UNIVERSITÀ degli STUDI di CATANIA
Dipartimento di Agricoltura, Alimentazione e Ambiente
Di3A

UNIVERSITÀ DEGLI STUDI DI CATANIA

PhD in

AGRICULTURAL, FOOD AND ENVIRONMENTAL SCIENCE

Modelling of bioenergy crops on marginal lands

Sebastiano Andrea Corinzia

Advisor:
Prof. Salvatore Luciano Cosentino
Dr. Danilo Scordia

Coordinator:
Prof. Cherubino Leonardi

Ph. D. attended during 2017/2020

Table of content

1 General introduction

Among renewable energy sources, biomasses derived from non-food or feed sources as energy dedicated crops, agricultural and agro-industrial waste are one of the most interesting solutions in the short and medium term for several reasons: the ability to produce energy *in situ* or on a short range, the relatively low investments, the opportunity to give an alternative to traditional crops that are unable to withstand the competition of a globalized market, the possibility to storage significant amounts of carbon in the soil, the opportunity to recover marginal and abandoned land by offering new market opportunities to farms avoiding competition with food production. Several energetic crops that are suitable for marginal areas where no food or feed crop can be grown sustainably have been identified during last years. However, the opportunity to exploit marginal areas for biomass production must be evaluated in relation to the particular pedoclimatic conditions and to the economic feasibility, concerning also the positive externalities and environmental impacts resulting from the agricultural activity. Cultivating energy crops on marginal land unsuitable for food production is consistently proposed as a viable alternative to minimize land-use competition for food production, and its adverse effects (direct or indirect) on food security, land based GHG emissions and biodiversity loss.

The main aim of this thesis is to provide forecasting tools that can help Mediterranean agriculture to deal with the climate change scenario and extreme climatic events, to identify new exploitable lands for energy production from biomass and energy crops for biorefinery purpose among marginal areas, to define the best management practices, including the choice of the crop species, suitable for these areas, and to quantify the environmental impact of these crops.

The aim is achievable by implementing biophysical models to simulate the response of crops under different climatic and environmental conditions and thus to produce a geo-spatial analysis of the results.
Two lines of research can be identified within this project

1. agronomic trial to collect data concerning morphology (stem height, leaf area), physiology (net photosynthesis rate, transpiration rate, stomatal conductance) and biomass yield components of three perennial lignocellulosic grasses (*Arundo donax* L., *Miscanthus* x *giganteum*, *Saccharum spontaneum* L. spp. *Aegyptiacum*) under three different soil moisture regimes
2. modellistic study that aims are to provide predictions for biomass and energy crops phenology and production, on marginal scenarios and to define marginal suitable areas and optimized agronomic management practices for biomass and energy crops grown in these areas; two energetic crop have been studied: *Ricinus communis* L. and *Miscanthus* x *giganteum*

2 Biomass yield and gas exchange of three perennial lignocellulosic grasses under different soil moisture regimes

2.1 Introduction

2.1.1 *Marginal Lands*

The definition of marginal land is not univocal and depends upon the point of view, which can be agronomical, economic or social, or upon the geographical context (Lewis and Kelly, 2014). From the agronomical point of view, marginal areas are characterized by under optimal growth conditions, which can be climatic, as temperature extremes, damage causing precipitations, drought or flooding; or pedological, as poor chemical, physical and biological soil properties, soil contaminants, excess slope. Under these conditions, the crop potential production cannot be achieved if an agronomic intervention meant to restore the optimal conditions is not provided. The yield that can be achieved under limiting conditions is called attainable yield; this can be further reduced down to the actual yield due to biotic constraints.

Focusing on Mediterranean area, marginal lands are those affected by severe drought, slope and salinity conditions (Cosentino et al., 2015b).Climate change projections indicates that it is likely that in arid and semi-arid regions, including Mediterranean area, where evapotranspiration exceed precipitations, reduced water availability, and duration of drought may increase (Cosentino et al., 2012; Edenhofer et al., 2014).

2.1.2 *Lignocellulosic perennial grasses*

Lignocellulosic perennial grasses are herbaceous plants of monocotyledonous class belonging to the Poaceae family. They have C4 (*Miscanthus* spp. and *Saccharum spontaneum* spp. *aegyptiacum*) (Cosentino et al., 2015b) or C3 (*Arundo donax* L.) photosynthetic pathway plants. The main advantages of lignocellulosic perennial grasses for biomass production are the resistance and resilience to abiotic stresses (Volaire et al., 2014) and thus the suitability for marginal lands; and the suitability for a multifunctional agriculture because of their multiple uses as feedstock for modern biorefineries to produce a number of high-added value products, as biomaterials for building, crafting and mulching, as biofuels and bioenergy source and as providers of ecosystem services, such as the protection of soil erosion and degradation, C-sequestration, restoration of severely degraded and heavily contaminated lands.

Perennial grasses possess some morphological, phenological and physiological traits that could cope with the stresses experienced under marginal conditions (Jones et al., 2015). Among perennial grasses, some species that have been considered suitable for biomass production for bio-energy purpose, as *Arundo donax* and *Miscanthus* x giganteus hybrid, proved to possess traits of avoidance or tolerance to severe stresses, as salinity on *Arundo* (Nackley and Kim, 2015; Stavridou et al., 2017), on cold tolerance on *Miscanthus* x giganteus (Clifton-Brown and Lewandowski, 2000; Dražić et al., 2017), on waterlogging or on water stress conditions (Cosentino et al., 2014, 2007; McDonald et al., 2002), on contaminated soils by heavy metals (Barbosa et al., 2015). Nevertheless, the suitability of very unproductive lands for biomass production remains questionable (Monti and Alexopoulou, 2017). Many studies suggest the suitability of minimum soil tillage techniques for these crops (Scordia et al.,

2015). Moreover, perennial lignocellulosic grasses are resistant to biotic stresses and disease and generally the cultivation is not aided by pesticide (Zegada-Lizarazu et al., 2010)

The suitability for marginal lands implies the possibility to minimize the competition with food crops on indirect land use change (iLUC) effects (Schmidt et al., 2015). Another advantage of perennial lignocellulosic grasses is the high environmental and energetic sustainability deriving from the long plantation life, spanning from 10 to 25 years, which limits the agronomic requirements to the crop establishment and yearly harvest (Alexopoulou et al., 2015b). Therefore the energy retourn on investment (EROI) and the greenhouse gases balance are generally positive (Lewandowski et al., 2003; Zanetti et al., 2019), and the soil organic carbon tends to increase. Many lignocellulosic perennial grasses have an increasing biomass yield during the first two to four year, followed by a period of stable yields, fluctuating only as a result of environmental conditions, and finally a gradual decrease associated with stand decline (Alexopoulou et al., 2015b).

Most of the lignocellulosic perennial grasses are currently undomesticated or at the early stages of crop development and improvement and thus biomass yield and other agronomic traits can be further improved by breeding (for fertile species), genotype and ecotype selection (for sterile and clonal populations) (Zegada-Lizarazu et al., 2010).

Lewandowsky et al. defined the hybridus *Miscanthus* x *giganteum*, canary grass (Phalaris arundinacea L.), switchgrass (Panicum virgatum L.) and giant reed (*Arundo donax* L.) as the most suitable perennial grasses for the European environmental conditions (Lewandowski et al., 2003)

(Cosentino et al., 2015b) suggested *Saccharum spontaneum* L. spp. *aegyptiacum* (Willd.) Hack. as a suitable lignocellulosic

perennial biomass crop for the sub-humid area of the Mediterranean

Perennial lignocellulosic grasses have a high resource-use efficiency due to the long leaf area duration, the extensive root system, high nitrogen use efficiency (NUE) (Cosentino et al., 2014) and, in the case of C4 species, the high radiation use efficiency (RUE) and water use efficiency (WUE) (Cosentino et al., 2007, 2015b; Scordia and Cosentino, 2019). Perennial lignocellulosic grasses are suited for low or no input agronomic management, but through input calibration in response to meteorological data and soil moisture measurements it is possible to reduce irrigation input (keeping the soil moisture in the range of 40 to 60% of field capacity) and fertilization input (in the order of 60 kg ha^{-1}) without compromising yield of giant reed grown in a semi-arid environment and therefore maximizing WUE and NUE (Cosentino et al., 2016)

Perennial lignocellulosic grasses, being characterized by characterized by high biomass yield and low requirement of agronomic input, have a positive energy balance. (Zanetti et al., 2019) calculated the energy balance of low-input (unfertilized, rainfed, no weed and pest management) long-term plantations (more than 10 years) of switchgrass, *Miscanthus* and giant reed, finding a net energy gain of 161 GJ ha^{-1} for giant reed in Catania, 203 GJ ha^{-1} for switchgrass in Bologna, 107 and 299 GJ ha^{-1} for *Miscanthus* in Catania and Bologna respectively.

Crop establishment is considered as the most expensive agronomic intervention in terms of energetic and economic cost for lignocellulosic perennial grasses, both seeded and propagated by rhizomes (Scordia et al., 2015). Crop establishment is also the period during crop life that is most vulnerable to weed competition. The cause is the low initial growth rate of seeded grasses (switchgrass and reed canary grass) and the low plant density (10000 to 20000 rhizomes ha^{-1})

usually chosen for *Miscanthus* and giant reed in order to reduce establishment cost (Scordia et al., 2015). Solutions to address this problem could be micropropagation (Cavallaro et al., 2014) or stem cutting (Cavallaro et al., 2019; Copani et al., 2013). Yield and growth rate, especially during crop establishment, could be enhanced by intercropping with perennial low grasses and legumes (Bybee-Finley and Ryan, 2018)

Perennial lignocellulosic grasses demonstrated to provide ecosystem services and environmental benefits: the continuous presence of the root system, the extended duration of the canopy cover and the long period without soil disturbance reduce soil erosion (Cosentino et al., 2008; Wuest et al., 2006), improve soil structure and effect positively the local biodiversity (Lewandowski et al., 2003) and increase the carbon stock in soil and aboveground as plant residues (Scordia and Cosentino, 2019). In *Miscanthus* and giant reed trial conducted in sloping (27%) soil the Mediterranean area, the soil loss trough erosion was reduced to 0.09 or 0.07 Mg ha^{-1} from the 4.34, 4.81 and 10.1 Mg ha^{-1} of soil loss caused by fallow, Italian ryegrass and durum wheat cultivation systems, respectively (Cosentino et al., 2015a).Giant reed is able to accumulate 0.6 – 1.0 Mg C ha^{-1} $year^{-1}$ during long term trials (Monti and Zegada-Lizarazu, 2016). The risk of invasiveness is one of the negative environmental traits, potentially affecting biodiversity: giant reed and *Miscanthus sinensis* are considered a noxious weed outside their natural range (Global Invasive Species Database, 2020; Quinn et al., 2010). Infertile *Miscanthus* hybrids eliminate the risk of invasiveness from naturally dispersed, viable seed (Clifton-Brown et al., 2019).

Climate change could affect lignocellulosic perennial grasses differently in relation to the geographical area: at mid and high latitude the growing season length could extend, while in more southern latitude, the increase in evapotranspiration could lead

to a decrease in growing season length (Cosentino et al., 2012; Olesen et al., 2011). C3 plants could benefit more than C4 from rising C02 concentration, in response to higher RUE and reduce transpiration (Ainsworth and Ort, 2010; Drake et al., 1997; Poorter, 1993). For giant reed has been reported a reduction of transpiration and an increase in WUE from 4 to 12 µmol CO2 mmol $H2O^{-1}$ when the CO2 concentration increased from 400 to 800 µmol mol^{-1} in growth chamber (Nackley et al., 2014).

Biomass of perennial lignocellulosic grasses consist mainly of cellulose, hemicellulose, lignin, a small fraction of soluble organic components and minerals (Wyman, 1994) (Scordia et al., 2011).

Cellulose and hemicellulose can be converted through biochemical or thermochemical processes into monosaccharides for fermentation and production of ethanol. These processes have the aim to disrupt the lignocellulosic matrix in order to enhance the cellulose and hemicellulose conversion (Scordia et al., 2011; Zhu and Pan, 2010). The lignocellulosic biomass can be used to generate electricity through combustion, pyrolysis, gasification and anaerobic digestion (Kiesel et al., 2017; Ragaglini et al., 2014; Scordia and Cosentino, 2019). Biomass moisture content affects the suitability of the bioconversion processes: biomass with high humidity content, such as *S. spontaneum* biomass, is more suited to biochemical conversion, while drier biomass is suited to thermochemical conversions (McKendry, 2002). Herbaceous plants are generally rich in mineral content and their ash has a low melting point. These trait hinders the thermochemical conversions because of slagging (Jenkins et al., 1998; Monti et al., 2008). Winter harvest showed to reduce biomass moisture content, to reduce ash content and improve the structural compounds content (Scordia et al., 2016; Zanetti et al., 2019).

2.1.3 *Lignocellulosic perennial grasses species*

Arundo donax L. is a perennial rhizomatous grass of the Poaceae, having a C3 metabolism, naturalized in the Mediterranean basin and spontaneously widespread in tropical and warm-temperate areas of the world (Cosentino et al., 2014). According to its fast growth rate and ease of vegetative propagation, it is considered as invasive species in the USA warm-temperate regions with winter floods that widely disperse this plant (Cosentino et al., 2014). *Arundo* spreads only by vegetative reproduction, thus it has low genetic variability and ecotypes are discriminated only on the base of phenotype (De Stefano et al., 2018). *A. donax* shows limited genetic diversity due to the inability to produce viable seed caused by the high polyploidy. Even though, phenotypic variability exists in nature (Cosentino et al., 2006). *A. donax* has a C3-pathway metabolism, but it shows values of net photosynthesis similar to that of C4 plants (Rossa et al., 1998).

Saccharum spontaneum spp. *Aegyptiacum* is a perennial rhizomatous grass of the Poaceae native of northern Africa and widespread in South Mediterranean regions (Pignatti, 1982). *S. spontaneum* has a C4-pathway metabolism, with a ^{13}C value of $^{-1}3.19‰$ (O'Leary, 1988). It is suitable for semi-arid regions of the Mediterranean area (Cosentino et al., 2015b).

Miscanthus × *giganteus*, is a perennial grass hybrid of *M. sinensi*s and *M. sacchariflorus*, part of the family Poacee, native of Eastern Asia but well adapted to European cool-temperate climate (Clifton-Brown et al., 2017). It has a C4 metabolism and thus exhibits high photosynthetic efficiency and water use efficiency up to 5 g L^{-1} (Clifton-Brown et al., 2017; Stavridou et al., 2017). The hybrid is sterile and its clonal propagation occurs by rhizomes. *Miscanthus* can achieve adequate yields on marginal lands, up to 30 Mg ha^{-1} of dry biomass where soil water

is adequate (Stavridou et al., 2017), including heavy metal contaminated, where it shows phytostabilization potential (Dražić et al., 2017) and saline soils (Stavridou et al., 2017).

2.2 Materials and methods

2.2.1 *Field trial description*

The field trial was carried out at the Experimental Farm of the University of Catania (10 m a.s.l., 37°24′ N, 15°03′ E) in a typical Xerofluvents soil (USDA, 1999).
Six genotypes were evaluated in a split-plot experimental design with nine replications: two *Arundo donax* L. ecotypes, named ARCT and ARMO (clone Fondachello and clone Morocco), the commercial *Miscanthus* x giganteus (greef et Deuter) named MxG, two seed-based *Miscanthus* hybrids obtained from the breeding program led by the Institute of Biological, Environmental and Rural Sciences of Aberystwyth University (UK) and Terravesta Ltd (UK), named GNT9 and GNT10, and one ecotype of *Saccharum spontaneum* L. ssp. aegypticum Willd (Hack.), named SAC. The main factor assigned to the plots is the irrigation factor, with 3 levels: 100%, 50% and 0% of maximum crop evapotranspiration (ETm) restoration during the summer months (June-August). Genotype is the second factor, assigned to the sub-plots within the main irrigation plots. Each combination of irrigation and genotype is replicated 3 times within the main plots.
Irrigation is provided by a drip irrigation system. During the first year of plant establishment, irrigation was not differentiated, and all the plots received 100% of maximum crop evapotranspiration restoration during the summer months.
Rhizomes of SAC, ARMO and ARCT were collected from the in-situ germplasm collection located at the Experimental farm. Plantlets of MxG were provided by Energene sp. z o.o (Poland), while the GNT9 and the GNT10 by Terravesta Ltd (UK). Fresh rhizomes of approximately 100 g with 2-3 main buds (ARMO, ARCT and SAC) and plantlets (MxG, GNT9 and GNT10) were directly transplanted in a previously prepared soil bed, ploughed

in autumn, and disk harrowed in spring. Transplant was done by hand in May 2018 at a density of 1 rhizome or plant m–2. With the aim to reduce the external input supply, no fertilization was supplied before transplanting,

Weeds were controlled manually during the year of establishment by means of a grass trimmer when necessary. Plantlets were kept in well-watered condition through a drip irrigation system, from the establishment to the end of summertime, by restoring 100% ETm.

Irrigation was scheduled when the sum of daily ETm corresponded to the volume, subtracting rainfall events from the calculation. The daily ETm was calculated according to:

$$ETm = ET0 \times Kc$$

where ETm is the maximum daily evapotranspiration (mm); E0 is the evaporation of class-A pan (mm); Kp is the pan coefficient, equal to 0.80 in semi-arid environment. Crop coefficients (Kc) were those applied for *Miscanthus* × giganteus, *Arundo donax* and *Saccharum spontaneum* grown in the same environment (Cosentino et al., 2014, 2007; Panoutsou and Chiaramonti, 2020).

The irrigation volume was calculated according to the following equation:

$$V = 0.66 \times (FC - WP) \times \phi \times D \times 103$$

where V = water amount (mm); 0.66 = readily available water not limiting for evapotranspiration; FC = soil water content at field capacity (27% of dry soil weight); WP = soil water content at wilting point (11% of dry soil weight); ϕ = bulk density (1.1 g cm−3); and D = rooting depth (0.6 m).

At the end of summer season, when rainfall increases in frequency, the irrigation is suspended.

2.2.2 *Measurements*

During the growing seasons, meteorological conditions have been continuously measured through a weather station connected to a data logger (Delta-T, WS-GP1). Potential evapotranspiration is calculated according to Allen and Food and Agriculture Organization of the United Nations (1998).

Field measurement of stem height, stem density, solar radiation interception and gas exchanges have been measured with a 2 weeks frequency from shoot emission at the beginning of spring to leaves senescence in autumn. Stem sampling has been performed monthly starting from shoot emission until harvest in winter.

Soil water content has been measured every two weeks using Teros10 moisture sensors (Delta-T).

Solar radiation interception has been measured using an AccuPAR model LP-80 PAR/LAI Ceptometer (Decagon Devices, Inc.). The instrument calculates leaf area index by measuring the amount of radiation transmitted through the canopy and of radiation scattered by leaves within the canopy and comparing with the above canopy photosynthetically active radiation (PAR), adopting the model suggested by Norman and Campbell (1989).

Net photosynthesis (μmol $C0_2$ m^{-2} s^{-1}), transpiration (mmol H_20 m^{-2} s^{-1}) and stomatal conductance (mol H_20 m^{-2} s^{-1}) have been calculated by the LCi-SD Portable Photosynthesis system (ADC BioScientific Ltd.) on the basis of $C0_2$ and H_20 gas exchange. The instrument measures also PAR, leaf and atmospheric temperature.

Stem sampling consist of the collection of one (ARMO and ARCT) or 3 (all the other genotypes) representative stems from each plot of the trial, avoiding the inner $4m^2$ subplot that has been used for the estimation of total aboveground biomass yield at winter harvest.

The sampled stems have been measured for stem weight (g), thickness (mm) and height (m), number of leaves per stem, green leaf area per stem, biomass fraction and plant fresh and dry matter, the latter obtained by drying the biomass at 65°C until constant weight. Leaf area index has been calculated by multiplying stem density and leaf area per stem in order to obtain a second estimation that can be compared with the values calculated by the ceptometer. Total aboveground biomass has been estimated during the growing season by multiplying the stem density and the sample stem weight.
Total aboveground biomass has been harvested in January 2019 and 2020. The whole aboveground fresh biomass has been collected and weighted from a 4 m^2 subplot and then from the entire plot. The number of stems in the subplot has been measured. Five stems per plot were sampled for further measurements: stem weight (g), thickness (mm) and height (m), number of leaves per stem, biomass fraction and plant dry matter. Biomass was cut 5 cm above ground level and fresh sub-samples were randomly collected, immediately weighted and then dried to a constant weight at 65°C. The percentage dry weight was used to calculate the dry biomass yield, which was referred to the unit land area (DMY, Mg ha^{-1}).

2.2.3 *Analytical determinations*

The composition of the biomass harvested in January 2019 was determined by a Near InfraRed (NIR) spectroscopy (SpectraStar 2500XL-R, Unity Scientific). The spectroscopy analysed the diffuse reflectance between 680 and 2500 nm at 1 nm intervals. The absorption spectra have been used to predict the concentration of hemicellulose, cellulose, acid detergent lignin (ADL), ash and neutral detergent soluble (NDS) using a calibration obtained from spectra and correspondent analytic values measured on lignocellulosic biomass of herbaceous

plants adopting the developed calibration for lignocellulosic perennial grasses, as reported in (Scordia et al., 2017).

2.2.4 *Statistical analysis*

Biomass yield, stem dry weight and stem density measured during 2019 harvest, before the differentiation of the irrigation factors, were subjected to a one-way ANOVA with genotype as source of variance. Tukey's HSD test with 0.05 significant level has been performed to assess the differences among each genotype using RStudio software (RStudio, Boston, USA).
Two-way ANOVA with genotype and the irrigation factor as the sources of variance has been performed on the variables measured during 2020 harvest.
Three-factor ANOVA with date, genotype and the irrigation factor as the sources of variance has been performed on the variables measured during 2019 and 2020 growing season.

2.3 Results and discussion

2.3.1 *Meteorological conditions*

Soil moisture at 0-30 and 30-60 cm depth, as well as soil water content from 0 to 60 cm depth, showed the effect of the irrigation level (**Errore. L'origine riferimento non è stata trovata.**). During summer months, which correspond to the irrigation period, soil moisture decreased in I0 thesis for all the genotypes, both in 2019 and 2020, and approached the wilting point threshold. Soil water in I0 raised to more suitable levels between September and October of 2019 and 2020, due to the precipitation events. During 2020, soil water content from 0 to 60 cm depth in the I0 thesis remained at higher levels than in 2019, in response to the more favorable rainfall regime. The I50 and I100 thesis maintained an adequate soil water content during 2019 and 2020 growing seasons, with I100 having higher levels of soil moisture.

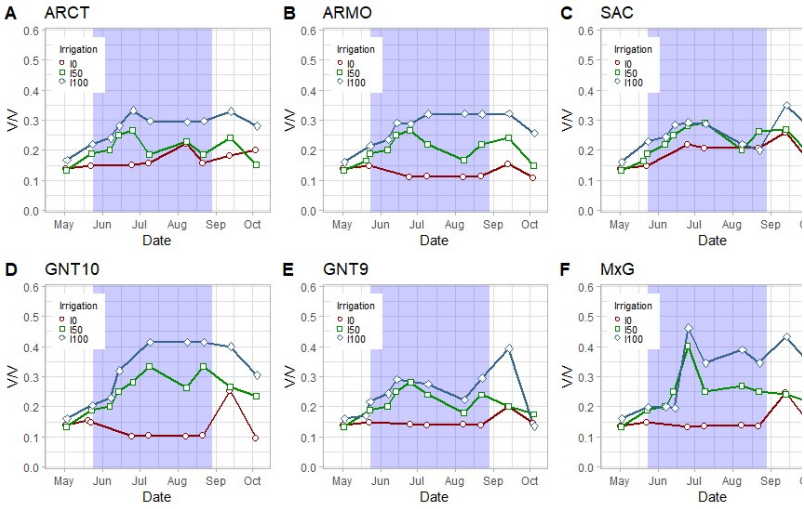

Figure 1 Soil water moisture from 0 to 30 cm depth (% V/V) trends over the vegetative stages (March to November 2019 for 3 water restoration levels (I0, I50, I100) and for 6 genotypes exanimated in this study: ARCT: *A. donax* ecotype Catania, ARMO: *A. donax* ecotype Morocco, SAC: *S. spontaneum*, GNT10: *Miscanthus* x *giganteus* hybrid 10, GNT9: *Miscanthus* x *giganteus* hybrid 9, MxG: *Miscanthus* x *giganteus*.

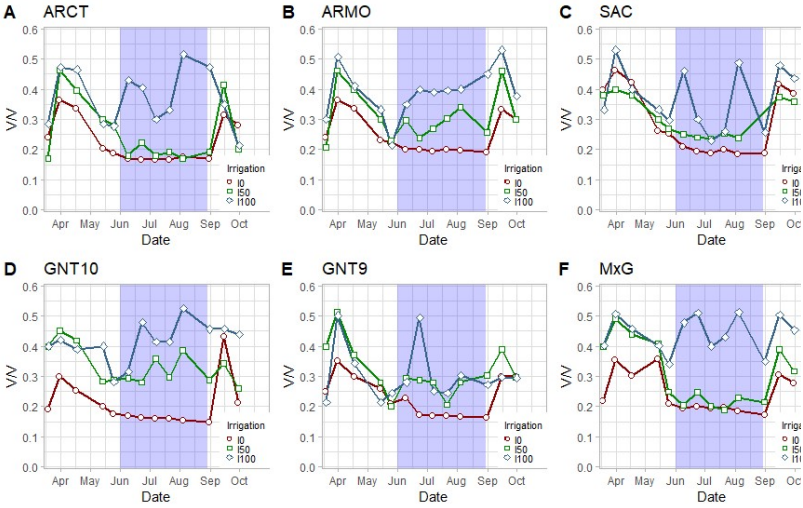

Figure 2 Soil water moisture from 0 to 30 cm depth (% V/V) trends over the vegetative stages (March to October 2020 for 3 water restoration levels (I0, I50, I100) and for 6 genotypes exanimated in this study: ARCT: *A. donax* ecotype Catania, ARMO: *A. donax* ecotype Morocco, SAC: *S. spontaneum*, GNT10: *Miscanthus* x *giganteus* hybrid 10, GNT9: *Miscanthus* x *giganteus* hybrid 9, MxG: *Miscanthus* x *giganteus*.

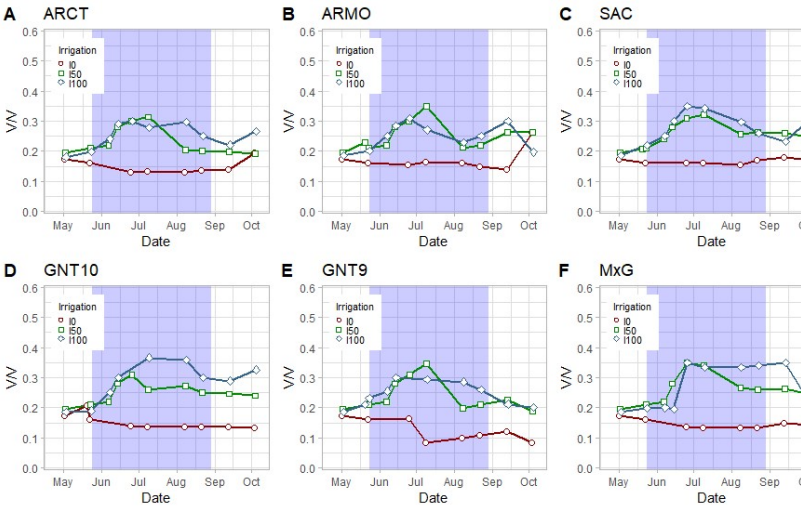

Figure 3 Soil water moisture from 30 to 60 cm depth (% V/V) trends over the vegetative stages (March to November 2019) for 3 water restoration levels (I0, I50, I100) and for 6 genotypes exanimated in this study: ARCT: *A. donax* ecotype Catania, ARMO: *A. donax* ecotype Morocco, SAC: *S. spontaneum*, GNT10: *Miscanthus* x *giganteus* hybrid 10, GNT9: *Miscanthus* x *giganteus* hybrid 9, MxG: *Miscanthus* x *giganteus*.

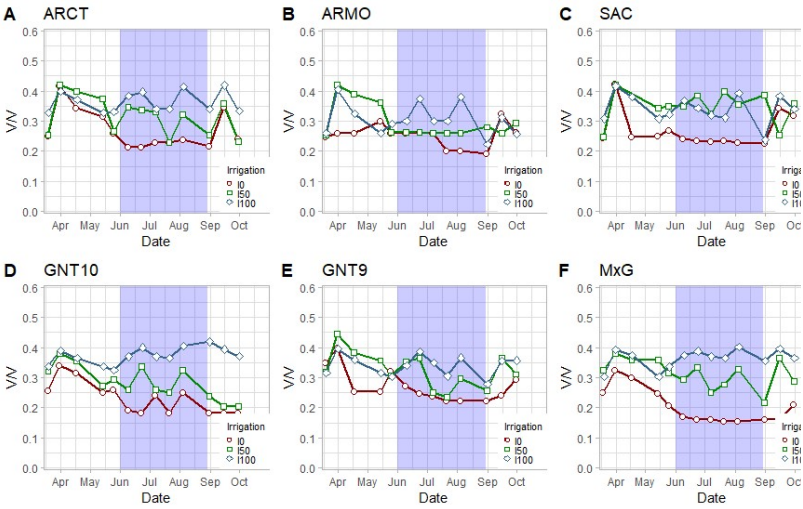

Figure 4 Soil water moisture from 30 to 60 cm depth (% V/V) trends over the vegetative stages (March to October 2020) for 3 water restoration levels (I0, I50, I100) and for 6 genotypes exanimated in this study: ARCT: *A. donax* ecotype Catania, ARMO: *A. donax* ecotype Morocco, SAC: *S. spontaneum*, GNT10: *Miscanthus* x *giganteus* hybrid 10, GNT9: *Miscanthus* x *giganteus* hybrid 9, MxG: *Miscanthus* x *giganteus*.

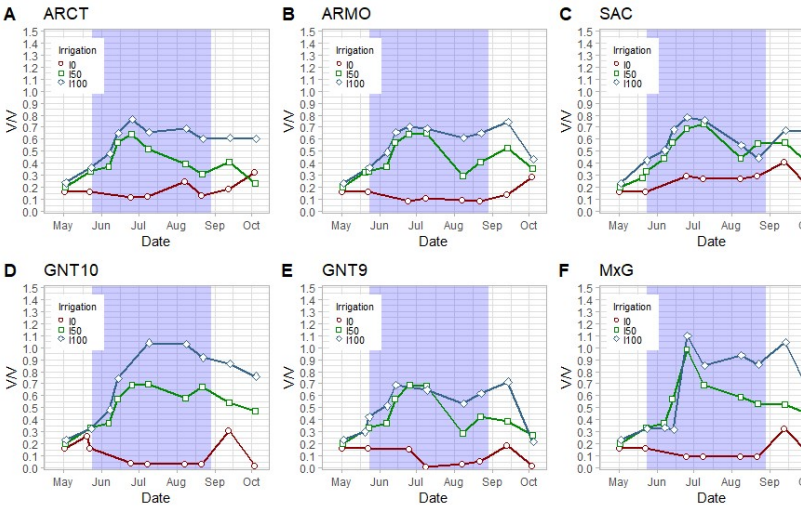

Figure 5 Available soil water content from 0 to 60 cm depth (% V/V) trends over the vegetative stages (March to November 2019) for 3 water restoration levels (I0, I50, I100) and for 6 genotypes exanimated in this study: ARCT: *A. donax* ecotype Catania, ARMO: *A. donax* ecotype Morocco, SAC: *S. spontaneum*, GNT10: *Miscanthus* x *giganteus* hybrid 10, GNT9: *Miscanthus* x *giganteus* hybrid 9, MxG: *Miscanthus* x *giganteus*.

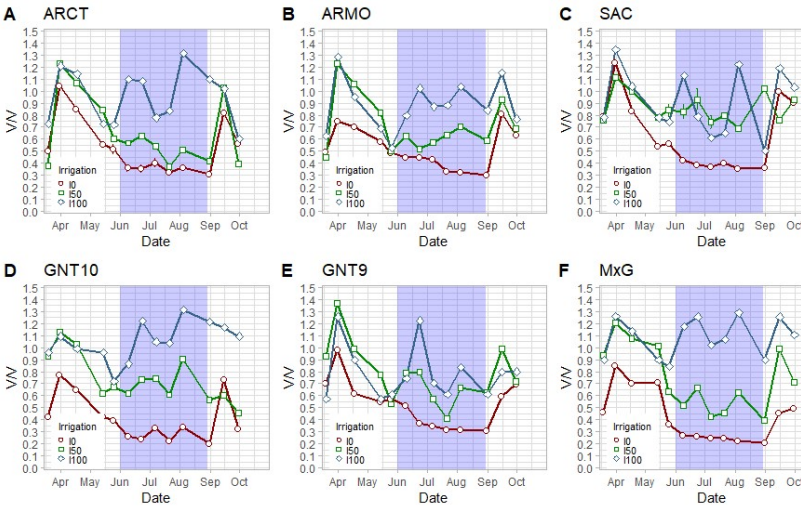

Figure 6 Available soil water content from 0 to 60 cm depth (% V/V) trends over the vegetative stages (March to October 2020) for 3 water restoration levels (I0, I50, I100) and for 6 genotypes exanimated in this study: ARCT: *A. donax* ecotype Catania, ARMO: *A. donax* ecotype Morocco, SAC: *S. spontaneum*, GNT10: *Miscanthus* x *giganteus* hybrid 10, GNT9: *Miscanthus* x *giganteus* hybrid 9, MxG: *Miscanthus* x *giganteus*.

2.3.2 *Growing season measurements*

2.3.2.1 Morphometric measurements

Genotype GNT9 had the highest stem density both in 2019 and 2020 growing seasons, peaking at 85 stems m-2 in the I100 thesis during 2019 growing season and at 102 stems m-2 in the I50 thesis during 2020 growing season (**Figure** 7, **Figure** 8). Both *A. donax* genotypes had the lowest stem density among the six genotypes for all the irrigation levels. Generally, stem density increases with the higher irrigation levels, however some exceptions have been reported, in particular during 2020 growing season. Date, genotype and irrigation have a statistically significant effect on stem density, while among the interactions, only date x genotype and irrigation x genotype have a statistically significant effect (**Errore. L'origine riferimento non è stata trovata.**). All the genotypes reached the maximum stem density at the end of summer or during autumn, excluding GNT9 that reached the maximum stem density in May and showed a decrease during summer. Stem density was higher in 2020 than 2019, in all the genotypes except for *S. spontaneum*, which showed similar values in both years, likely because of the faster rhizome propagation within the plots of this species.

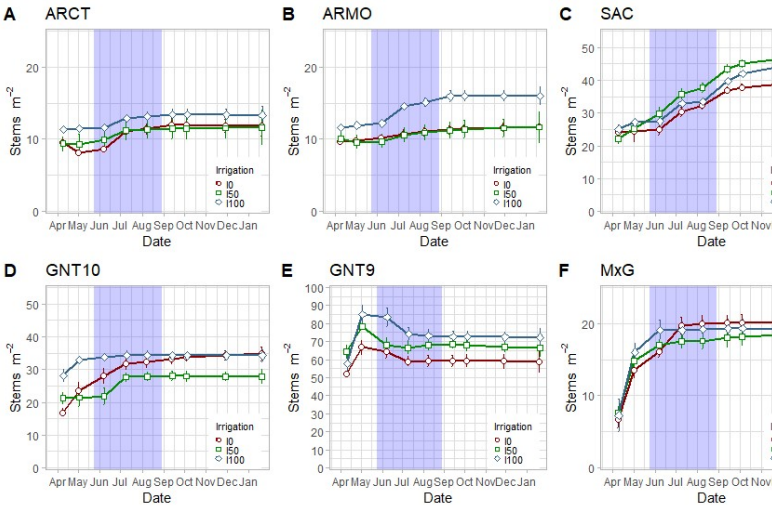

Figure 7 Stem density (stems m^{-2}) trends over the vegetative stages (March to November 2019) for 3 water restoration levels (I0, I50, I100) and for 6 genotypes exanimated in this study: ARCT: *A. donax* ecotype Catania, ARMO: *A. donax* ecotype Morocco, SAC: *S. spontaneum*, GNT10: *Miscanthus* x *giganteus* hybrid 10, GNT9: *Miscanthus* x *giganteus* hybrid 9, MxG: *Miscanthus* x *giganteus.*

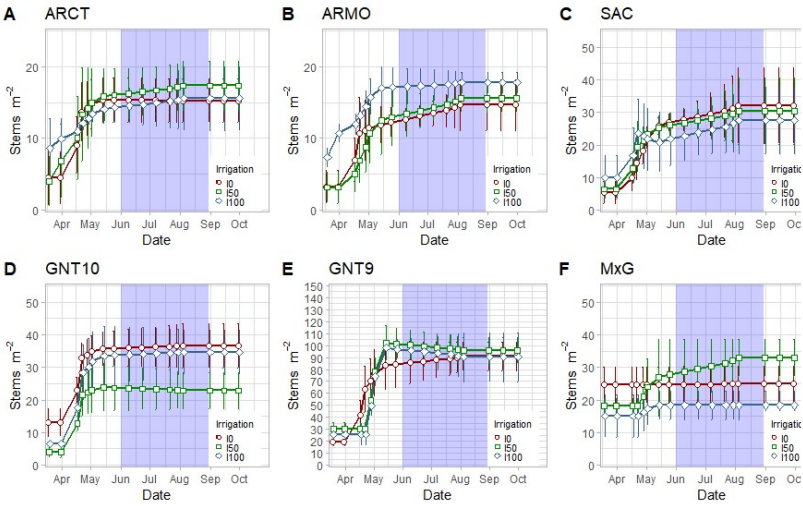

Figure 8 Stem density (stems m-2) trends over the vegetative stages (March to October 2020) for 3 water restoration levels (I0, I50, I100) and for 6 genotypes exanimated in this study: ARCT: *A. donax* ecotype Catania, ARMO: *A. donax* ecotype Morocco, SAC: *S. spontaneum*, GNT10: *Miscanthus* x giganteus hybrid 10, GNT9: *Miscanthus* x giganteus hybrid 9, MxG: *Miscanthus* x giganteus.

A. donax genotypes had the highest stem height in both 2019 and 2020, with ARMO peaking at almost 400 cm in 2019 and 550 cm in 2020, followed by *S. spontaneum*, while *Miscanthus* genotypes had the lowest stem height (**Figure** 9, **Figure** 10). Irrigation has a statistically significant positive effect on stem height (Anova Tables of growing season measurements), with I00 thesis showing higher stems for all the genotypes and I0 thesis showing the lowest. Date, genotype, irrigation and all factors interactions have a statistically significant effect on stem height (**Errore. L'origine riferimento non è stata trovata.**). Stem height increased continuously until late autumn in all the genotypes. *A. donax* genotypes showed an increase in 2020 stem

height compared to 2019, while *S. spontaneum* and *Miscanthus* genotypes maintained similar values in both years.

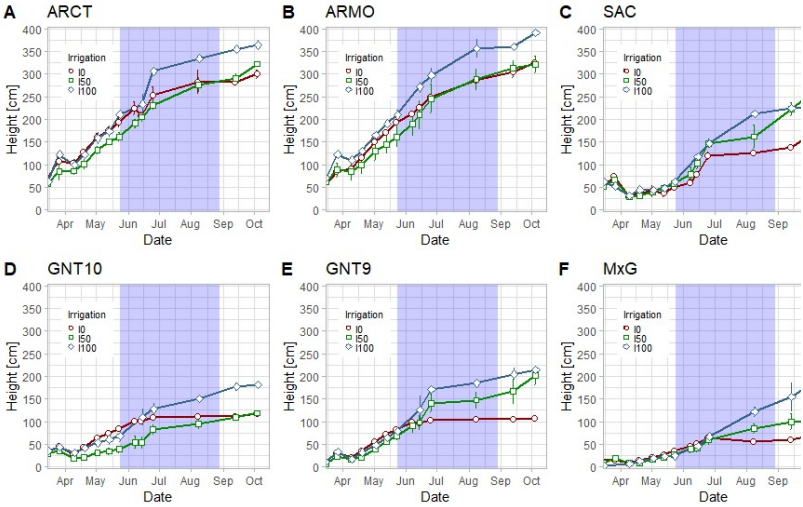

Figure 9 Mean stem height (stems m^{-2}) trends over the vegetative stages (March to November 2019) for 3 water restoration levels (I0, I50, I100) and for 6 genotypes exanimated in this study: ARCT: *A. donax* ecotype Catania, ARMO: *A. donax* ecotype Morocco, SAC: *S. spontaneum*, GNT10: *Miscanthus* x *giganteus* hybrid 10, GNT9: *Miscanthus* x *giganteus* hybrid 9, MxG: *Miscanthus* x *giganteus.*

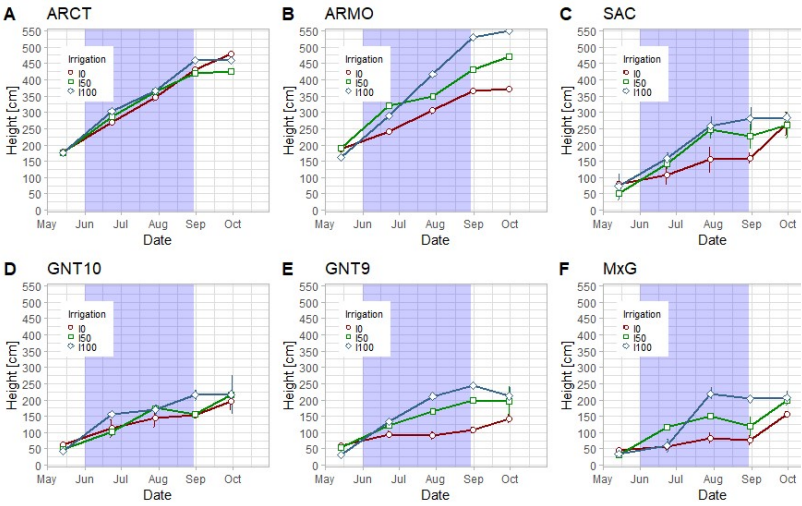

Figure 10 Mean stem height (stems m^{-2}) trends over the vegetative stages (May to October 2020) for 3 water restoration levels (I0, I50, I100) and for 6 genotypes exanimated in this study: ARCT: *A. donax* ecotype Catania, ARMO: *A. donax* ecotype Morocco, SAC: *S. spontaneum*, GNT10: *Miscanthus* x *giganteus* hybrid 10, GNT9: *Miscanthus* x *giganteus* hybrid 9, MxG: *Miscanthus* x *giganteus.*

GNT9 in the I100 theis showed the highest LAI (10.1) as measured by ceptometer among the genotypes and the irrigation thesis (**Figure** 11, **Figure** 12). Slightly lower LAI values have been measured for *A. donax* genotypes. Irrigation has a statistically significant positive effect on LAI in both years (Anova Tables of growing season measurements), with I00 thesis showing higher stems for all the genotypes and I0 thesis showing the lowest. GNT9 showed the highest effect on LAI by irrigation, with a marked difference between I0 values and 150 – I100 values both in 2019 and 2020. During 2019, all the genotypes reached the highest LAI in September, while in 2020 leaf area growth has been faster and LAI peak has been reached during summer months by all the genotypes.

Date, genotype, irrigation and all factors interactions, excluding the date x irrigation x genotype interaction in 2020, have a statistically significant effect on stem height (**Errore. L'origine riferimento non è stata trovata.**).

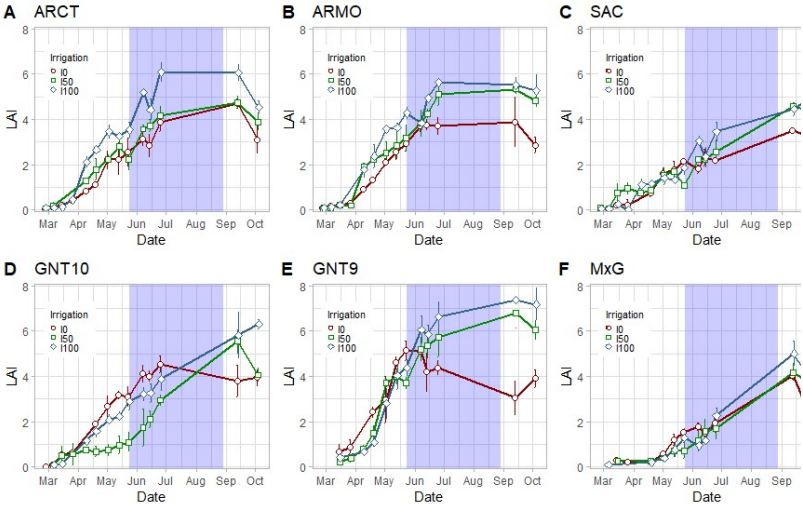

Figure 11 Leaf area index trends over the vegetative stages (March to November 2019) as measured by ceptometer for 3 water restoration levels (I0, I50, I100) and for 6 genotypes exanimated in this study: ARCT: *A. donax* ecotype Catania, ARMO: *A. donax* ecotype Morocco, SAC: *S. spontaneum*, GNT10: *Miscanthus* x giganteus hybrid 10, GNT9: *Miscanthus* x giganteus hybrid 9, MxG: *Miscanthus* x giganteus.

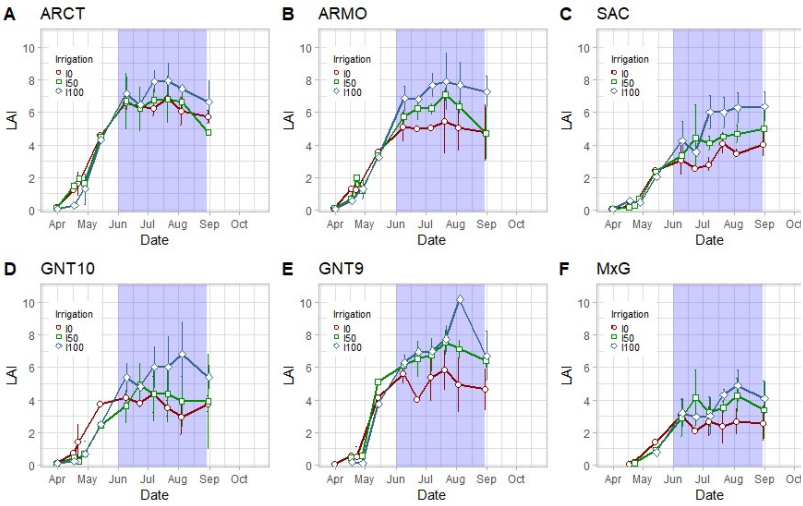

Figure 12 Leaf area index trends over the vegetative stages (April to September 2020) as measured by ceptometer for 3 water restoration levels (I0, I50, I100) and for 6 genotypes exanimated in this study: ARCT: *A. donax* ecotype Catania, ARMO: *A. donax* ecotype Morocco, SAC: *S. spontaneum*, GNT10: *Miscanthus* x *giganteus* hybrid 10, GNT9: *Miscanthus* x *giganteus* hybrid 9, MxG: *Miscanthus* x *giganteus.*

Solar radiation interception follows the same pattern of LAI measured by ceptometer, since the latter has been calculated on the basis of the solar radiation interception (**Figure** 13, **Figure** 14). Gnt9 and *A. donax* genotypes reached the highest solar radiation interception during both years, with the irrigated thesis showing higher values and the rainfed thesis having slightly lower values. Even for this variable, date, genotype, irrigation and all factors interactions have a statistically significant effect on stem height (**Errore. L'origine riferimento non è stata trovata.**).

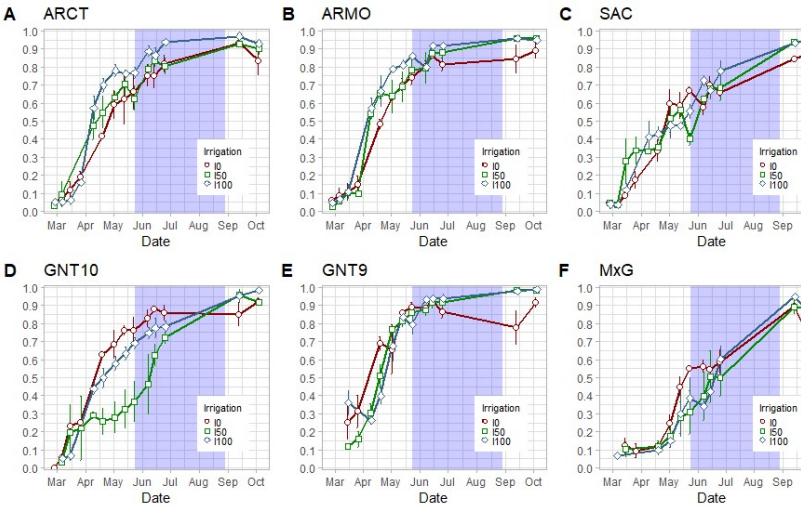

Figure 13 Solar radiation interception trends over the vegetative stages (March to November 2019) as measured by ceptometer for 3 water restoration levels (I0, I50, I100) and for 6 genotypes exanimated in this study: ARCT: *A. donax* ecotype Catania, ARMO: *A. donax* ecotype Morocco, SAC: *S. spontaneum*, GNT10: *Miscanthus* x *giganteus* hybrid 10, GNT9: *Miscanthus* x *giganteus* hybrid 9, MxG: *Miscanthus* x *giganteus.*

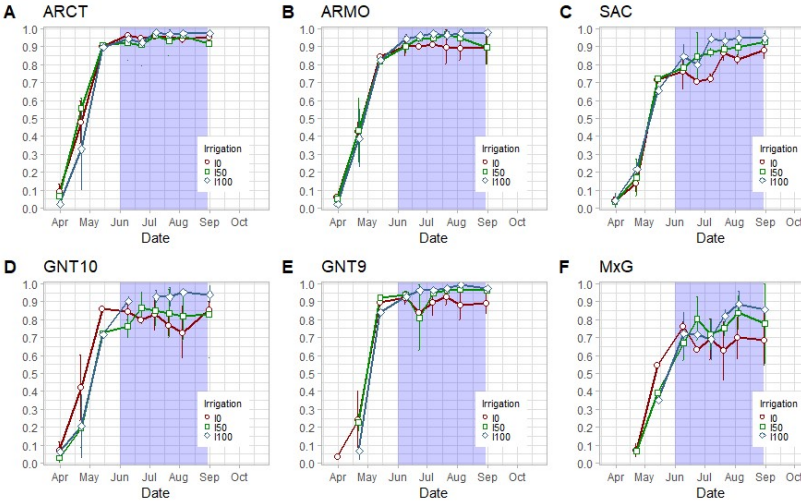

Figure 14 Solar radiation interception trends over the vegetative stages (April to September 2020) as measured by ceptometer for 3 water restoration levels (I0, I50, I100) and for 6 genotypes exanimated in this study: ARCT: *A. donax* ecotype Catania, ARMO: *A. donax* ecotype Morocco, SAC: *S. spontaneum*, GNT10: *Miscanthus* x *giganteus* hybrid 10, GNT9: *Miscanthus* x *giganteus* hybrid 9, MxG: *Miscanthus* x *giganteus.*

Stem leaf area has been measured in order to calculate LAI as a reference of LAI values measured by ceptometer. ARCT reached the highest LAI in 2020 in I100 thesis (13.2) (**Errore. L'origine riferimento non è stata trovata.**) and ARMO showed similar results, while GNT9 reached a LAI of 7.9 in 2020. Values of LAI in 2019 were lower, reaching a maximum of 5.7 in ARMO I100 (**Figure** 15). In 2019 maximum LAI has been reached between September and October for all the genotypes, while in 2020 the maximum has been reached during summer months. ANOVA was statistically significant for date, genotype, irrigation and all factors interactions, while

in 2020 only the date x irrigation and the date x irrigation x genotype effect was not statistically signicant (**Errore. L'origine riferimento non è stata trovata.**). LAI obtained from stem sapling tends to be underestimated in comparison with LAI measured by ceptometer with the exception of *A. donax* genotypes in 2020. GNT9 and GNT10 LAI values in 2020 showed the highest agreement, likely because of the high stem uniformity.

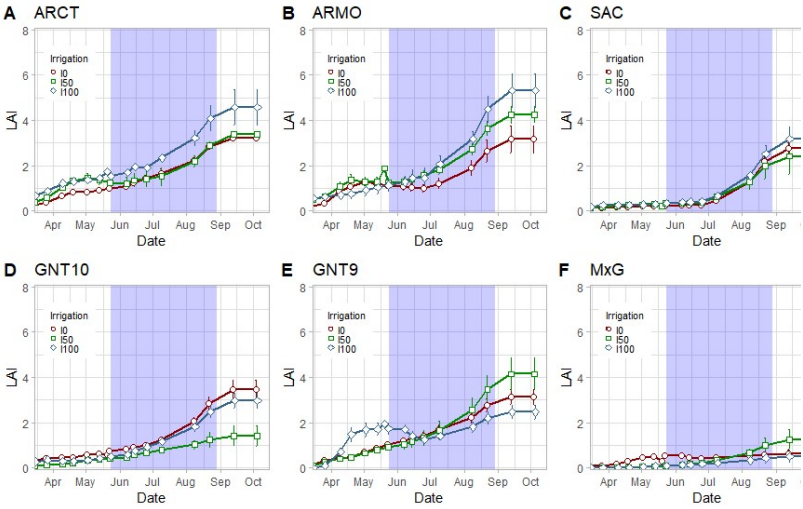

Figure 15 Leaf area index trends over the vegetative stages (March to November 2019) as calculated by measuring stem leaf area per stems and stem density for 3 water restoration levels (I0, I50, I100) and for 6 genotypes exanimated in this study: *A. donax* ecotype Catania, ARMO: *A. donax* ecotype Morocco, SAC: *S. spontaneum*, GNT10: *Miscanthus* x *giganteus* hybrid 10, GNT9: *Miscanthus* x *giganteus* hybrid 9, MxG: *Miscanthus* x *giganteus.*

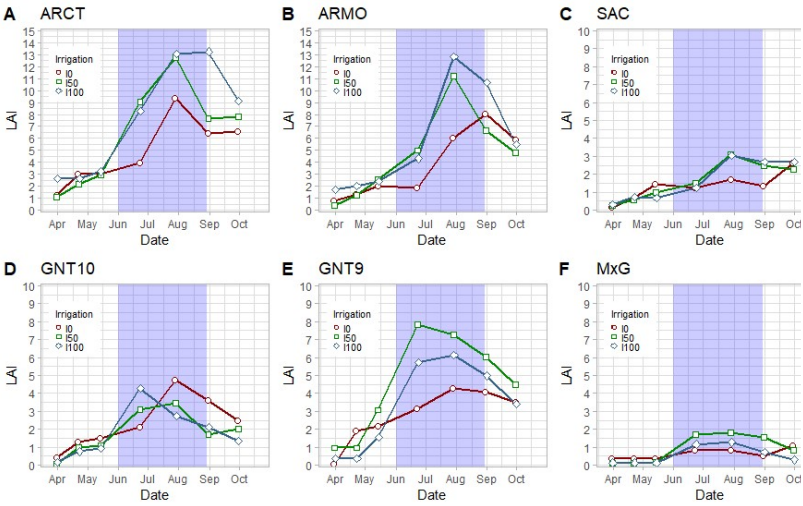

Figure 16 Leaf area index trends over the vegetative stages (April to October 2020) as calculated by measuring stem leaf area per stems and stem density for 3 water restoration levels (I0, I50, I100) and for 6 genotypes exanimated in this study: *A. donax* ecotype Catania, ARMO: *A. donax* ecotype Morocco, SAC: *S. spontaneum*, GNT10: *Miscanthus* x *giganteus* hybrid 10, GNT9: *Miscanthus* x *giganteus* hybrid 9, MxG: *Miscanthus* x *giganteus.*

Mean stem dry weight showed a high variability among genotypes (F-value of 1830 in 2019 and 1100 in 2020, Anova Tables of growing season measurements), with values ranging from 302 g for ARMO to 13.5 g for MxG in the I100 thesis in 2019 (**Figure** 17) and from 577 g for ARMO to 44 g for GNT9 in the I100 thesis in 2020 (**Figure** 18**Figure** 18). *A. donax* genotypes showed the highest stem dry weight during the whole growing season for all the irrigation thesis, both in 2019 and 2020. *S. spontaneum* and GNT10 showed intermediate values, while GNT9 and MxG had the lowest stem dry weights. Irrigation has a statistically significant positive effect on stem dry weight. Date, genotype, irrigation and all factors interactions

have a statistically significant effect on stem height (**Errore. L'origine riferimento non è stata trovata.**).

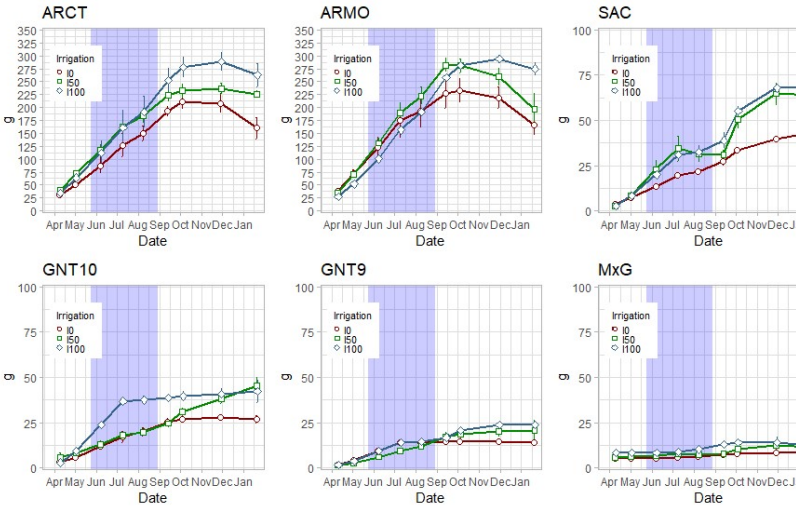

Figure 17 Mean stem dry weight (g stems^{-1}) trends over the vegetative stages (March to November 2019) for 3 water restoration levels (I0, I50, I100) and for 6 genotypes exanimated in this study: ARCT: *A. donax* ecotype Catania, ARMO: *A. donax* ecotype Morocco, SAC: *S. spontaneum*, GNT10: *Miscanthus* x *giganteus* hybrid 10, GNT9: *Miscanthus* x *giganteus* hybrid 9, MxG: *Miscanthus* x *giganteus.*

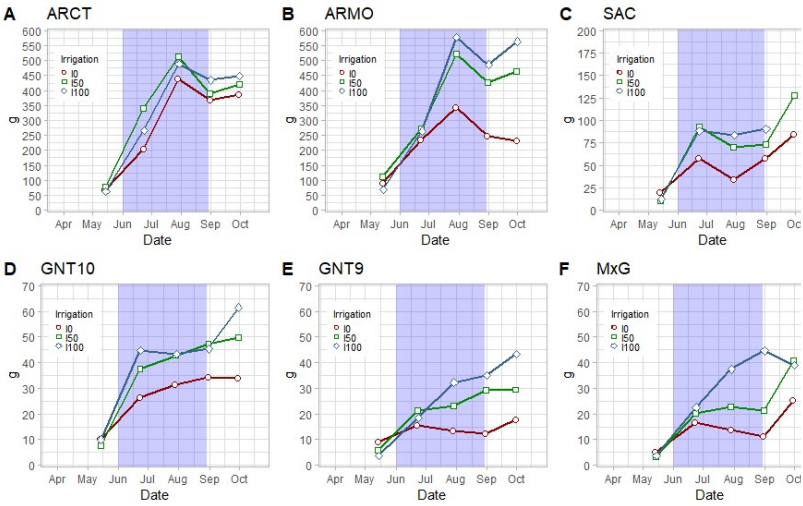

Figure 18 Mean stem dry weight (g stems^{-1}) trends over the vegetative stages (April to October 2020) for 3 water restoration levels (I0, I50, I100) and for 6 genotypes exanimated in this study: ARCT: *A. donax* ecotype Catania, ARMO: *A. donax* ecotype Morocco, SAC: *S. spontaneum*, GNT10: *Miscanthus* x *giganteus* hybrid 10, GNT9: *Miscanthus* x *giganteus* hybrid 9, MxG: *Miscanthus* x *giganteus.*

Total aboveground biomass showed a high variability among genotypes (F-value of 1466 in 2019 and 524 in 2020, Anova Tables of growing season measurements). Irrigation induced a lower variability among irrigation thesis in 2019 (F-value of 51) and was not statistically significant in 2020 (F-value of 0.55 and p-value of 58). In 2019, *A. donax* genotypes showed a decrease of the total aboveground biomass before the winter harvest (2019). This trend is due to the translocation of photosynthate to the rhizomes (Cosentino et al., 2014). In 2020, this trend has not been observed yet. The other genotypes showed an increase of the total aboveground biomass through the whole growing season. In 2019, date,

genotype, irrigation and all factors interactions, excluding the date x irrigation x genotype, have a statistically significant effect on stem height (**Errore. L'origine riferimento non è stata trovata.**). In 2020, the factors date and genotype and the interactions date genotype and irrigation x genotype have a a statistically significant effect on stem height (**Errore. L'origine riferimento non è stata trovata.**).

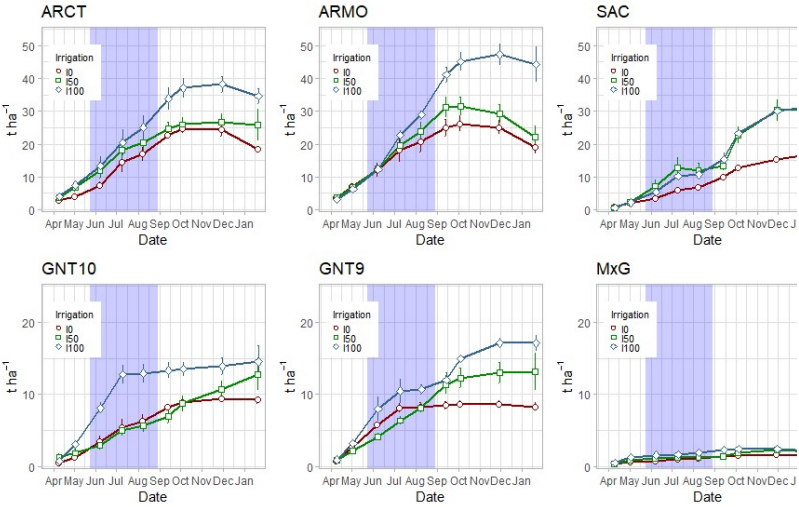

Figure 19 Total aboveground biomass (Mg ha^{-1}) trends over the vegetative stages (March to November 2019) for 3 water restoration levels (I0, I50, I100) and for 6 genotypes exanimated in this study: ARCT: *A. donax* ecotype Catania, ARMO: *A. donax* ecotype Morocco, SAC: *S. spontaneum*, GNT10: *Miscanthus* x *giganteus* hybrid 10, GNT9: *Miscanthus* x *giganteus* hybrid 9, MxG: *Miscanthus* x *giganteus.*

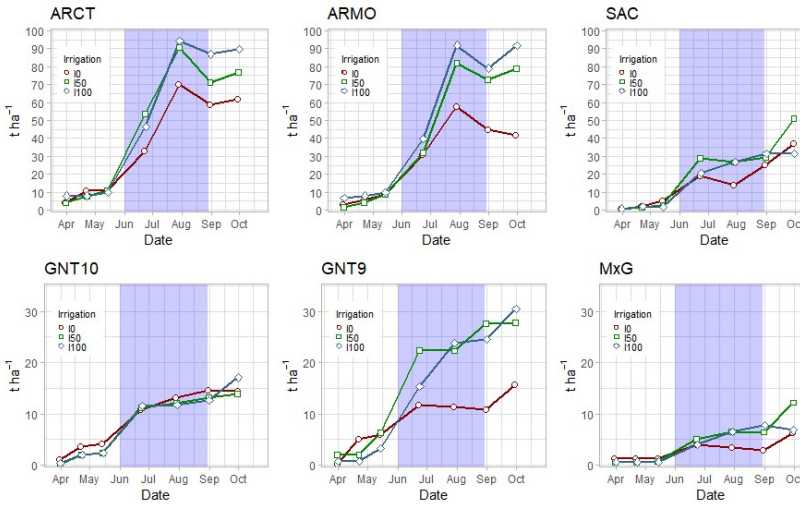

Figure 20 Total aboveground biomass (Mg ha^{-1}) trends over the vegetative stages (March to November 2019) for 3 water restoration levels (I0, I50, I100) and for 6 genotypes exanimated in this study: ARCT: *A. donax* ecotype Catania, ARMO: *A. donax* ecotype Morocco, SAC: *S. spontaneum*, GNT10: *Miscanthus* x *giganteus* hybrid 10, GNT9: *Miscanthus* x *giganteus* hybrid 9, MxG: *Miscanthus* x *giganteus.*

2.3.2.2 Physiologic measurements

C3 *A. donax* genotypes had higher values of stomatal conductance than C4 genotypes (*S. spontaneum* and *Miscanthus* hybrids) (**Figure** 21, **Figure** 22), in agreement with scientific literature (Knapp, 1993). Among C4 genotypes, GNT10 had the lowest stomatal conductance values. According to Anova, the genotype factor explains most of the variance (F-value of 120 in 2019 and 182 in 2020) (**Errore. L'origine riferimento non è stata trovata.**). Irrigation thesis, varying in soil water content, induced variations in stomatal conductance: while before the irrigation period the values were similar, during and after the

irrigation period the two irrigated thesis, I50 and I100, showed higher values than the rainfed thesis. The variability within the factors is ascribable to the variation in soil water content, atmospheric temperature and humidity, solar radiation and age of the leaves. Date, genotype, irrigation and all factors interactions, excluding the date x irrigation x genotype, have a statistically significant effect on stem height (**Errore. L'origine riferimento non è stata trovata.**).

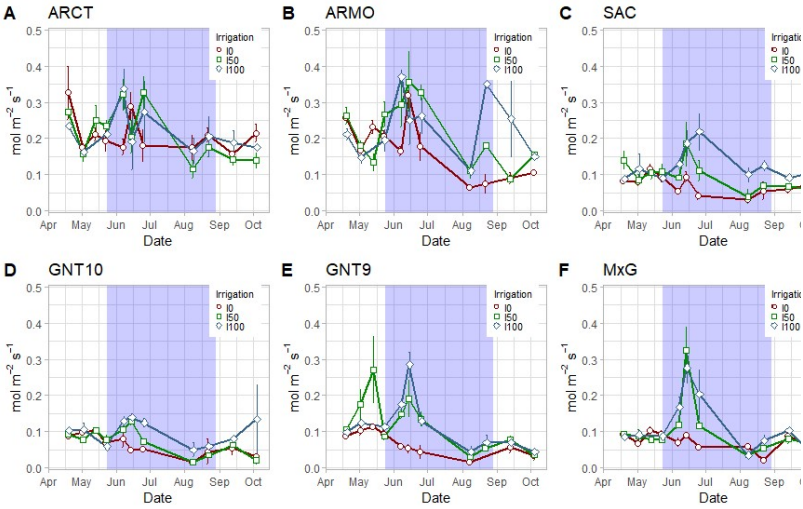

Figure 21 Stomatal conductance (mol m^{-2} s^{-1}) trends over the vegetative stages (March to November 2019) as measured by ADC LCi -SD gas exchange system for 3 water restoration levels (I0, I50, I100) and for 6 genotypes exanimated in this study: ARCT: *A. donax* ecotype Catania, ARMO: *A. donax* ecotype Morocco, SAC: *S. spontaneum*, GNT10: *Miscanthus* x *giganteus* hybrid 10, GNT9: *Miscanthus* x *giganteus* hybrid 9, MxG: *Miscanthus* x *giganteus.*

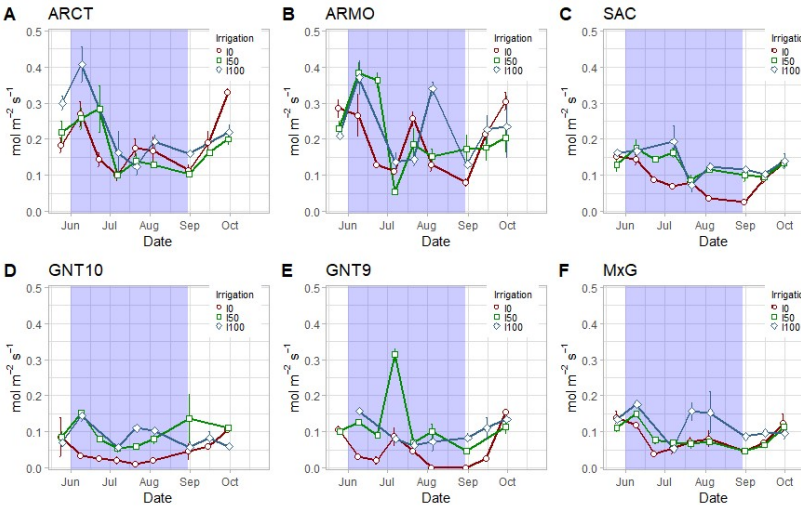

Figure 22 Stomatal conductance (mol m^{-2} s^{-1}) trends over the vegetative stages (March to November 2019) as measured by ADC LCi -SD gas exchange system for 3 water restoration levels (I0, I50, I100) and for 6 genotypes exanimated in this study: ARCT: *A. donax* ecotype Catania, ARMO: *A. donax* ecotype Morocco, SAC: *S. spontaneum*, GNT10: *Miscanthus* x *giganteus* hybrid 10, GNT9: *Miscanthus* x *giganteus* hybrid 9, MxG: *Miscanthus* x *giganteus.*

Net photosynthesis depends on stomatal conductance, thus the irrigated thesis, which have higher stomatal conductance, showed higher values of net photosynthesis (**Figure** 23, **Figure** 24). According to Anova, irrigation explains most of the variance both in 2019 and 2020 (F-value of 1005 and 784 respectively) (**Errore. L'origine riferimento non è stata trovata.**). The effect of genotype is statistically significant, and some trends can be observed among genotypes: *A. donax* genotypes, despite of the C3 metabolism, maintained higher net photosynthesis during summer months in comparison with *S. spontaneum* and particularly with *Miscanthus* hybrids, while *Miscanthus* hybrids showed a higher decrease in net

photosynthesis, particularly in the I0 theisis. The sustained high rate of net photosynthesis of *A. donax* in the I0 thesis during periods of low soil water availability can be explained by the deep root system as reported by Cosentino et al., (2014), who observed water uptake by the crop up to 160 cm depth. As for stomatal conductance, the variability within the factors is ascribable to the variation in soil water content, atmospheric temperature and humidity, solar radiation and age of the leaves. Date, genotype, irrigation and all factors interactions, excluding the date x irrigation x genotype, have a statistically significant effect on stem height (**Errore. L'origine riferimento non è stata trovata.**).

The high photosynthetic capacity of giant reed has been widely recognized, with rates higher than 30 _mol CO2 m□2 s□1 in optimal growing conditions [A C3 species with unusually high photosynthetic capacity.]

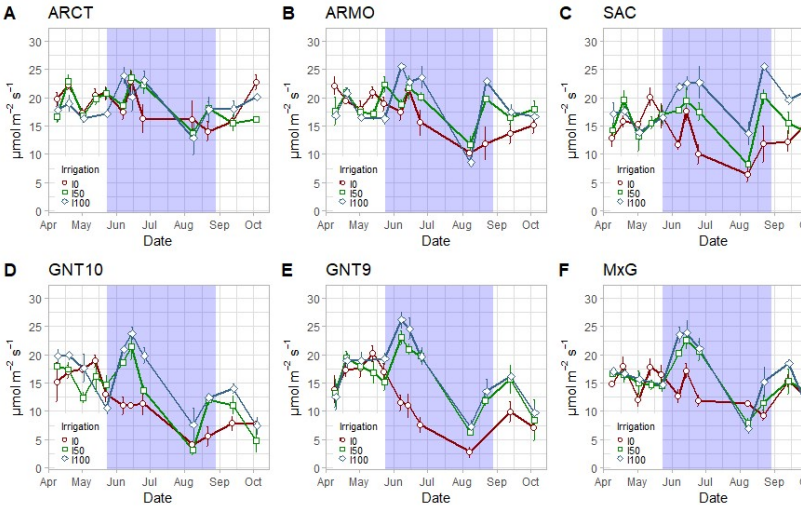

Figure 23 Net photosynthesis rate (µmol m^{-2} s^{-1}) trends over the vegetative stages (March to November 2019) as measured by ADC LCi -SD gas exchange system for 3 water restoration levels (I0, I50,

I100) and for 6 genotypes exanimated in this study: ARCT: *A. donax* ecotype Catania, ARMO: *A. donax* ecotype Morocco, SAC: *S. spontaneum*, GNT10: *Miscanthus* x *giganteus* hybrid 10, GNT9: *Miscanthus* x *giganteus* hybrid 9, MxG: *Miscanthus* x *giganteus.*

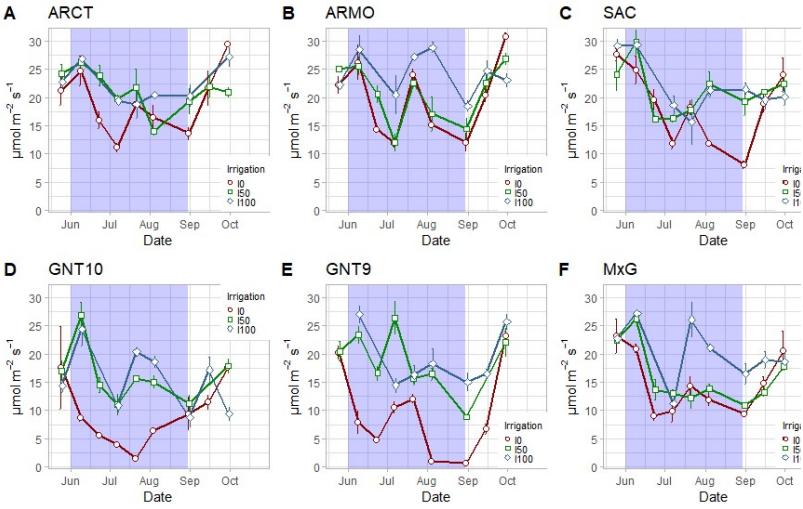

Figure 24 Net photosynthesis rate (µmol m^{-2} s^{-1}) trends over the vegetative stages (May to October 2020) as measured by ADC LCi -SD gas exchange system for 3 water restoration levels (I0, I50, I100) and for 6 genotypes exanimated in this study: ARCT: *A. donax* ecotype Catania, ARMO: *A. donax* ecotype Morocco, SAC: *S. spontaneum*, GNT10: *Miscanthus* x *giganteus* hybrid 10, GNT9: *Miscanthus* x *giganteus* hybrid 9, MxG: *Miscanthus* x *giganteus.*

Transpiration rate is an other physiological trait that is strongly dependent on stomatal conductance, therefore irrigated shows higher transpiration rates than rainfed thesis (**Figure** 25, **Figure** 26). Irrigation has the most significant effect on transpiration rate in 2019 (F-value of 117), while in 2020 the genotype factor has the most significant effect (F-value of 108). As for net photosynthesis, the effect of

genotype is statistically significant in both years, and different genotypes show different transpiration patterns in relation to date and irrigation: having a C3 metabolism, *A. donax* genotypes maintained higher transpiration rates than the other genotypes, especially in the rainfed thesis. In addition to the C3 metabolism, the deeper root system of *A. donax* (Cosentino et al., 2014) allows for crop water uptake even in periods of low water availability in the upper soil layers and thus explains both the higher net photosynthesis and transpiration rate in comparison with the genotypes that are characterized by shallower root systems. The variability of transpiration rate during the growing season is due to the variation of soil water content, atmospheric temperature and humidity, solar radiation and age of the leaves. Date, genotype, irrigation and all factor interactions have a statistically significant effect on transpiration rate (ref).

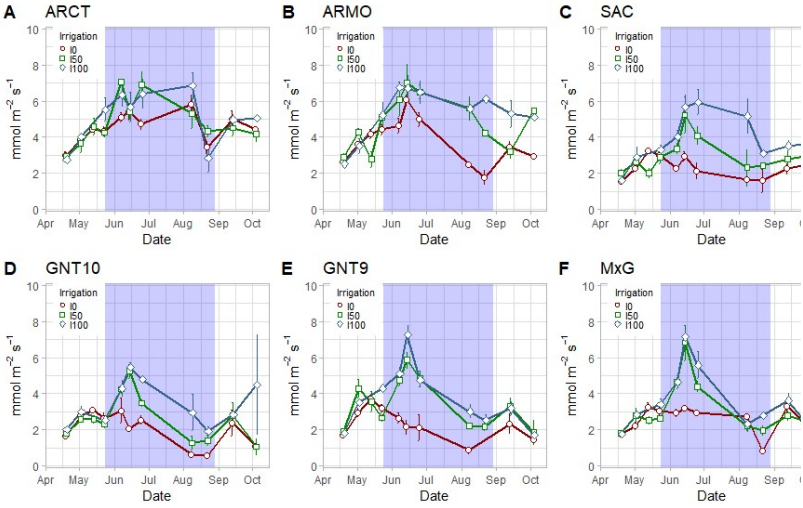

Figure 25 Transpiration rate (mmol m^{-2} s^{-1}) trends over the vegetative stages (March to November 2019) as measured by ADC LCi -SD gas exchange system for 3 water restoration levels (I0, I50, I100) and for 6 genotypes exanimated in this study: ARCT: *A.*

donax ecotype Catania, ARMO: *A. donax* ecotype Morocco, SAC: *S. spontaneum*, GNT10: *Miscanthus* x *giganteus* hybrid 10, GNT9: *Miscanthus* x *giganteus* hybrid 9, MxG: *Miscanthus* x *giganteus.*

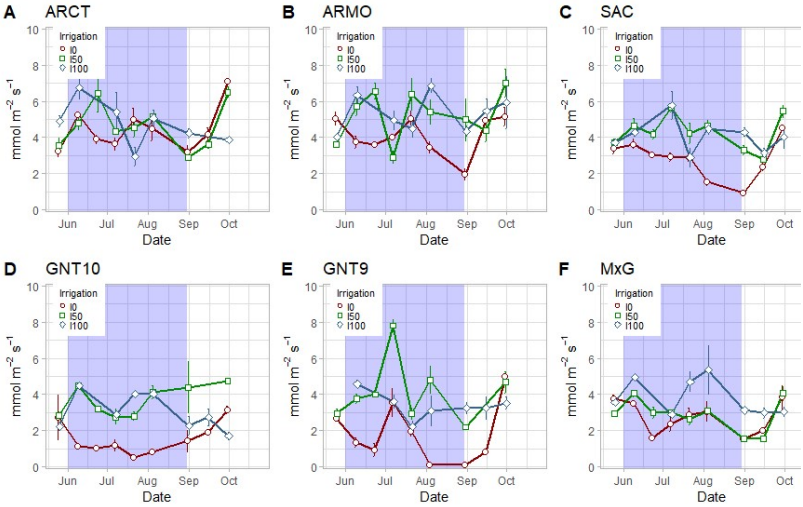

Figure 26 Transpiration rate (mmol m^{-2} s^{-1}) trends over the vegetative stages (March to November 2019) as measured by ADC LCi -SD gas exchange system for 3 water restoration levels (I0, I50, I100) and for 6 genotypes exanimated in this study: ARCT: *A. donax* ecotype Catania, ARMO: *A. donax* ecotype Morocco, SAC: *S. spontaneum*, GNT10: *Miscanthus* x *giganteus* hybrid 10, GNT9: *Miscanthus* x *giganteus* hybrid 9, MxG: *Miscanthus* x *giganteus.*

Instant water use efficiency (IWUE), calculated as the ratio between net photosynthesis rate and transpiration rate, is directly dependant by the previous physiological traits. IWUE can be used to define which genotype has the most efficient photosysnthesis system in relation to the water consumption by transpiration: *A. donax* genotypes, having a C3 metabolism, are characterized by a lower net photosynthesis rate in comparison with C4 plants in analogue condition of water uptake and thus

show lower IWUE. *S. spontaneum*, having a C4 metabolism and morphological adaptation that limit transpiration (cit) showed the highest IWUE among the genotypes in this study. Among the experimental factors, date has the most significant effect on IWUE (F-value of 219 in 2019 and 49 in 2020). Date, genotype, irrigation and all factor interactions excluding the irrigation x genotype interaction have a statistically significant effect on IWUE (ref). Durign summer months, characterized by high temperature and vapour pressur deficit, which limit the efficiency of photosystems and increase the atmospheric water uptake, the IWUE was generally lower for all the genotypes. The highest values of IWUE were recorded in May, which is characterized by high levels of solar radiation and lower temperature and vapour pressur deficit than summer months.

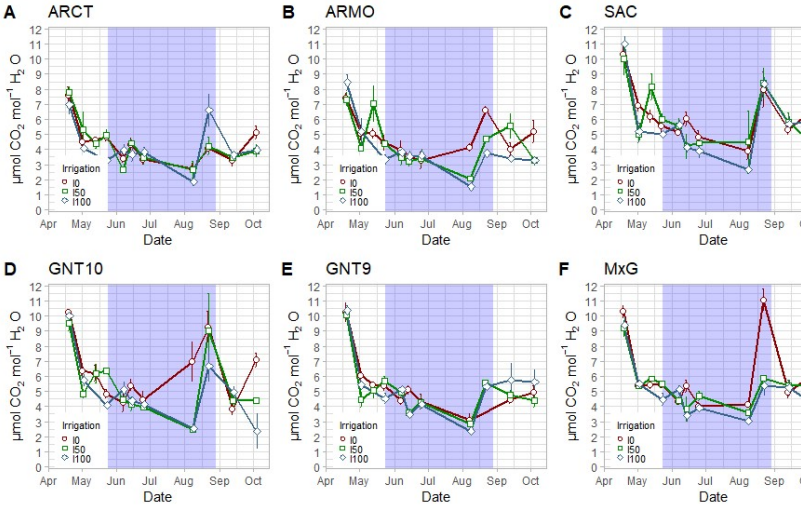

Figure 27 Instant water use efficiency (IWUE) (µmol CO_2 $mmol^{-1}$ H_2O) trends over the vegetative stages (March to November 2019) as calculated from photosynthesis and transpiration rate for 3 water restoration levels (I0, I50, I100) and for 6 genotypes exanimated in

this study: ARCT: *A. donax* ecotype Catania, ARMO: *A. donax* ecotype Morocco, SAC: *S. spontaneum*, GNT10: *Miscanthus* x *giganteus* hybrid 10, GNT9: *Miscanthus* x *giganteus* hybrid 9, MxG: *Miscanthus* x *giganteus.*

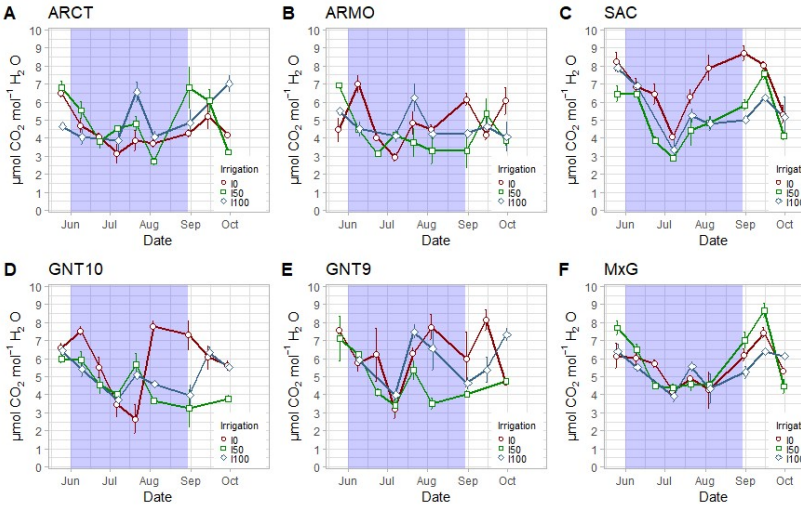

Figure 28 Instant water use efficiency (IWUE) (µmol CO_2 $mmol^{-1}$ H_2O) trends over the vegetative stages (March to November 2019) as calculated from photosynthesis and transpiration rate for 3 water restoration levels (I0, I50, I100) and for 6 genotypes exanimated in this study: ARCT: *A. donax* ecotype Catania, ARMO: *A. donax* ecotype Morocco, SAC: *S. spontaneum*, GNT10: *Miscanthus* x *giganteus* hybrid 10, GNT9: *Miscanthus* x *giganteus* hybrid 9, MxG: *Miscanthus* x *giganteus.*

2.3.3 *Harvest measurements*

2.3.3.1 Morphology and yield

At the first year harvest, stem density was the highest for GNT9 (45.1 stems m^{-2}) and the lowest for ARMO (5.3 stems m^{-2}), MxG (5.2 stems m^{-2}) and ARCT (5.1 stems m^{-2}) with no statistical difference among them. SAC and GNT10 had 24.4 and 11.9 stems m^{-2}, respectively (**Figure** 29).

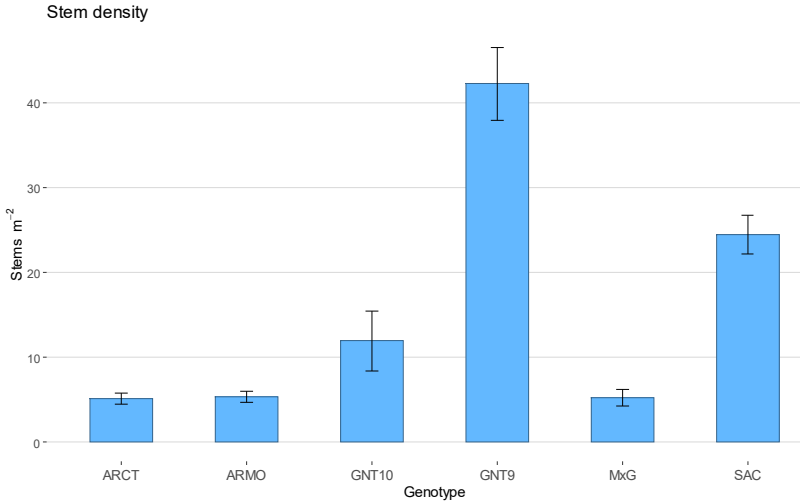

Figure 29 Stem density at 2019 harvest (stems m^{-2}) for 6 genotypes exanimated in this study: ARCT: *A. donax* ecotype Catania, ARMO: *A. donax* ecotype Morocco, SAC: *S. spontaneum*, GNT10: *Miscanthus* x *giganteus* hybrid 10, GNT9: *Miscanthus* x *giganteus* hybrid 9, MxG: *Miscanthus* x *giganteus.*

At the second year harvest (January 2020), GNT9 had again the highest stem density for all the irrigation thesis, with the higher levels of irrigation having higher stem density than the lower level of irrigation. *S. spontaneum* had the second highest stem density, followed by GNT10 and MxG. Both *A. donax* had the lowest stem density with negligible differences

among the irrigation thesis, with the exclusion of ARMO in the I100 thesis, which had a higher stem density. The genotype factor explains most of the variance of stem density (F-value of 172), while irrigation has a weaker significance (ref). All the genotype had a higher stem density in 2020 than in 2019.

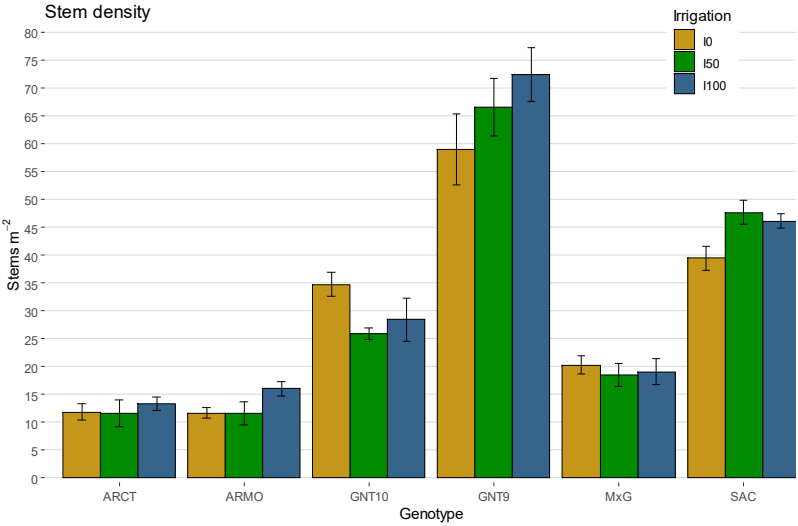

Figure 30 Stem density at 2020 harvest (stems m^{-2}) for 3 water restoration levels (I0, I50, I100) and for 6 genotypes exanimated in this study: ARCT: *A. donax* ecotype Catania, ARMO: *A. donax* ecotype Morocco, SAC: *S. spontaneum*, GNT10: *Miscanthus* x *giganteus* hybrid 10, GNT9: *Miscanthus* x *giganteus* hybrid 9, MxG: *Miscanthus* x *giganteus*.

At the first year harvest, stem dry weight resulted the highest for *A. donax* ecotypes (135.4 and 144.9 g for ARCT and ARMO ecotypes respectively), followed by SAC (73.6 g). The lowest for *Miscanthus* hybrids (19.7 g for GNT10, 16.1 g for GNT9, 13.6 g for MxG (the differences were not statistically different among hybrids) (**Errore. L'origine riferimento non è stata trovata.**).

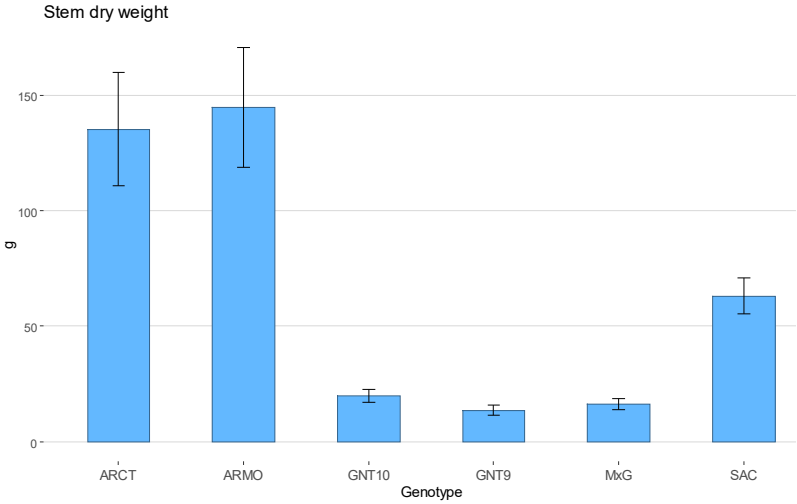

Figure 31 Stem dry weight at 2019 harvest (g) for 6 genotypes exanimated in this study: ARCT: *A. donax* ecotype Catania, ARMO: *A. donax* ecotype Morocco, SAC: *S. spontaneum*, GNT10: *Miscanthus* x *giganteus* hybrid 10, GNT9: *Miscanthus* x *giganteus* hybrid 9, MxG: *Miscanthus* x *giganteus.*

Figure 32 Stem dry weight at 2020 harvest (g) for 3 water restoration levels (I0, I50, I100) and for 6 genotypes exanimated in this study: ARCT: *A. donax* ecotype Catania, ARMO: *A. donax* ecotype Morocco, SAC: *S. spontaneum*, GNT10: *Miscanthus* x

giganteus hybrid 10, GNT9: *Miscanthus* x *giganteus* hybrid 9, MxG: *Miscanthus* x *giganteus*.

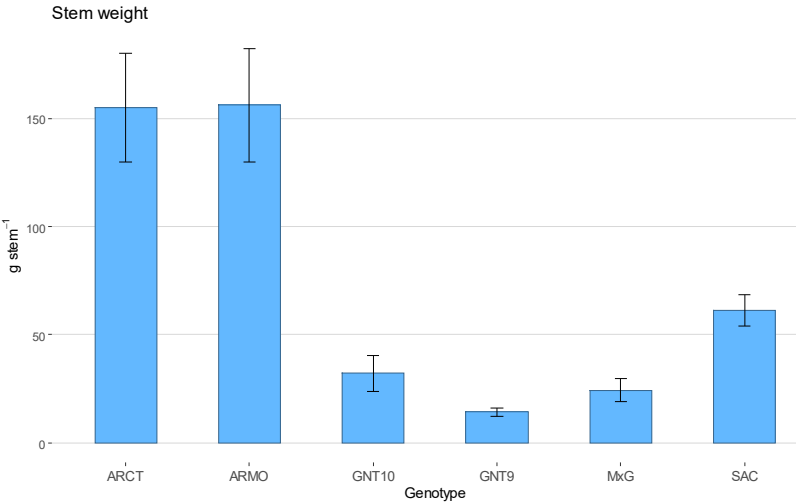

Figure 33 Mean stem dry weight at 2019 harvest (g) as calculated from aboveground biomass yield and stem density for 6 genotypes exanimated in this study: ARCT: *A. donax* ecotype Catania, ARMO: *A. donax* ecotype Morocco, SAC: *S. spontaneum*, GNT10: *Miscanthus* x *giganteus* hybrid 10, GNT9: *Miscanthus* x *giganteus* hybrid 9, MxG: *Miscanthus* x *giganteus.*

At the second year harvest, *A. donax* genotypes had again the highest stem weight for all the irrigation thesis, with no statistically significant differences between ARCT and ARMO and with the higher levels of irrigation having higher stem weight than the lower level of irrigation. *S. spontaneum* had the second highest stem weight, followed by GNT10, followed by GNT9 and MxG. The genotype factor explains most of the variance of stem density (F-value of 133), while irrigation and the interaction genotype x irrigation have a weaker significance (ref). All the genotype had a higher stem weight in 2020 than in 2019, except for *S. spontaneum*, which mantained similar values.

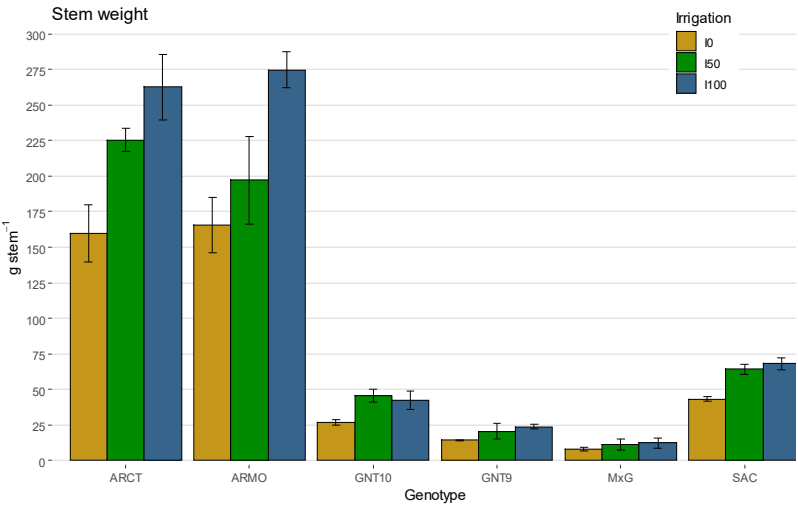

Figure 34 Mean stem dry weight at 2020 harvest (g) as calculated from aboveground biomass yield and stem density for 3 water restoration levels (I0, I50, I100) and for 6 genotypes exanimated in this study: ARCT: *A. donax* ecotype Catania, ARMO: *A. donax* ecotype Morocco, SAC: *S. spontaneum*, GNT10: *Miscanthus* x *giganteus* hybrid 10, GNT9: *Miscanthus* x *giganteus* hybrid 9, MxG: *Miscanthus* x *giganteus*.

At the first year harvest, *S. spontaneum* performed the highest dry biomass yield among the tested genotypes (15.1 Mg ha^{-1}), followed by ARMO and ARCT (8.0 and 7.9 Mg ha^{-1} with no significant difference among them). Among *Miscanthus* genotypes, GNT9 produced 6.0 Mg ha^{-1} of dry biomass followed by GNT10 and finally by MxG 3.8 and 1.3 Mg ha^{-1}, respectively (**Figure** 4).

About biomass fractions, in *A. donax* and *S. spontaneum* stems were the predominant component of the yield, while leaves were the predominant component of the yield in *Miscanthus*

genotypes. The contribution of the inflorescences was negligible for all genotypes.

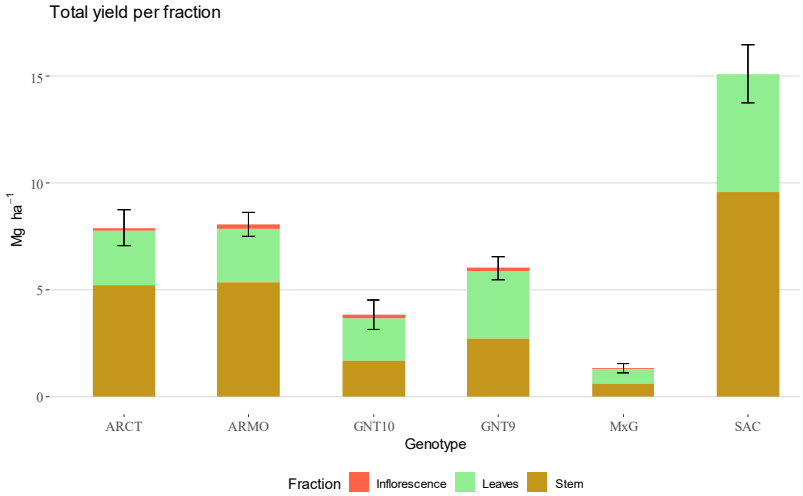

Figure 35 Total aboveground biomass, divided per fraction, at 2019 harvest (Mg ha^{-1}) for 6 genotypes exanimated in this study: ARCT: *A. donax* ecotype Catania, ARMO: *A. donax* ecotype Morocco, SAC: *S. spontaneum*, GNT10: *Miscanthus* x *giganteus* hybrid 10, GNT9: *Miscanthus* x *giganteus* hybrid 9, MxG: *Miscanthus* x *giganteus*.

At the second harvest, the highest aboveground biomass yield has been oberved in *A. donax* ecotype ARMO in the I100 thesis, with 44.3 Mg ha^{-1}. This yield is statistically significantly higher than the yield of ARCT and S. spontaeum in the I100 thesis, which had a yield of 34.6 and 31.4 Mg ha^{-1} respectively. The difference among the latter is not statistically significant (ref). Lower yields have been observed for GNT9 and GNT10 in the I100 (17.1 and 14.5 Mg ha^{-1} respectively, with a non statistically significant difference). The lowest yield within the I100 thesis has been observed for MxG, which produced 2.2 Mg ha^{-1} of aboveground biomass.

S. spontaneum produced the highest biomass yiled among the I50 thesis, followed by ARCT and ARMO (30.5, 25.8 and 22.1 Mg ha^{-1} in order). As for I100 thesis, GNT9 and GNT10 had lower yield and MxG had the lowest yield among the genotypes (13.2, 11.8 and 2.1 Mg ha^{-1} in order).
Considering the I0 thesis, ARMO produced the highest yield, followed by ARCT and *S. spontaneum* (16.1, 18.4 and 17 Mg ha^{-1} in order. The difference among these genotypes is not statistically significant (ref). Lower yields have been achieved by GNT10 and GNT9 (9.3 and 8.3 Mg ha^{-1} respectively, with a non signficant different). The *Miscanthus* hybridus MxG preduced the lowest biomass yield in the I0 thesis, 1.6 Mg ha^{-1}.
Stem fraction was the dominant fraction of aboveground biomass for all the genotypes, and leaf fraction constituted only a minor fraction, except fot GNT10 and GNT9, in which the leaf fraction constituted ...% and ...% of the aboeground biomass respectively. The contribution of the inflorescences was negligible for all genotypes.
It is worth to note that biomass at harvest was quite dry for *Miscanthus* genotypes (15-20%), while the moisture content approached 45-50% in *A. donax* and *Saccharum*. The higher moisture content detected in *Arundo* and *Saccharum* were already observed in a previous study in the same area and were explained by the fact that they are naturalized and well adapted to Southern Mediterranean environments, can maintain gas exchange activities with the atmosphere even in early winter when the climatic conditions are favorable. Vice versa, *Miscanthus*, native from a tropical area and adapted to live in dry cold temperate environments, showed senesced stems and leaves in winter time, and as consequence reduced significantly the biomass moisture content (Scordia et al., 2014). In accordance with that study, morphology, such as stem density was higher in *Miscanthus* followed by *Saccharum* and by

Arundo, while the weight of a single stem showed the opposite trend.

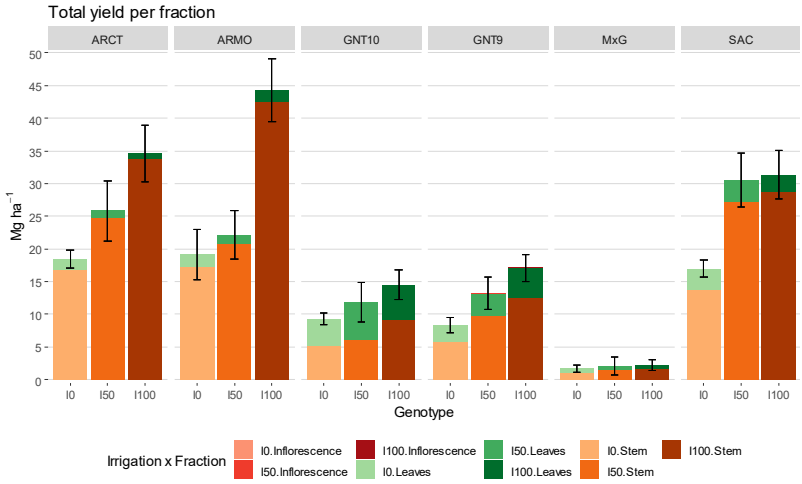

Figure 36 Total aboveground biomass, divided per fraction, at 2020 harvest (Mg ha^{-1}) for 3 water restoration levels (I0, I50, I100) and for 6 genotypes exanimated in this study: ARCT: *A. donax* ecotype Catania, ARMO: *A. donax* ecotype Morocco, SAC: *S. spontaneum*, GNT10: *Miscanthus* x *giganteus* hybrid 10, GNT9: *Miscanthus* x *giganteus* hybrid 9, MxG: *Miscanthus* x *giganteus.*

2.3.3.2 Biomass composition

At the first year harvest, biomass composition showed significant differences among the study genotypes (**Figure** 5). The neutral detergent soluble (NDS) were the significantly highest in ARCT and ARMO, followed by SAC, with *Miscanthus* showing the lowest value, particularly the GNT9.
On the contrary, hemicellulose content was the highest in *Miscanthus* and not statistically different among the three hybrids, followed by SAC and ARMO, with ARCT showing the lowest value overall. The cellulose content was the highest in GNT9 and GNT10, followed by MxG, by SAC and by ARMO and ARCT. Acid detergent lignin was the highest in ARMO and ARCT, followed by SAC, and by the three *Miscanthus*, which were not statistically different. Surprisingly, the ash content was the highest in the three *Miscanthus* than both *Arundo* and *Saccharum* which were not statistically different.
Miscanthus is notoriously poorer in ash content than all the other perennial grasses (Scordia et al., 2016; Scordia and Cosentino, 2019), therefore the higher ash content achieved in the present study can be explained by the higher leaf to stem ratio at the first harvest after the establishment. Indeed, leaves are much richer in ash content than stems (Monti et al., 2008) and it has likely contributed to the high ash amount. Interestingly, the high hemicellulose and cellulose and low lignin content shown by the two seed-based hybrid suggest a biomass with lower recalcitrance, that is a barrier for advanced bioconversions

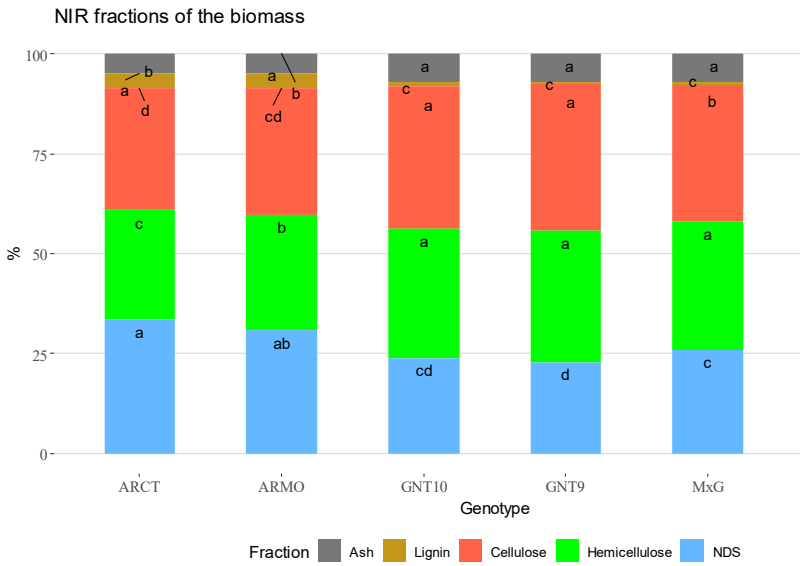

Figure 37 Fractions of the biomass assessed by Near InfraRed spectrometry at 2019 harvest (%) for 6 genotypes exanimated in this study: ARCT: *A. donax* ecotype Catania, ARMO: *A. donax* ecotype Morocco, SAC: *S. spontaneum*, GNT10: *Miscanthus* x *giganteus* hybrid 10, GNT9: *Miscanthus* x *giganteus* hybrid 9, MxG: *Miscanthus* x *giganteus*. Different letters indicate groups that are significantly different (p-value <0.05)

2.4 Conclusions

S. spontaneum performed the highest dry biomass yield during the first year of the trial due to the combination of stem density and stem dry weight. Low stem density affected the yield of *A. donax* ecotypes, despite of the highest stem weight. On the contrary, the yield of *Miscanthus* genotypes was constrained by the lowest stem weight overall. Both GNT9 and GNT10 performed better than MxG during the trial. These results are obtained from one harvest during the first year of crop establishment. In order to prove the productivity of perennial grasses, further harvests during the years following crop establishment are necessary. The present experiment plans to differentiate water availability to ascertain the yield performances and biomass quality of the study genotypes under different soil water availability, namely not limiting water, reduced irrigation and rainfed conditions.

2.5 Annex

2.5.1 *Anova* Tables *of growing season measurements*

2019

Stem density

Error: Block	Degrees of freedom	Sum of squares	Mean of squares
Date	2	87.08	43.54

Error: Within	Degrees of freedom	Sum of squares	Mean of squares	Fvalue	pvalue	
Date	18	43923	2440	103.052	$2.00E^{-1}6$	***
Irrigation	2	3431	1716	72.454	$2.00E^{-1}6$	***
Genotype	5	163823	32765	1383.709	$2.00E^{-1}6$	***
Date:Irrigation	28	674	24	1.016	0.445	
Date:Genotype	71	34396	484	20.459	$2.00E^{-1}6$	***
Irrigation:Genotype	10	1476	148	6.232	6.62E-09	***

Date:Irrigation:Genotype	98	1877	19	0.809	0.898	
Residuals	415	9827	24			

Photosynthesis

Error:	Block		
	Degrees of freedom	Sum of squares	Mean of squares
Date	2	483.6	241.8

Error:	Within					
	Degrees of freedom	Sum of squares	Mean of squares	Fvalue	pvalue	
Date	11	5423	493	44.06	$2.00E^{-1}6$	***
Irrigation	2	2010	1004.8	89.791	$2.00E^{-1}6$	***
Genotype	5	2228	445.5	39.814	$2.00E^{-1}6$	***
Date:Irrigation	21	3282	156.3	13.966	$2E^{-1}6$	***
Date:Genotype	55	2070	37.6	3.363	$7.56E^{-1}4$	***
Irrigation:Genotype	10	688	68.8	6.147	4.67E-09	***
Date:Irrigation:Genotype	104	1615	15.5	1.388	0.00951	**

Residuals	760	8505	11.2

Transpiration

Error:	Block		
	Degrees of freedom	Sum of squares	Mean of squares
Date	2	66.96	33.48

Error:	Within					
	Degrees of freedom	Sum of squares	Mean of squares	Fvalue	pvalue	
Date	10	797.5	79.75	87.098	$2.00E^{-1}6$	***
Irrigation	2	213.7	106.87	116.72	$2.00E^{-1}6$	***
Genotype	5	523.9	104.78	114.439	$2.00E^{-1}6$	***
Date:Irrigation	19	192.6	10.14	11.071	$2E^{-1}6$	***
Date:Genotype	50	152.2	3.04	3.325	$1.34E^{-1}2$	***
Irrigation:Genotype	10	24.4	2.44	2.669	3.29E-03	**
Date:Irrigation:Genotype	94	146.5	1.56	1.703	0.000104	***
Residuals	723	662	0.92			

Stomatal conductance

Error: Block	Degrees of freedom	Sum of squares	Mean of squares
Date	2	0.091	0.0455

Error: Within	Degrees of freedom	Sum of squares	Mean of squares	Fvalue	pvalue	
Date	10	0.99	0.099	20.757	$2.00E^{-1}6$	***
Irrigation	2	0.329	0.1646	34.499	$4.90E^{-1}5$	***
Genotype	5	2.858	0.5715	119.788	$2.00E^{-1}6$	***
Date:Irrigation	19	0.412	0.0217	4.549	$6.63E^{-1}0$	***
Date:Genotype	50	0.627	0.0125	2.627	2.62E-08	***
Irrigation:Genotype	10	0.083	0.0083	1.75	6.62E-02	.
Date:Irrigation:Genotype	94	0.728	0.0077	1.624	0.000385	***
Residuals	723	3.45	0.0048			

Stem height

Error: Block	Degrees of freedom	Sum of squares	Mean of squares
Date	2	9526	4763

Error: Within	Degrees of freedom	Sum of squares	Mean of squares	Fvalue	pvalue	
Date	13	2425800	186600	642.954	$<2e^{-1}6$	***
Irrigation	2	79211	39606	136.467	$<2e^{-1}6$	***
Genotype	5	2090862	418172	1440.866	$<2e^{-1}6$	***
Date:Irrigation	25	114549	4582	15.788	$<2e^{-1}6$	***
Date:Genotype	63	431836	6855	23.618	$<2e^{-1}6$	***
Irrigation:Genotype	10	32230	3223	11.105	$<2e^{-1}6$	***
Date:Irrigation:Genotype	120	39796	332	1.143	0.17	
Residuals	438	127118	290			

IWUE

Error: Block	Degrees of freedom	Sum of squares	Mean of squares
Date	2	9.288	4.644

Error: Within	Degrees of freedom	Sum of squares	Mean of squares	Fvalue	pvalue	
Date	10	2400.8	240.08	219.352	2.00E^{-1}6	***
Irrigation	2	21.9	10.97	10.022	5.09E-05	***
Genotype	5	323.8	64.77	59.177	2.00E^{-1}6	***
Date:Irrigation	19	141.1	7.43	6.786	2E^{-1}6	***
Date:Genotype	50	149.2	2.98	2.725	6.82E-09	***
Irrigation:Genotype	10	10.3	1.03	0.938	4.98E-01	
Date:Irrigation:Genotype	94	183.7	1.95	1.785	2.47E-05	***
Residuals	723	791.3	1.09			

Stem thickness

Error:	Block		
	Degrees of freedom	Sum of squares	Mean of squares
Date	2	3.074	1.537

Error:	Within					
	Degrees of freedom	Sum of squares	Mean of squares	Fvalue	pvalue	
Date	4	23	5.7	3.26	1.37E-02	*
Irrigation	2	49	24.4	14.017	2.80E-06	***
Genotype	5	5341	1068.3	612.876	$2.00E^{-1}6$	***
Date:Irrigation	6	7	1.2	0.694	0.65503	
Date:Genotype	15	40	2.7	1.547	9.67E-02	.
Irrigation:Genotype	10	49	4.9	2.786	3.57E-03	**
Date:Irrigation:Genotype	30	15	0.5	0.285	0.99992	
Residuals	141	246	1.7			

LAI

Error: Block	Degrees of freedom	Sum of squares	Mean of squares
Date	2	5.621	2.811

Error: Within	Degrees of freedom	Sum of squares	Mean of squares	Fvalue	pvalue	
Date	13	1477.3	113.64	280.867	$2.00E^{-1}6$	***
Irrigation	2	41.8	20.88	51.613	$2.00E^{-1}6$	***
Genotype	5	355.7	71.14	175.842	$2.00E^{-1}6$	***
Date:Irrigation	26	79.6	3.06	7.568	$2E^{-1}6$	***
Date:Genotype	61	145.2	2.38	5.883	$2.00E^{-1}6$	***
Irrigation:Genotype	10	42.1	4.21	10.417	$9.00E^{-1}6$	***
Date:Irrigation:Genotype	107	68	0.64	1.571	0.000953	***
Residuals	419	169.5	0.4			

H30

	Degrees of freedom	Sum of squares	Mean of squares	Fvalue	pvalue	
Date	19	0.947	0.0498	2.41E+29	$<2e^{-1}6$	***
Irrigation	2	0.9255	0.4628	2.24E+30	$<2e^{-1}6$	***
Genotype	5	0.1983	0.0397	1.92E+29	$<2e^{-1}6$	***
Date:Irrigation	37	0.4983	0.0135	6.51E+28	$<2e^{-1}6$	***
Date:Genotype	90	0.1861	0.0021	1.00E+28	$<2e^{-1}6$	***
Irrigation:Genotype	10	0.2277	0.0228	1.10E+29	$<2e^{-1}6$	***
Date:Irrigation:Genotype	180	0.5325	0.003	1.43E+28	$<2e^{-1}6$	***
Residuals	326	0	0			

H60

	Degrees of freedom	Sum of squares	Mean of squares	Fvalue	pvalue	
Date	19	0.4213	0.0222	1.01E+29	$<2e^{-1}6$	***
Irrigation	2	0.8175	0.4088	1.87E+30	$<2e^{-1}6$	***
Genotype	5	0.0494	0.0099	4.51E+28	$<2e^{-1}6$	***
Date:Irrigation	37	0.5221	0.0141	6.45E+28	$<2e^{-1}6$	***
Date:Genotype	90	0.1051	0.0012	5.34E+27	$<2e^{-1}6$	***
Irrigation:Genotype	10	0.0539	0.0054	2.46E+28	$<2e^{-1}6$	***
Date:Irrigation:Genotype	180	0.1729	0.001	4.39E+27	$<2e^{-1}6$	***
Residuals	326	0	0			

ASWC

	Degrees of freedom	Sum of squares	Mean of squares	Fvalue	pvalue	
Date	19	8.373	0.441	2.12E+29	$<2e^{-1}6$	***
Irrigation	2	11.69	5.845	2.81E+30	$<2e^{-1}6$	***
Genotype	5	1.354	0.271	1.30E+29	$<2e^{-1}6$	***
Date:Irrigation	37	6.651	0.18	8.63E+28	$<2e^{-1}6$	***
Date:Genotype	90	1.348	0.015	7.20E+27	$<2e^{-1}6$	***
Irrigation:Genotype	10	1.23	0.123	5.91E+28	$<2e^{-1}6$	***
Date:Irrigation:Genotype	180	3.001	0.017	8.01E+27	$<2e^{-1}6$	***
Residuals	326	0	0			

2020

Stem density

Error:	Block		
	Degrees of freedom	Sum of squares	Mean of squares
Residuals	2	96.41	48.2

Error:	Within					
	Degrees of freedom	Sum of squares	Mean of squares	Fvalue	pvalue	
Date	6	27152	4525	88.688	2.00E^{-1}6	***
Irrigation	2	135	67	1.319	2.69E-01	
Genotype	5	171719	34344	673.076	2.00E^{-1}6	***
Date:Irrigation	12	759	63	1.24	0.256	
Date:Genotype	30	30749	1025	20.088	2.00E^{-1}6	***
Irrigation:Genotype	10	3251	325	6.37	1.01E-08	***
Date:Irrigation:Genotype	60	3696	62	1.207	0.162	
Residuals	250	12756	51			

Net hotosynthesis rate

Error: Block	Degrees of freedom	Sum of squares	Mean of squares
Date	2	1518	758.7

Error: Within	Degrees of freedom	Sum of squares	Mean of squares	Fvalue	pvalue	
Date	8	5501	687.6	89.958	$2.00E^{-1}6$	***
Irrigation	2	1569	784.3	102.6	$2.00E^{-1}6$	***
Genotype	5	3816	763.3	99.85	$2.00E^{-1}6$	***
Date:Irrigation	15	1273	84.9	11.106	$2E^{-1}6$	***
Date:Genotype	40	1546	38.7	5.057	$2.00E^{-1}6$	***
Irrigation:Genotype	10	814	81.4	10.646	$2.78E^{-1}5$	***
Date:Irrigation:Genotype	73	2127	29.1	3.811	$5.15E^{-1}6$	***
Residuals	279	2133	7.6			

Transpiration rate

Error: Block	Degrees of freedom	Sum of squares	Mean of squares
Date	2	12.82	6.408

Error: Within	Degrees of freedom	Sum of squares	Mean of squares	Fvalue	pvalue	
Date	8	199.12	24.89	46.993	$2.00E^{-1}6$	***
Irrigation	2	100.21	50.1	94.601	$2.00E^{-1}6$	***
Genotype	5	286.42	57.28	108.158	$2.00E^{-1}6$	***
Date:Irrigation	15	103.59	6.91	13.038	$2E^{-1}6$	***
Date:Genotype	40	111.9	2.8	5.282	$2.00E^{-1}6$	***
Irrigation:Genotype	10	52.01	5.2	9.821	$4.53E^{-1}4$	***
Date:Irrigation:Genotype	73	132.61	1.82	3.43	$9.96E^{-1}4$	***
Residuals	279	147.77	0.53			

Stomatal conductance

Error: Block	Degrees of freedom	Sum of squares	Mean of squares
Date	2	0.2448	0.1224

Error: Within	Degrees of freedom	Sum of squares	Mean of squares	Fvalue	pvalue	
Date	8	0.3593	0.04492	35.027	2.00E^{-1}6	***
Irrigation	2	0.0826	0.04132	32.222	2.57E^{-1}3	***
Genotype	5	1.1686	0.23372	182.262	2.00E^{-1}6	***
Date:Irrigation	15	0.1719	0.01146	8.938	2E^{-1}6	***
Date:Genotype	40	0.4044	0.01011	7.885	2.00E^{-1}6	***
Irrigation:Genotype	10	0.0536	0.00536	4.181	2.07E-05	***
Date:Irrigation:Genotype	73	0.351	0.00481	3.75	1.2E^{-1}5	***
Residuals	279	0.3578	0.00128			

Stem eight

Error:	Block		
	Degrees of freedom	Sum of squares	Mean of squares
Residuals	2	1690	845

Error:	Within					
	Degrees of freedom	Sum of squares	Mean of squares	Fvalue	pvalue	
Date	4	1386299	346575	190.847	2.00E^{-1}6	***
Irrigation	2	172153	86077	47.399	2.00E^{-1}6	***
Genotype	5	2675563	535113	294.669	2.00E^{-1}6	***
Date:Irrigation	8	119856	14982	8.25	1.76E-09	***
Date:Genotype	20	184329	9216	5.075	7.55E^{-1}0	***
Irrigation:Genotype	10	64324	6432	3.542	2.71E-04	***
Date:Irrigation:Genotype	40	96425	2411	1.327	0.109833	
Residuals	178	323245	1816			

IWUE

Error: Block	Degrees of freedom	Sum of squares	Mean of squares
Date	2	22.2	11.1

Error: Within	Degrees of freedom	Sum of squares	Mean of squares	Fvalue	pvalue	
Date	8	283.09	35.39	49.386	$2.00E^{-1}6$	***
Irrigation	2	32.93	16.46	22.978	$5.79E^{-1}0$	***
Genotype	5	107.08	21.42	29.888	$2.00E^{-1}6$	***
Date:Irrigation	15	114.12	7.61	10.618	$2E^{-1}6$	***
Date:Genotype	40	108.81	2.72	3.797	$2.60E^{-1}1$	***
Irrigation:Genotype	10	58.8	5.88	8.206	$1.20E^{-1}1$	***
Date:Irrigation:Genotype	73	159.57	2.19	3.051	$1.97E^{-1}1$	***
Residuals	279	199.91	0.72			

LAI

Error: Block	Degrees of freedom	Sum of squares	Mean of squares
Date	2	7.337	3.668

Error: Within	Degrees of freedom	Sum of squares	Mean of squares	Fvalue	pvalue	
Date	8	1543.5	192.94	319.032	$2.00E^{-1}6$	***
Irrigation	2	114.5	57.24	94.644	$2.00E^{-1}6$	***
Genotype	5	405.4	81.08	134.069	$2.00E^{-1}6$	***
Date:Irrigation	16	90	5.62	9.297	$2E^{-1}6$	***
Date:Genotype	39	85.7	2.2	3.635	$5.86E^{-1}0$	***
Irrigation:Genotype	10	21.8	2.18	3.611	1.79E-04	***
Date:Irrigation:Genotype	75	31	0.41	0.683	0.97264	
Residuals	226	136.7	0.6			

Solar radiation interception

Error: Block	Degrees of freedom	Sum of squares	Mean of squares
Date	2	0.04938	0.02469

Error: Within	Degrees of freedom	Sum of squares	Mean of squares	Fvalue	pvalue	
Date	8	31.83	3.979	900.199	$2.00E^{-1}6$	***
Irrigation	2	0.09	0.046	10.388	4.83E-05	***
Genotype	5	2.13	0.426	96.465	$2.00E^{-1}6$	***
Date:Irrigation	16	0.45	0.028	6.328	$1.27E^{-1}1$	***
Date:Genotype	39	0.89	0.023	5.154	$1.01E^{-1}5$	***
Irrigation:Genotype	10	0.08	0.008	1.799	6.18E-02	.
Date:Irrigation:Genotype	75	0.98	0.013	2.961	$2.64E^{-1}0$	***

Residuals	226	1	0.004			

H30

	Degrees of freedom	Sum of squares	Mean of squares	Fvalue	pvalue	
Date	14	1.1607	0.0829	5.97E+05	$<2e^{-1}6$	***
Irrigation	2	1.1245	0.5623	4.05E+06	$<2e^{-1}6$	***
Genotype	5	0.0518	0.0104	7.46E+04	$<2e^{-1}6$	***
Date:Irrigation	27	0.4627	0.0171	1.23E+05	$<2e^{-1}6$	***
Date:Genotype	65	0.3144	0.0048	3.48E+04	$<2e^{-1}6$	***
Irrigation:Genotype	10	0.2068	0.0207	1.49E+05	$<2e^{-1}6$	***
Date:Irrigation:Genotype	126	0.4225	0.0034	2.41E+04	$<2e^{-1}6$	***
Residuals	120	0	0			

H60

	Degrees of freedom	Sum of squares	Mean of squares	Fvalue	pvalue	
Date	14	0.4143	0.0296	6.43E+29	$<2e^{-1}6$	***
Irrigation	2	0.619	0.30952	6.73E+30	$<2e^{-1}6$	***
Genotype	5	0.1075	0.0215	4.67E+29	$<2e^{-1}6$	***
Date:Irrigation	27	0.2125	0.00787	1.71E+29	$<2e^{-1}6$	***
Date:Genotype	65	0.1297	0.00199	4.34E+28	$<2e^{-1}6$	***
Irrigation:Genotype	10	0.099	0.0099	2.15E+29	$<2e^{-1}6$	***
Date:Irrigation:Genotype	126	0.1989	0.00158	3.43E+28	$<2e^{-1}6$	***
Residuals	136	0	0			

ASWC

	Degrees of freedom	Sum of squares	Mean of squares	Fvalue	pvalue	
Date	14	9.536	0.681	6.85E+02	$<2e^{-1}6$	***
Irrigation	2	11.59	5.795	5.83E+03	$<2e^{-1}6$	***
Genotype	5	0.475	0.095	9.56E+01	$<2e^{-1}6$	***
Date:Irrigation	27	3.885	0.144	1.45E+02	$<2e^{-1}6$	***
Date:Genotype	65	2.003	0.031	3.10E+01	$<2e^{-1}6$	***
Irrigation:Genotype	10	1.618	0.162	1.63E+02	$<2e^{-1}6$	***
Date:Irrigation:Genotype	127	2.841	0.022	2.25E+01	$<2e^{-1}6$	***
Residuals	136	0.135	0.001			

2.5.2 *Anova* Tables *of harvest measurements*

2019

Response: Stem density

	Df	Sum Sq	Mean Sq	F valu	Pr(F)	
Genotype	5	10137.9	2027.58	135.96	$2.20E^{-1}6$	***
Residuals 48	715.8	14.91				

	Stem density	groups
ARCT	5.055556	d
ARMO	5.277778	d
GNT10	11.861111	c
GNT9	42.222222	a
MxG	5.194444	d
SAC	24.416667	b

Response: Mean Stem weight

	Df	Sum Sq	Mean Sq	F valu	Pr(F)	
Genotype	5	191840	38368	66.683	$2.20E^{-1}6$	***
Residuals 48	27618	575				

	Mean stem weight	groups
ARCT	155.00435	a
ARMO	156.32645	a
GNT10	32.10001	bc
GNT9	14.12332	c
MxG	24.25429	c
SAC	61.31644	b

Response: stem dry weight

	Df	Sum Sq	Mean Sq	F valu	Pr(F)	
Genotype	5	497273	99455	62.172	$2.20E^{-1}6$	***
Residuals	156	249547	1600			

	stem dry weight	groups
ARCT	135.35934	a
ARMO	144.88149	a
GNT10	19.74541	c
GNT9	13.57045	c
MxG	16.11226	c
SAC	62.95589	b

2020

Response: Stem density m-2

	Df	Sum Sq	Mean Sq	F valu	Pr(F)	
Genotype	5	19887.1	3977.4	171.8762	$2.00E^{-1}6$	***
Irrigation	2	162.3	81.2	3.5076	0.04057	*
Genotype:Irrigation	10	418.6	41.9	1.8091	0.09432	.
Residuals	36	833.1	23.1			

	Stem density m-2	groups
ARCT	12.25	e
ARMO	13.11111	de
GNT10	31.61111	c
GNT9	65.94444	a
MxG	19.27778	d
SAC	44.38889	b

I0		
	Stem density m-2	groups
ARCT	11.83333	c
ARMO	11.66667	c
GNT10	34.75	b
GNT9	58.91667	a
MxG	20.25	c
SAC	39.41667	b

I50		
	Stem density m-2	groups
ARCT	11.58333	d
ARMO	11.66667	d
GNT10	25.91667	c
GNT9	66.58333	a
MxG	18.5	cd
SAC	47.66667	b

	I100	
	Stem density m-2	groups
ARCT	13.33333	d
ARMO	16	d
GNT10	34.16667	c
GNT9	72.33333	a
MxG	19.08333	d
SAC	46.08333	b

Response: Stem weight

	Df	Sum Sq	Mean Sq	F valu	Pr(F)	
Genotype	5	426283	85257	133.0764	$2.20E^{-1}6$	***
Irrigation	2	18420	9210	14.3756	2.58E-05	***
Genotype:Irrigation	10	20286	2029	3.1664	0.005259	**
Residuals	36	23064	641			

	Stem weight	groups
ARCT	219.53027	a
ARMO	215.29147	a
GNT10	38.19148	bc
GNT9	19.46008	c
MxG	10.54268	c
SAC	58.49715	b

I0		
	Stem weight	groups
ARCT	159.778392	a
ARMO	165.720218	a
GNT10	26.844187	b
GNT9	14.179324	b
MxG	8.066452	b
SAC	43.169263	b
I50		
	Stem weight	groups
ARCT	236.18507	a
ARMO	202.02771	a
GNT10	45.33578	b
GNT9	20.43314	b
MxG	11.23203	b
SAC	64.13502	b

	I100	
	Stem weight	groups
ARCT	262.62734	a
ARMO	278.12648	a
GNT10	42.39447	bc
GNT9	23.76778	bc
MxG	12.32954	c
SAC	68.18716	b

Response: Stem dry weight MEAN

	Df	Sum Sq	Mean Sq	F valu	Pr(F)	
Genotype	5	123006	24601.3	99.438	$4.25E^{-1}6$	***
Irrigation	2	3737	1868.5	7.5525	0.002594	**
Genotype:Irrigation	10	7739	773.9	3.128	0.009416	**
Residuals	26	6432	247.4			

	Stem dry weight MEAN	groups
ARCT	128.691655	a
ARMO	132.353637	a
GNT10	23.244	c
GNT9	12.4705	c
MxG	7.691714	c
SAC	64.229064	b

	I0	
	Stem dry weight MEAN	groups
ARCT	101.052391	b
ARMO	149.882283	a
GNT10	19.071333	c
GNT9	8.944667	c
MxG	6.380667	c
SAC	45.875485	c

	I50	
	Stem dry weight MEAN	groups
ARCT	105.03123	a
ARMO	107.69351	a
GNT10	24.076	bc
GNT9	12.14267	c
MxG	9.928	c
SAC	75.63057	ab

	I100	
	Stem dry weight MEAN	groups
ARCT	164.21773	a
ARMO	139.48512	a
GNT10	34.93	bc
GNT9	18.251	c
MxG	4.916	c
SAC	74.98164	b

Response: Dry matter yield subplot t ha^{-1}

	Df	Sum Sq	Mean Sq	F valu	Pr(F)	
Genotype	5	5118.7	1023.73	150.824	2.20E^{-1}6	***
Irrigation	2	1246	622.99	91.784	7.33E^{-1}5	***
Genotype:Irrigation	10	839	83.9	12.361	6.39E-09	***
Residuals	36	244.4	6.79			

	Dry matter yield subplot t ha^{-1}	groups
ARCT	26.269952	a
ARMO	28.513353	a
GNT10	11.860447	b
GNT9	12.86636	b
MxG	1.972138	c
SAC	26.299699	a

I0		
	Dry matter yield subplot t ha^{-1}	groups
ARCT	18.398474	a
ARMO	19.115453	a
GNT10	9.253559	b
GNT9	8.298034	b
MxG	1.625107	c
SAC	16.963652	a

I50		
	Dry matter yield subplot t ha^{-1}	groups
ARCT	25.802769	ab
ARMO	22.099891	b
GNT10	11.827822	c
GNT9	13.220453	c
MxG	2.058538	d
SAC	30.53698	a

	I100	
	Dry matter yield subplot t ha^{-1}	groups
ARCT	34.60861	b
ARMO	44.32472	a
GNT10	14.49996	c
GNT9	17.08059	c
MxG	2.23277	d
SAC	31.39846	b

2.6 References

Ainsworth, E.A., Ort, D.R., 2010. How do we improve crop production in a warming world? Plant physiology 154, 526–530.

Alexopoulou, E., Papatheohari, Y., Zanetti, F., Tsiotas, K., Papamichael, I., Christou, M., Namatov, I., Monti, A., 2015a. Comparative studies on several castor (Ricinus communis L.) hybrids: Growth, yields, seed oil and biomass characterization. Industrial Crops and Products, Advances in Industrial Crops and Products Worldwide: AAIC 2014 international conference 75, 8–13. https://doi.org/10.1016/j.indcrop.2015.07.015

Alexopoulou, E., Zanetti, F., Scordia, D., Zegada-Lizarazu, W., Christou, M., Testa, G., Cosentino, S.L., Monti, A., 2015b. Long-term yields of switchgrass, giant reed, and Miscanthus in the Mediterranean basin. Bioenergy Research 8, 1492–1499.

Allan, R., Pereira, L., Smith, M., 1998. Crop evapotranspiration-Guidelines for computing crop water requirements-FAO Irrigation and drainage paper 56.

Allen, R.G., Food and Agriculture Organization of the United Nations (Eds.), 1998. Crop evapotranspiration: guidelines for computing crop water requirements, FAO irrigation and drainage paper. Food and Agriculture Organization of the United Nations, Rome.

Barbosa, B., Boléo, S., Sidella, S., Costa, J., Duarte, M.P., Mendes, B., Cosentino, S.L., Fernando, A.L., 2015. Phytoremediation of heavy metal-contaminated soils using the perennial energy crops Miscanthus spp. and *Arundo donax* L. BioEnergy Research 8, 1500–1511.

Bybee-Finley, K., Ryan, M.R., 2018. Advancing intercropping research and practices in industrialized agricultural landscapes. Agriculture 8, 80.

Cavallaro, V., Patanè, C., Cosentino, S.L., Di Silvestro, I., Copani, V., 2014. Optimizing in vitro large scale production of giant reed (*Arundo donax* L.) by liquid medium culture. Biomass and Bioenergy 69, 21–27.

Cavallaro, V., Scordia, D., Cosentino, S.L., Copani, V., 2019. Up-scaling agamic propagation of giant reed (*Arundo donax* L.) by means of single-node stem cuttings. Industrial Crops and Products 128, 534–544.

Clifton-Brown, J., Harfouche, A., Casler, M.D., Dylan Jones, H., Macalpine, W.J., Murphy-Bokern, D., Smart, L.B., Adler, A., Ashman, C., Awty-Carroll, D., 2019. Breeding progress and preparedness for mass-scale deployment of perennial lignocellulosic biomass crops switchgrass, miscanthus, willow and poplar. Gcb Bioenergy 11, 118–151.

Clifton-Brown, J., Hastings, A., Mos, M., McCalmont, J.P., Ashman, C., Awty-Carroll, D., Cerazy, J., Chiang, Y.-C., Cosentino, S., Cracroft-Eley, W., 2017. Progress in upscaling Miscanthus biomass production for the European bio-economy with seed-based hybrids. Gcb Bioenergy 9, 6–17.

Clifton-Brown, J.C., Lewandowski, I., 2000. Overwintering problems of newly established Miscanthus plantations can be overcome by identifying genotypes with improved rhizome cold tolerance. New Phytologist 148, 287–294.

Copani, V., Cosentino, S.L., Testa, G., Scordia, D., 2013. Agamic propagation of giant reed (*Arundo donax* L.) in semi-arid Mediterranean environment. Ital J Agron 8, e4.

Cosentino, S.L., Copani, V., D'Agosta, G.M., Sanzone, E., Mantineo, M., 2006. First results on evaluation of *Arundo donax* L. clones collected in Southern Italy. Industrial Crops and Products 23, 212–222.

Cosentino, S.L., Copani, V., Mantineo, M., 2008. Sod seeding and soil erosion in a semi-arid Mediterranean environment of south of Italy. Italian Journal of Agronomy 3, 47–48.

Cosentino, S.L., Copani, V., Scalici, G., Scordia, D., Testa, G., 2015a. Soil erosion mitigation by perennial species under Mediterranean environment. BioEnergy Research 8, 1538–1547.

Cosentino, S.L., Copani, V., Testa, G., Scordia, D., 2015b. Saccharum spontaneum L. ssp. aegyptiacum (Willd.) Hack. a potential perennial grass for biomass production in marginal land in semi-arid Mediterranean environment. Industrial Crops and Products 75, 93–102.

Cosentino, S.L., Patanè, C., Sanzone, E., Copani, V., Foti, S., 2007. Effects of soil water content and nitrogen supply on the productivity of Miscanthus×giganteus Greef et Deu. in a Mediterranean environment. Industrial Crops and Products 25, 75–88. https://doi.org/10.1016/j.indcrop.2006.07.006

Cosentino, S.L., Patanè, C., Sanzone, E., Testa, G., Scordia, D., 2016. Leaf gas exchange, water status and radiation use efficiency of giant reed (*Arundo donax* L.) in a changing soil

nitrogen fertilization and soil water availability in a semi-arid Mediterranean area. European Journal of Agronomy 72, 56–69.

Cosentino, S.L., Scordia, D., Sanzone, E., Testa, G., Copani, V., 2014. Response of giant reed (*Arundo donax* L.) to nitrogen fertilization and soil water availability in semi-arid Mediterranean environment. European Journal of agronomy 60, 22–32.

Cosentino, S.L., Testa, G., Scordia, D., Alexopoulou, E., 2012. Future yields assessment of bioenergy crops in relation to climate change and technological development in Europe. Ital J Agronomy 7, 22. https://doi.org/10.4081/ija.2012.e22

De Stefano, R., Cappetta, E., Guida, G., Mistretta, C., Caruso, G., Giorio, P., Albrizio, R., Tucci, M., 2018. Screening of giant reed (*Arundo donax* L.) ecotypes for biomass production under salt stress. Plant Biosystems-An International Journal Dealing with all Aspects of Plant Biology 152, 911–917.

Drago, A., 2005. Atlante climatologico della Sicilia - Seconda Edizione. Rivista Italiana di Agrometeorologia 2, 67–83.

Drake, B.G., Gonzàlez-Meler, M.A., Long, S.P., 1997. More efficient plants: a consequence of rising atmospheric CO2? Annual review of plant biology 48, 609–639.

Dražić, G., Milovanović, J., Stefanović, S., Petrić, I., 2017. Potential of Miscanthus$\\times$ Giganteus for Heavy Metals Removing from Industrial Deposol. Acta Regionalia et Environmentalica 14, 56–58.

Edenhofer, O., Pichs-Madruga, R., Sokona, Y., Agrawala, S., Bashmakov, I.A., Blanco, G., Broome, J., Bruckner, T., Brunner, S., Bustamante, M., 2014. Summary for policymakers.

Global Invasive Species Database, 2020. GISD [WWW Document]. URL http://www.iucngisd.org/gisd/species.php?sc=112 (accessed 11.10.20).

Jenkins, Bm., Baxter, L.L., Miles Jr, T.R., Miles, T.R., 1998. Combustion properties of biomass. Fuel processing technology 54, 17–46.

Jones, M.B., Finnan, J., Hodkinson, T.R., 2015. Morphological and physiological traits for higher biomass production in perennial rhizomatous grasses grown on marginal land. Gcb Bioenergy 7, 375–385.

Kiesel, A., Wagner, M., Lewandowski, I., 2017. Environmental performance of miscanthus, switchgrass and maize: Can C4 perennials increase the sustainability of biogas production? Sustainability 9, 5.

Knapp, A.K., 1993. Gas Exchange Dynamics in C^3 and C^4 Grasses: Consequence of Differences in Stomatal Conductance. Ecology 74, 113–123. https://doi.org/10.2307/1939506

Kumar, P.V., Ramakrishna, Y.S., Rao, B.V.R., Victor, U.S., Srivastava, N.N., Subba Rao, A.V.M., 1997. Influence of moisture, thermal and photoperiodic regimes on the productivity of castor beans (Ricinus communis L.). Agricultural and Forest Meteorology 88, 279–289. https://doi.org/10.1016/S0168-^{1}923(97)00019^{-1}

Lewandowski, I., Scurlock, J.M., Lindvall, E., Christou, M., 2003. The development and current status of perennial rhizomatous grasses as energy crops in the US and Europe. Biomass and bioenergy 25, 335–361.

Lewis, S., Kelly, M., 2014. Mapping the Potential for Biofuel Production on Marginal Lands: Differences in Definitions, Data and Models across Scales. IJGI 3, 430–459. https://doi.org/10.3390/ijgi3020430

McDonald, M.P., Galwey, N.W., Colmer, T.D., 2002. Similarity and diversity in adventitious root anatomy as related to root aeration among a range of wetland and dryland grass species. Plant, Cell & Environment 25, 441–451.

McKendry, P., 2002. Energy production from biomass (part 1): overview of biomass. Bioresource technology 83, 37–46.

Monti, A., Alexopoulou, E., 2017. Non-food crops in marginal land: an illusion or a reality? Biofuels, Bioprod. Bioref. 11, 937–938. https://doi.org/10.1002/bbb.1820

Monti, A., Di Virgilio, N., Venturi, G., 2008. Mineral composition and ash content of six major energy crops. Biomass and Bioenergy 32, 216–223. https://doi.org/10.1016/j.biombioe.2007.09.012

Monti, A., Zegada-Lizarazu, W., 2016. Sixteen-year biomass yield and soil carbon storage of giant reed (*Arundo donax* L.) grown under variable nitrogen fertilization rates. BioEnergy research 9, 248–256.

Nackley, L.L., Kim, S.-H., 2015. A salt on the bioenergy and biological invasions debate: salinity tolerance of the invasive biomass feedstock A rundo *donax*. Gcb Bioenergy 7, 752–762.

Nackley, L.L., Vogt, K.A., Kim, S.-H., 2014. *Arundo donax* water use and photosynthetic responses to drought and elevated CO2. Agricultural Water Management 136, 13–22.

Norman, J.M., Campbell, G.S., 1989. Canopy structure, in: Plant Physiological Ecology. Springer, pp. 301–325.

O'Leary, M.H., 1988. Carbon isotopes in photosynthesis. Bioscience 38, 328–336.

Olesen, J.E., Trnka, M., Kersebaum, K.C., Skjelvåg, A.O., Seguin, B., Peltonen-Sainio, P., Rossi, F., Kozyra, J., Micale, F., 2011. Impacts and adaptation of European crop production systems to climate change. European Journal of Agronomy 34, 96–112. https://doi.org/10.1016/j.eja.2010.11.003

Panoutsou, C., Chiaramonti, D., 2020. Socio-Economic Opportunities from Miscanthus Cultivation in Marginal Land for Bioenergy. Energies 13, 2741. https://doi.org/10.3390/en13112741

Pignatti, S., 1982. Flora d'Italia. Edagricole.

Poorter, H., 1993. Interspecific variation in the growth response of plants to an elevated ambient CO 2 concentration, in: CO2 and Biosphere. Springer, pp. 77–98.

Quinn, L.D., Allen, D.J., Stewart, J.R., 2010. Invasiveness potential of Miscanthus sinensis: implications for bioenergy production in the United States. Gcb Bioenergy 2, 310–320.

Ragaglini, G., Dragoni, F., Simone, M., Bonari, E., 2014. Suitability of giant reed (*Arundo donax* L.) for anaerobic digestion: effect of harvest time and frequency on the biomethane yield potential. Bioresource technology 152, 107–115.

Rossa, B., Tüffers, A.V., Naidoo, G., Von Willert, D.J., 1998. *Arundo donax* L.(Poaceae)—a C3 species with unusually high photosynthetic capacity. Botanica Acta 111, 216–221.

Schmidt, T., Fernando, A.L., Monti, A., Rettenmaier, N., 2015. Life cycle assessment of bioenergy and bio-based products from perennial grasses cultivated on marginal land in the Mediterranean region. Bioenergy Research 8, 1548–1561.

Scordia, D., Cosentino, S., 2019. Perennial Energy Grasses: Resilient Crops in a Changing European Agriculture. Agriculture 9, 169. https://doi.org/10.3390/agriculture9080169

Scordia, D., Cosentino, S.L., Lee, J.-W., Jeffries, T.W., 2011. Dilute oxalic acid pretreatment for biorefining giant reed (*Arundo donax* L.). biomass and bioenergy 35, 3018–3024.

Scordia, D., Testa, G., Copani, V., Patanè, C., Cosentino, S.L., 2017. Lignocellulosic biomass production of Mediterranean wild accessions (*Oryzopsis miliacea, Cymbopogon hirtus, Sorghum halepense* and *Saccharum spontaneum*) in a semi-arid environment. Field Crops Research 214, 56–65.

Scordia, D., Testa, G., Cosentino, S.L., 2014. Perennial grasses as lignocellulosic feedstock for second-generation bioethanol production in Mediterranean environment. Ital J Agronomy 9, 84. https://doi.org/10.4081/ija.2014.581

Scordia, D., van den Berg, D., van Sleen, P., Alexopoulou, E., Cosentino, S.L., 2016. Are herbaceous perennial grasses suitable feedstock for thermochemical conversion pathways? Industrial Crops and Products 91, 350–357. https://doi.org/10.1016/j.indcrop.2016.07.019

Scordia, D., Zanetti, F., Varga, S.S., Alexopoulou, E., Cavallaro, V., Monti, A., Copani, V., Cosentino, S.L., 2015. New insights into the propagation methods of switchgrass, miscanthus and giant reed. BioEnergy Research 8, 1480–1491.

Stavridou, E., Hastings, A., Webster, R.J., Robson, P.R., 2017. The impact of soil salinity on the yield, composition and physiology of the bioenergy grass Miscanthus$\times$ giganteus. Gcb Bioenergy 9, 92–104.

Volaire, F., Barkaoui, K., Norton, M., 2014. Designing resilient and sustainable grasslands for a drier future: adaptive strategies, functional traits and biotic interactions. European Journal of Agronomy 52, 81–89.

Wuest, S.B., Williams, J.D., Gollany, H.T., 2006. Tillage and perennial grass effects on ponded infiltration for seven semi-arid loess soils. Journal of soil and water conservation 61, 218–223.

Wyman, C.E., 1994. Ethanol from lignocellulosic biomass: technology, economics, and opportunities. Bioresource Technology 50, 3–15.

Zanetti, F., Chieco, C., Alexopoulou, E., Vecchi, A., Bertazza, G., Monti, A., 2017. Comparison of new castor (Ricinus communis L.) genotypes in the mediterranean area and possible valorization of residual biomass for insect rearing. Industrial Crops and Products 107, 581–587.

Zanetti, F., Scordia, D., Calcagno, S., Acciai, M., Grasso, A., Cosentino, S.L., Monti, A., 2019. Trade-off between harvest date and lignocellulosic crop choice for advanced biofuel production in the Mediterranean area. Industrial Crops and Products 138, 111439. https://doi.org/10.1016/j.indcrop.2019.06.002

Zegada-Lizarazu, W., Elbersen, H.W., Cosentino, S.L., Zatta, A., Alexopoulou, E., Monti, A., 2010. Agronomic aspects of future energy crops in Europe. Biofuels, Bioprod. Bioref. 4, 674–691. https://doi.org/10.1002/bbb.242

Zhu, J.Y., Pan, X.J., 2010. Woody biomass pretreatment for cellulosic ethanol production: technology and energy consumption evaluation. Bioresource technology 101, 4992–5002.

3 Biomass yield, water use efficiency, energy content, and energy return on investment of diverse perennial grasses in autumn and winter harvest regimes in the Mediterranean area

3.1 Introduction

Sustainable biomass production mostly relies on cultivation practices employing low external input supply. In Europe, research activities deemed a few perennial grasses for biomass production, in relation to the variable climatic conditions. Perennial grasses are lignocellulosic feedstock, the most abundant and low-cost raw material on earth, tailored to develop a competitive, resource efficient and low-carbon economy in Europe (Scarlat et al., 2015). The C4 perennial grasses, *Miscanthus* x giganteus and Panicum virgatum, are high-yielding in temperate environments of northern and central Europe (Lewandowski et al., 2003), while the C3 *Arundo donax* is reported to be more productive in southern Europe (Mantineo et al., 2009; Cosentino et al., 2014; Cosentino et al., 2016). In the Mediterranean basin, however, there is a remarkable plant diversity still largely unexplored. The investigation of site-specific wild germplasms for biomass production would mitigate the effect of land use competition and might provide new genetic resource for breeding programs aiming at the development of relevant varieties able to thrive under limiting conditions (Scordia et al., 2017). High-resource-use-efficient species could maximize natural resources, thus limiting the use of external input meeting in this way the environmental sustainability by achieving positive energy balances (Tilman et al., 2006). Biomass quality is as important as biomass yield in view of industrial conversions. One of the major determinant of biomass productivity, stand longevity and quality of perennial

grasses is the harvest time (Monti et al., 2015). Decisions about the optimal harvest time of perennial energy grasses have important implications for economic and environmental objectives, as trade-offs between harvestable yield, qualitative traits for specific bioenergy processes, and environmental costs/benefits are still required. The aim of the present study was to assess the biomass dry matter yield (DM), the water use efficiency (WUE), the energy content (EC) and the energy return on investment (EROI) at the farm gate of several perennial grasses already established at the experimental farm of the University of Catania.

3.2 Materials and methods

3.2.1 *Field trial description*

Field trials employing *Arundo donax* (AD), *Miscanthus* x giganteus (MxG), *Saccharum spontaneum* spp. *aegyptiacum* (SS), *Sorghum halepense* (SA), *Oryzopsis miliacea* (OM) and *Cymbopogon* hirthus (CH) established at the Experimental farm of the University of Catania, Italy (37°25' N., 15°03' E., 10 m a.s.l.) were used. Trial main characteristics are shown in **Table** 1. For further experimental details, see [4, 6, 8]. Briefly, in all field trials soil was ploughed 0.4 m depth in autumn and disk-harrowed 0.2 m depth in spring before transplanting. Micro-propagated *Miscanthus* plants (*Miscanthus* x giganteus Greef et Deuter), provided by Piccoplant (Old- enburg, Germany), were transplanted (4 plants m−2) in summer 1993. Giant reed (*Arundo donax* L.) plantlets were produced at the University of Catania from stem cuttings of the local ecotype 'Fondachello' then transplanted in spring 1997 (2.5 plants m−2). Both crops were constantly irrigated until establishment was successfully achieved. The experimental design was a randomized block with

three replications. Nitrogen fertilization was applied only in the first three years. Both crops were harvested in winter until 2010. Since 2011, autumn (late September/October) and winter (mid-February) harvestings were differentiated. In spring 2010, *Oryzopsis miliacea* (L.) Asch. & Schweinf., *Cymbopogon hirtus* (L.) Janchen, *Sorghum halepense* (L.) Pers., and *Saccharum spontaneum* L. ssp. *aegyptiacum* (Willd.) Hackel were established at a density of 1 plant m-2 , in a split-plot randomized block design. Propagation material was collected at the experimental farm. The main plots were used for the species, while the sub-plots were used to analyse the harvest time, namely autumn and winter (as above). Species were constantly irrigated until establishment was successfully achieved, while no fertilization was supplied, neither at establishment nor subsequently.

Table I: Field-trial main characteristics

Species	EY	MT	RF
MxG	1993	Harvest time (from 2011)	[9]
AD	1997	Harvest time (from 2011)	[4]
SS, SA, OM, CH	2010	Harvest time (from 2011)	[6]

3.2.2 *Measurements on field*

Throughout the 2014/2015 growing season, main meteorological parameters, as maximum and minimum temperatures, and rainfall, were measured by a weather station connected to a data logger (Delta-T, WS-GP1 Compact) located nearby the field trials. The reference crop evapotranspiration (ET0) was calculated from the evaporation pan (mm d^{-1}) by the pan coefficient of 0.80. At harvest, edge plants were removed in

each plot to weight the biomass within 12 m2. Dry biomass yield was calculated by weighing sub-samples of fresh biomass and after oven drying it at 65 °C until constant weight. The whole season crop water use efficiency (g L−1) was calculated as the ratio between dry biomass yield and crop water use (CWU) from regrowth up to harvest, in both winter and autumn growing seasons.

3.2.3 *Analytical determinations*

Oven-dried samples (whole aboveground biomass) collected at the autumn or winter harvest were ground through a 1-mm sieve in an IKA mill (IKA-WERFE, Gmbh & Co., KG, Staufenim Breisgau, Germany). Cellulose, hemicellulose, acid detergent lignin (ADL), proteins, lipids and ash were determined by a near- infrared spectrometer (NIR, SpectraStarTM 2500XL-R, Unity Scientific) provided with a tungsten halogen lamp as light source and a high performance ultra-cooled InGaAs extended range detector. Samples were placed in small powder cups and scanned in duplicate in diffuse reflection measurement mode, wavelength range of 680- 2500 nm and accuracy < 0.1 nm. A previous calibration developed by the Ucal complete chemometric calibration software (InfoStar 3.11.0 version) was adopted. The calibration consisted of a regression that correlates spectra and analytic determinations of 240 different lignocellulosic raw materials of *Arundo donax* clones and *Miscanthus* species (stems, leaves or the whole biomass) grown under different agronomic practices and growing seasons. Following a first scan run, spectra of *Oryzopsis*, *Cymbopogon* , Sorghum and *Saccharum* were also used for further calibration development in the Ucal software. Biomass energy content (MJ kg^{-1}) was determined as biomass composition in terms of carbohydrates, proteins and lipids. Carbohydrate energy conversion factor was also applied for lignin (ADL). Energy

input referred only to harvesting, accounting for 2.94 GJ ha^{-1} . The energy return on investment (EROI) was calculated as the ratio of usable energy (output) to the amount of energy used to obtain that resource.

3.2.4 *Statistical analysis*

Biomass yield, water use efficiency, energy content and energy return on investment were subjected to a two- way analysis of variance (ANOVA) with species and harvest time as main effects. The Duncan's post-hoc test was used for mean separation at 95% confidence level.

3.3 Results and discussions

3.3.1 *Meteorological conditions*

In the autumn growing season (from October to October) temperatures averaged 24.2°C for maximum, 13.0°C for the minimum and 18.6°C for the mean. Winter growing season (February to February) was cooler, 22.8°C and 18.1°C for the maximum and mean temperatures, whilst minimum temperatures were warmer, 13.4°C (**Figure** 1). Rainfall was much lower in autumn than winter, 354.1 and 518.5 mm, respectively. It was 102 mm between September and November and only 87.6 mm in the period March to September, namely the period that covers the main growth phases of perennial grasses. Overall ET0 was higher in autumn than winter season (1101.2 and 985.5 mm, respectively), averaging at 2.89 and 2.59 mm day^{-1} in autumn and winter season, respectively. Obviously the period with the highest ET0 was from late spring to the end of summertime (on average 4.21 mm day^{-1}).

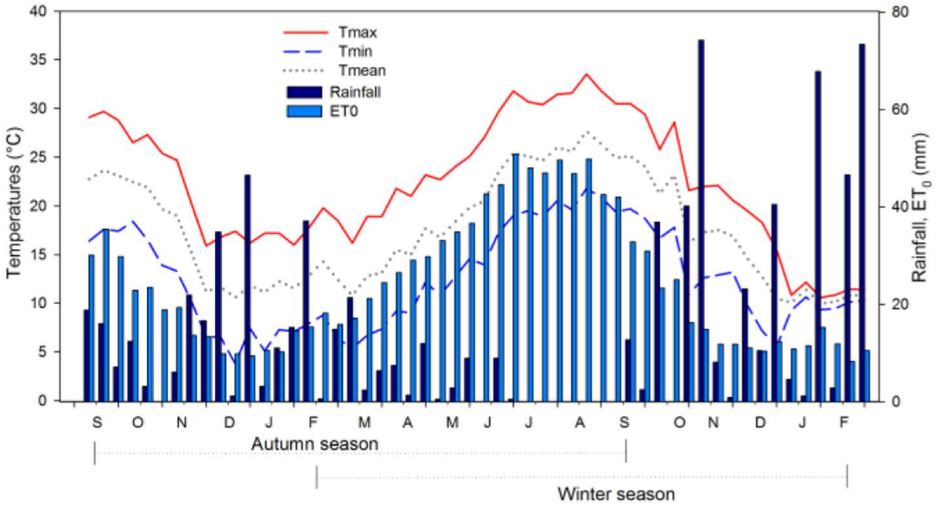

Figure 1: Main meteorological parameters registered in Autumn and Winter growing season at the Experimental farm of the University of Catania, Italy (37°25' N., 15°03' E., 10 m a.s.l.)

The dryness index (P/ET), according to the criteria and thresholds set in the Regulation EU (1305) 2013, was much lower in autumn (0.32) than winter season (0.53) and both are lower than the threshold of 0.6 suggested by the JRC report on the delineation of agricultural areas affected by specific biophysical constraints (Confalonieri et al., 2014). Thus, the environment where the trial was carried out can be considered constrained by "dryness" as biophysical constraint.

3.3.2 *Biomass yield and water use efficiency*

The analysis of variance showed that species and harvest time main effect, and interaction on water use efficiency (WUE) was significant, while only species and the interaction of species per harvest time was significant on biomass yield (DM) (**Table** II).

Table II: ANOVA for species (S) and harvest time (HT) main effect, and interaction (S x HT) on biomass yield (DM) and water use efficiency (WUE) of perennial grasses. Degree of freedom (df), adjusted mean square (Adj MS) and significance: P≤0.01 (**), P≤0.05 (*), Not significant (ns)

Source	df	DM	WUE
		Adj MS	
S	5	3.49**	20.99**
HT	1	121719ns	11.22**
S x HT	5	254964*	3.26*

Across the average of species, harvest time main effect was not significant for biomass dry matter yield (DM), and averaged 9.9 and 8.7 Mg ha^{-1} in autumn and winter harvest, respectively (**Figure** 2). On the other hand, it was significant different on WUE (2.79 and 1.67 g L^{-1} in autumn and winter harvest, respectively). Across the average of harvest time, species main effect was significant on both DM and WUE (P≤0.05). Harvest time x species interaction was significant as well (P≤0.05). *Saccharum* showed the highest DM and WUE across harvest time (23.1 Mg ha^{-1} and 5.6 g L^{-1}, respectively) followed by *Arundo* (13.5 Mg ha^{-1} and 3.3 g L^{-1} , respectively). Cymbopgon showed the lowest DM and WUE (3.7 Mg ha^{-1} and 0.9 g L^{-1} , respectively), however did not differ from *Miscanthus* and *Oryzopsis* for DM and *Miscanthus* only for WUE (**Figure** 2 and 3). Sorghum was at the middle range for both DM and WUE (6.5 Mg ha^{-1} and 0.9 g L^{-1} , respectively). The yield reduction observed for *Saccharum* and *Arundo*, but also for *Cymbopogon* and *Oryzopsis* from autumn to winter harvest is in line with other perennial grasses [4, 11, 12].

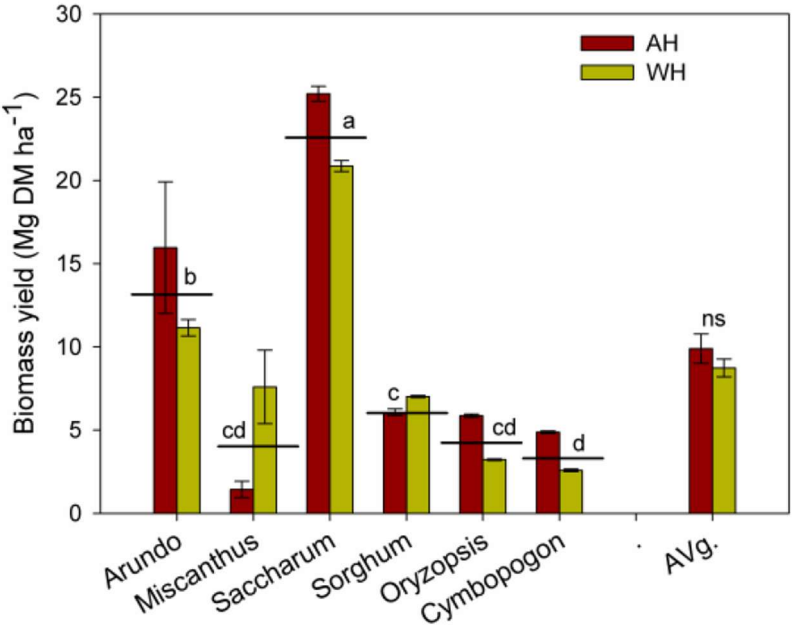

Figure 2: Biomass dry matter yield (Mg ha^{-1}) of perennial grasses under autumn harvest (AH) and winter harvest (WH). Different letters indicate significantly different means ($P \leq 0.05$). LSD of species and harvest time interaction ($P \leq 0.05$), 2.79

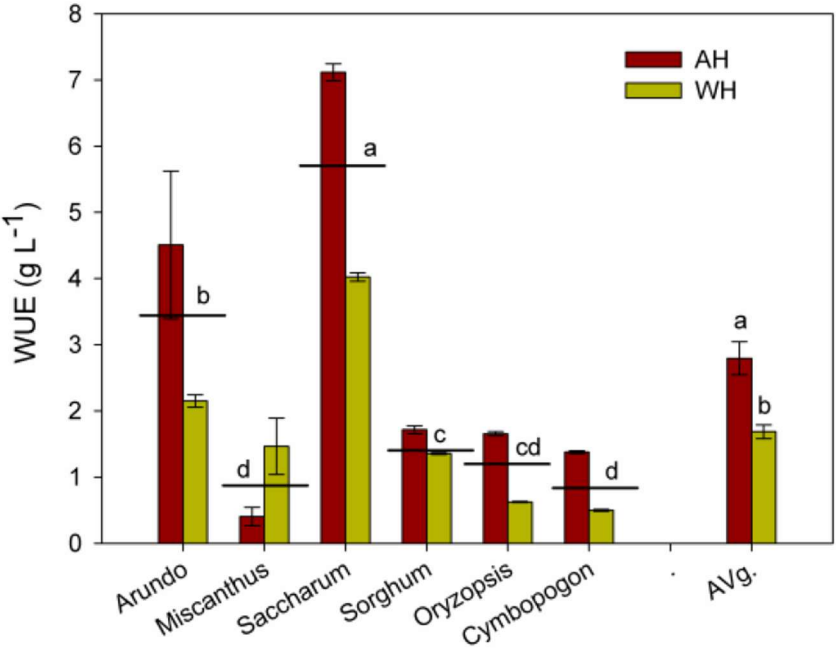

Figure 3: Water use efficiency (g L^{-1}) of perennial grasses under autumn harvest (AH) and winter harvest (WH). Different letters indicate significantly different means (P≤0.05). LSD of species and harvest time interaction (p≤0.05), 0.72

It can be ascribed to leaves senescence and losses, and nutrient translocation from aerial to undergrounds part that usually occurs at the onset of the cool season (in late autumn in the present environment). *Miscanthus* did not show the typical behaviour described above (Strullu et al., 2011), as the stand is very old (>20 years) and the autumn harvest is constantly leading to rhizome depletion due to nutrient translocation interruption. Thus, plots harvested in autumn in *Miscanthus* are steadily decreasing biomass yield. Sorghum was not affected by harvest regimes, and showed almost the same yield between

harvests. In *Saccharum*, both biomass yield and water use efficiency were in agreement with previous studies conducted in the same environment by Cosentino et al. (Cosentino et al., 2015) and Scordia et al. (Scordia et al., 2015) in rainfed conditions.

3.3.3 *Energy Content and Energy Return On Investment*

The analysis of variance showed that species, and interaction of species and harvest time interactions was significant on EC and EROI, while harvest time was not significant on both parameters (**Table** 3).

Table III: ANOVA for species (S) and harvest time (HT) main effect, and interaction (S x HT) on energy content (EC) and energy return on investment (EROI) of perennial grasses. Degree of freedom (df), adjusted mean square (Adj MS) and significance: P≤0.01 (**), P≤0.05 (*), Not significant (ns)

Source	df	EC	EROI
		Adj MS	
S	5	0.98**	9332.1**
HT	1	0.13ns	345.9ns
S x HT	5	0.58*	765.4**

Across the average of species, harvest time main effect was not significant on energy content (EC). On the other hand, across the average of harvest time, species main effect was significant (P≤0.05). There were significant harvest time x species interaction (P≤0.05). Across harvest time, *Miscanthus*, Sorghum and *Cymbopogon* showed the highest EC and not statistically different (15.9, 15.8 and 15.7 MJ kg^{-1} , respectively). *Saccharum*, *Arundo* and *Oryzopsis* showed the lowest and not

different EC (15.3, 15.1 and 14.9 MJ kg^{-1} , respectively) (**Figure** 4).

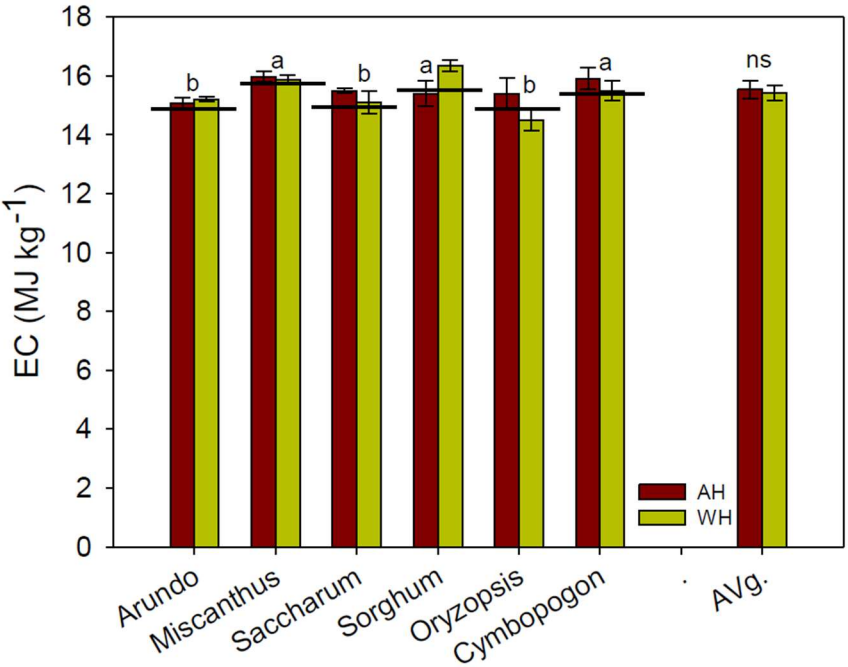

Figure 4: Energy content (MJ kg^{-1}) of perennial grasses under autumn harvest (AH) and winter harvest (WH). Different letters indicate significantly different means ($p \leq 0.05$). LSD of species and harvest time interaction ($p \leq 0.05$), 0.51

Across the average of species, harvest time main effect was not significant on the energy return on investment (EROI). Across the average of harvest time, species main effect was significant on EROI ($P \leq 0.05$). A significant harvest time x species interaction was observed ($P \leq 0.05$). *Saccharum* showed the highest EROI (120:1) followed by *Arundo* (69.8:1) and Sorghum (35.4:1) across the average of harvest time. *Cymbopgon*, *Oryzopsis* and *Miscanthus* showed the lowest and

not statistically different EROI (20:1, 23.3:1 and 24.3:1, respectively) (**Figure** 5).

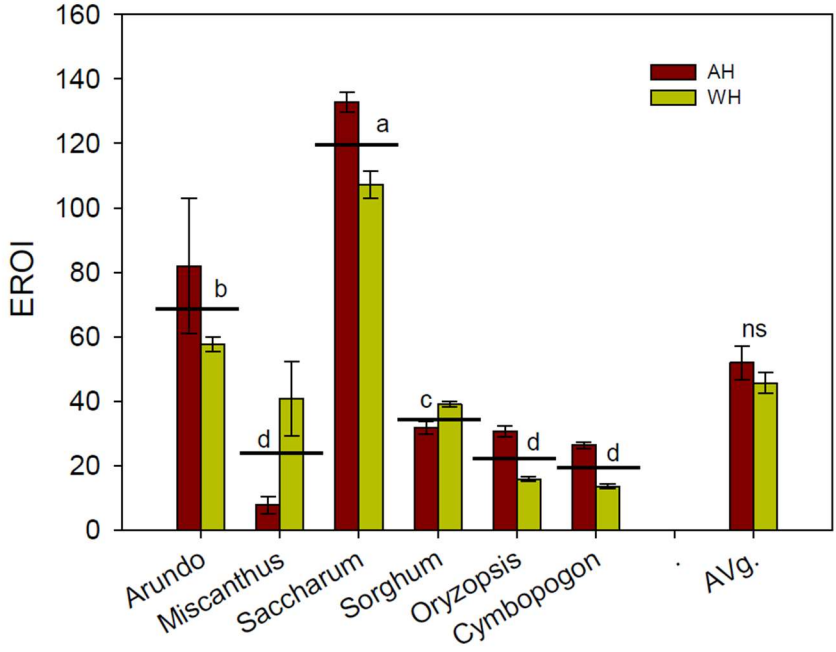

Figure 5: EROI of perennial grasses under autumn harvest (AH) and winter harvest (WH). Different letters indicate significantly different means (P≤0.05).

LSD of species and harvest time interaction (P≤0.05), 15.0 The EROI of *Saccharum* was impressive, since it was achieved at the fifth year of plantation, and the crop never received irrigation water, fertilization and other input. This result could be well comparable to those obtained by Angelini et al. (Angelini et al., 2005), with *A. donax* grown in a more wet environment (North Italy) and quite higher than the *A. donax* and M. x giganteus values reported by Mantineo et al. (Mantineo et al., 2009) in a similar semi-arid environment. *Arundo* was the second highest

species, confirming the exceptional adaptability to the growing conditions of the area, even almost 20 years after the establishment. In this case as well, the crop did not benefit from any input supply.

3.4 Conclusions

The dryness index (P/ET) was much lower in autumn (0.32) than winter season (0.53), and both were lower than the threshold of 0.6 set in (Confalonieri et al., 2014). *S. spontaneum* was clearly the outstanding species. It is worth nothing, however, that stands present different age, with *Miscanthus* and *Arundo* being older (22 and 18 years, respectively) than the other species (4 years). This may bias the present analysis. Overall, species widespread in semi-arid Mediterranean environment were able to produce similar (*Oryzopsis* and *Cymbopogon*) or higher (*Saccharum*, *Arundo* and Sorghum) biomass yield and WUE than *Miscanthus* x giganteus, which is more suited to colder and wetter environments. The energy content of perennial grasses, although significant, was in the range of 1.0 MJ kg^{-1} between the most (*Miscanthus*, 15.9 MJ kg^{-1}) and the least (*Oryzopsis*, 14.9 MJ kg^{-1}) species. This indicate that perennial grasses are characterized by a quite similar composition, which is a positive feature in a bioenergy chain. Indeed, a stable biomass composition delivered at the bioconversion site avoids continual modifications to processing operations, in turn avoiding to incur in costly and risky operations. All species can be considered sustainable from the energy point of view as evidenced by the EROI value which was the highest in *Saccharum* (120:1), and the lowest, but still positive, in *Cymbopogon* (20:1). Further research in agronomy is needed on native Mediterranean perennial grasses as biomass crops or as candidate species for breeding programs in environments characterized by severe drought stress. 5

3.5 References

Angelini, L.G., Ceccarini, L., Bonari, E., 2005. Biomass yield and energy balance of giant reed (*Arundo donax* L.) cropped in central Italy as related to different management practices. Eur. J. Agron. 22, 375–389.

Angelini, L.G., Ceccarini, L., Nassi o Di Nasso, N., Bonari, E., 2009. Comparison of *Arundo donax* L. and Miscanthus x giganteus in a long-term field experiment in Central Italy: analysis of productive characteristics and energy balance. Biomass Bioenergry 33, 635–643.

Confalonieri, R., Jones, B., Van Diepen, K., Van Orshoven, J., 2014. Scientific contribution on combining biophysical criteria underpinning the delineation of agricultural areas affected by specific constraints. Editors: JM. Terres, A. Hagyo, A. Wania. European Commission, Joint Research Centre, Institute for Environment and Sustainability. JRC92686, EUR 26940 EN, ISBN 978-92-79-44340-4.

Cosentino, S.L., Patanè, C., Sanzone, E., Copani, V., Foti, S., 2007. Effect of soil water content and nitrogen supply on the productivity of Miscanthus × giganteus in Mediterranean environment. Industrial Crops and Products 25(1),75–88.

Cosentino, S.L., Scordia, D., Sanzone, E., Testa, G., Copani, V., 2014. Response of giant reed (*Arundo donax* L.) to nitrogen fertilization and soil water availability in semi-arid Mediterranean environment. European Journal of Agronomy 60, 22–32.

Cosentino, S.L., Copani, V., Testa, G., Scordia, D., 2015. Saccharum spontaneum L. ssp. aegyptiacum (Willd.) Hack. a

potential perennial grass for biomass production in marginal land in semi-arid Mediterranean environment. Ind. Crop. Prod. 75, 93–102.

Cosentino, S.L., Patanè, C., Sanzone, E., Testa, G., Scordia, D., 2016. Leaf gas exchange, water status and radiation use efficiency of giant reed (*Arundo donax* L.) in a changing soil nitrogen fertilization and soil water availability in a semi-arid Mediterranean area. European Journal of Agronomy 72, 56–69.

Lewandowski, I., Scurlock, J.M.O., Lindvall, E., Christou, M., 2003. The development and current status of perennial rhizomatous grasses as energy crops in the US and Europe. Biomass and Bioenergy 25, 335–361.

Mantineo, M., D'Agosta, G.M., Copani, V., Patanè, C., Cosentino, S.L., 2009. Biomass yield and energy balance of three perennial crops for energy use in the semi-arid Mediterranean environment. Field Crops Research 114, 204–213.

Monti, A., Zanetti, F., Scordia, D., Testa, G., Cosentino, S.L., 2015. What to harvest when? Autumn, winter, annual and biennial harvesting of giant reed, Miscanthus and switchgrass in northern and southern Mediterranean area. Industrial Crops and Products, 75, 129–134.

Nassi o Di Nasso, N., Roncucci, N., Triana, F., Tozzini, C., Ragaglini, G., Bonari, E.,2011. Productivity of giant reed (*Arundo donax* L.) and Miscanthus (Miscanthus × giganteus Greef et Deuter) as energy crops: growth analysis. Ital. J. Agron.6, e22.

Scarlat, N., Dallemand, J.F., Monforti-Ferrario, F., Nita, V., 2015. The role of biomass and bioenergy in a future bioeconomy: Policies and facts. Environmental Development, 15, 3–34.

Scordia, D., Testa, G., Cosentino, S.L., Copani, V., Patanè, C., 2015. Soil water effect on crop growth, leaf gas exchange, water and radiation use efficiency of Saccharum spontaneum L. ssp. aegyptiacum (Willd.) Hackel in semi-arid Mediterranean environment. Ital. J Agron. 10 (672), 185–191.

Scordia, D., Testa, G., Copani, V., Patanè C., Cosentino, S.L., 2017. Lignocellulosic biomass production of Mediterranean wild accessions (*Oryzopsis* miliacea, *Cymbopogon* hirtus, Sorghum halepense and Saccharum spontaneum) in a semi-arid environment. Field Crops Research, 214, 56.

Strullu, L., Cadoux, S., Preudhomme, M., Jeuffroy, M.H., Beaudoin, N., 2011.Biomass production and nitrogen accumulation and remobilization by Miscanthus × giganteus as influenced by nitrogen stocks in belowground organs. Field Crop Res. 121, 381–391.

Tilman, D., Hill, J., Lehman, C., 2006. Carbon- negative biofuels from low-input high-diversity grassland biomass. Science 314, 1598-1600.

4 A model to describe *Miscanthus* x *giganteum* gas exchanges in relation to environmental conditions

4.1 Materials and methods

Miscanthus x *giganteum* gas exchanges have been measured from a field trial carried out at the Experimental Farm of the University of Catania (10 m a.s.l., 37°24′ N, 15°03′ E) in a typical Xerofluvents soil (USDA, 1999) in which other five genotypes were evaluated in a split-plot experimental design with nine replications: two *Arundo donax* L. ecotypes, named ARCT and ARMO (clone Fondachello and clone Morocco), the commercial *Miscanthus* x giganteus (greef et Deuter) named MxG, two seed-based *Miscanthus* hybrids obtained from the breeding program led by the Institute of Biological, Environmental and Rural Sciences of Aberystwyth University (UK) and Terravesta Ltd (UK), named GNT9 and GNT10, and one ecotype of *Saccharum spontaneum* L. ssp. aegypticum Willd (Hack.), named SAC. The main factor assigned to the plots is the irrigation level, with 3 levels: 100%, 50% and 0% of maximum crop evapotranspiration (ETm) restoration during the summer months (June-August). Genotype is the second factor, assigned to the sub-plots within the main irrigation plots. Each combination of irrigation and genotype is replicated 3 times within the main plots.

During the growing seasons, meteorological conditions have been continuously measured through a weather station connected to a data logger (Delta-T, WS-GP1). Potential evapotranspiration is calculated according to Allen and Food and Agriculture Organization of the United Nations (1998). Soil water content has been measured every two weeks using Teros10 moisture sensors (Delta-T). Net photosynthesis (μmol $C0_2$ m^{-2} s^{-1}),

transpiration (mmol H_20 m^{-2} s^{-1}), stomatal conductance (mol H_20 m^{-2} s^{-1}), photosynthetically active radiation, carbon dioxide concentration in the atmosphere, atmospheric H_2O concentration and atmospheric temperature have been measured or calculated by the LCi-SD Portable Photosynthesis system (ADC BioScientific Ltd.) on the basis of $C0_2$ and H_20 gas exchange.
Vapour pressure deficit has been calculated as suggested by (Allan et al., 1998).
Simulated values have been calculated according to the following equations:

$$gs(vpd) = maxgs \cdot e^{\frac{-(vpd \cdot k2)^2}{\left(k2/k5\right)^2}} \quad \text{Eq. 1}$$

$$gs(asw) = maxgs \cdot (1 - e^{-asw \cdot k7}) \quad \text{Eq. 2}$$

$$gs(Q) = maxgs \cdot \frac{1}{1+e^{-\frac{Q-k4}{k6}}} \quad \text{Eq. 3}$$

$$gs(T) = maxgs \cdot e^{\frac{-(T*k10)^2}{\left(k10/k11\right)^2}} \quad \text{Eq. 4}$$

$$gs(doy) = maxgs \cdot \frac{1}{1+e^{\frac{doy-doe-k9}{k8}}} \quad \text{Eq.5}$$

doe = date of shoots emission = 105

$$gs(vpd, Q, asw, T, doy) = \quad \text{Eq. 6}$$

$$maxgs \cdot e^{\frac{-(vpd*k2)^2}{\left(k2/k5\right)^2}} \cdot \frac{1}{1+e^{-\frac{Q-k4}{k6}}} \cdot (1 - e^{-asw \cdot k7}) \cdot maxgs \cdot e^{\frac{-(T*k10)^2}{\left(k10/k11\right)^2}} \cdot \frac{1}{1+e^{\frac{doy-doe-k}{k8}}}$$

$$A(gs) = maxA \cdot (1 - e^{-gs \cdot c6}) \quad \text{Eq. 7}$$

$$A(vpd) = maxA \cdot (1 - e^{-gs(vpd) \cdot c6}) \quad \text{Eq. 8}$$

$$A(asw) = maxA \cdot (1 - e^{-gs(asw) \cdot c6}) \quad \text{Eq. 9}$$

$$A(Q) = maxA \cdot \frac{1}{1+e^{-\frac{Q-c4}{c7}}} \quad \text{Eq. 10}$$

$$A(T) = maxA \cdot e^{\frac{-(T*c2)^2}{(c2/c3)^2}} \quad \text{Eq. 11}$$

$$A(CO_2) = maxA \cdot (1 - e^{-CO_2 \cdot c5}) \quad \text{Eq. 12}$$

$$A(doy) = maxA \cdot \frac{1}{1+e^{\frac{doy-doe-c9}{c8}}} \quad \text{Eq. 13}$$

with doe = date of the emission of the culm

$$A(vpd, asw, Q, T, CO_2, doy) = \quad \text{Eq. 14}$$

$$maxA \cdot (1 - e^{-gs(vpd,asw,Q) \cdot c6}) \cdot e^{\frac{-(T*c2)^2}{(c2/c3)^2}} \cdot \frac{1}{1+e^{-\frac{Q-c4}{c7}}} \cdot (1 - e^{-CO_2 \cdot c5}) \cdot \frac{1}{1+e^{\frac{doy-doe-c9}{c8}}}$$

The parameters maxgs, k2, k3, k4, k5, k6, k7, k8, k9, k10 and k11 have been calculated in order to minimize the function

$$f(vpd, asw, Q, T) = \frac{\sum(gs\ sim - gs\ obs)^2}{\sum(\bar{X} - gs\ obs)^2}$$

in which $gs\ obs$ is the value observed for the given set of environmental variables (vpd, asw, Q, T), $gs\ sim$ has been calculated according to the equation 6 using the set of environmental variables (vpd, asw, Q, T), $\bar{X}$ is the mean of $gs\ obs$.
The parameters maxA, c2, c3, c4, c5, c6, c7, c8 and c9 have been calculated in order to minimize the function

$$f(vpd, asw, Q, T) = \frac{\sum(A\ sim - A\ obs)^2}{\sum(\bar{X} - A\ obs)^2}$$

in which $A\ obs$ is the value observed for the given set of environmental variables $(vpd, asw, Q, T, CO_2, doy)$, $A\ sim$ has been calculated according to the equation 14 using the set of environmental variables $(vpd, asw, Q, T, CO_2, doy)$, $\bar{X}$ is the mean of $A\ obs$.

4.2 Results and discussion

Observed stomatal conductance ranged between 0.02 and 0.21 mol m^{-2} s^{-1}, while simulated stomatal conductance ranged between 0.022 and 0.191 mol m^{-2} s^{-1}. The highest observed stomatal conductance has been measured with VPD at 1.64 kPa. Observed values tend to decrease at high level of VPD (above 2.5 kPa). The relation between VPD and simulated stomatal conductance has been modelled as a Gaussian function with an optimum at 0.24 mol m^{-2} s^{-1} and 1.58 kPa (k2). The highest simulated stomatal conductance has been calculated at 1.24 kPa of VPD.

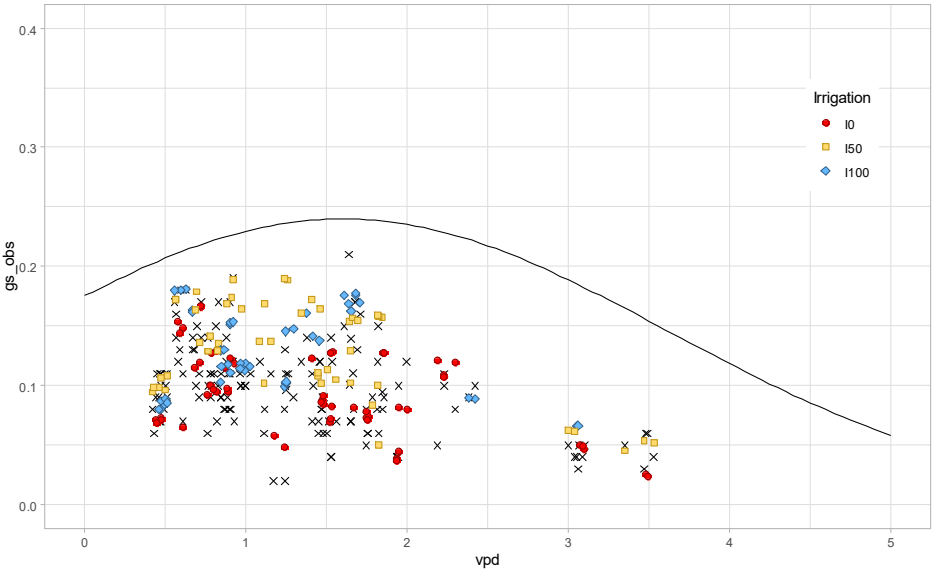

Figure 1 Stomatal conductance (gs) expressed in mol m^{-2} s^{-1} in relation to vapour pressure deficit (VPD) expressed in kPa. The observed values are shown as crosses, the simulated values are shown in different shapes and colours according to the irrigation level. The continuous line represents the equation 1.

In relation to available soil water (ASW), the maximum observed value has been observed at 71.3% of field capacity, while the minimum at 9.1% of field capacity. Observed values tend to decrease at ASW below 15% of field capacity. The relation between ASW and simulated stomatal conductance has been modelled as an exponential function with the asymptote at 0.24 mol m^{-2} s^{-1} and a slope coefficient (k7) of 6.9. The highest simulated stomatal conductance has been calculated at 57.4% of field capacity.

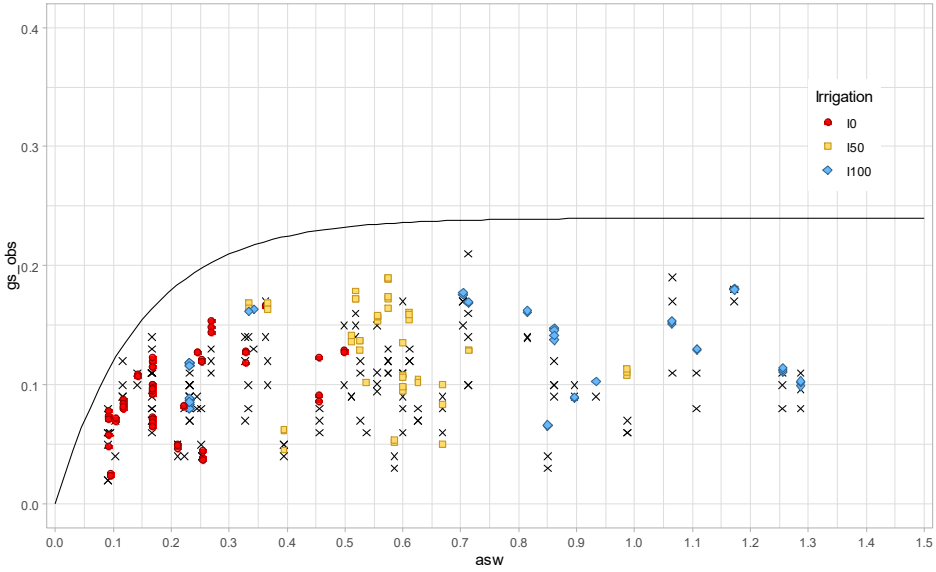

Figure 2 Stomatal conductance (gs) expressed in mol m^{-2} s^{-1} in relation to available soil water (ASW) expressed as fraction of field capacity. The observed values are shown as crosses, the simulated values are shown in different shapes and colours according to the irrigation level. The continuous line represents the equation 2.

In relation to photosynthetically active radiation (Q), the maximum observed value has been observed at 1674 mol m^{-2} s^{-1}, while the minimum at 1221 mol m^{-2} s^{-1}. The relation between

Q and simulated stomatal conductance has been modelled as a sigmoid function with the inflection point at 990 mol m^{-2} s^{-1} (k4). The highest simulated stomatal conductance has been calculated at 1655 mol m^{-2} s^{-1} and the minimum at 1398 mol m^{-2} s^{-1}.

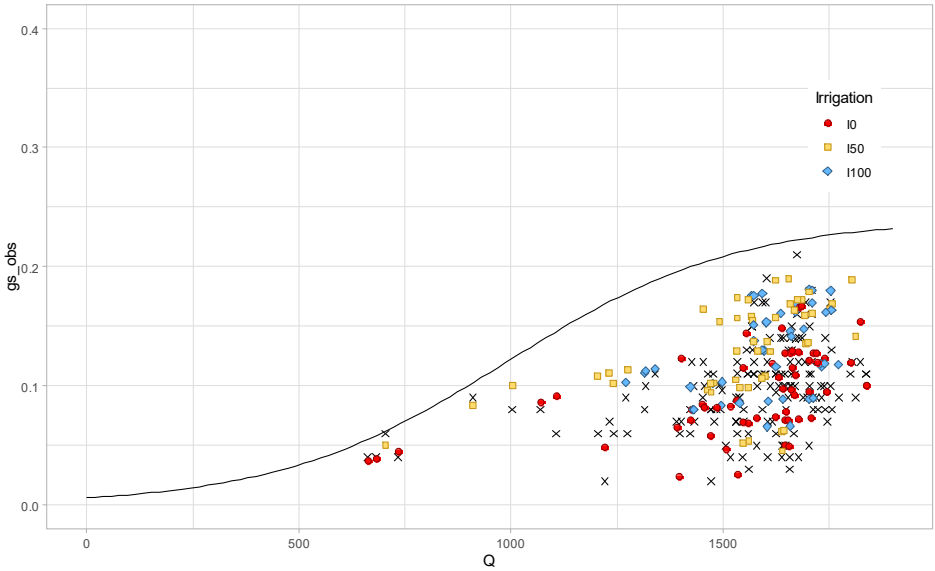

Figure 3 Stomatal conductance (gs) expressed in mol m^{-2} s^{-1} in relation to photosynthetically active radiation (Q) expressed in µmol m^{-2} s^{-1}. The observed values are shown as crosses, the simulated values are shown in different shapes and colours according to the irrigation level. The continuous line represents the equation 3.

In relation to temperature (temp), the maximum observed value has been observed at 30.5°C, while the minimum at 34.4°C. Observed values tend to decrease at temperature below 20°C or above 30°C. The relation between temperature and simulated stomatal conductance has been modelled as a Gaussian function with an optimum at 25.6°C (k10), with the parameter K11=2.2. The highest simulated stomatal conductance has been calculated at 27.4°C.

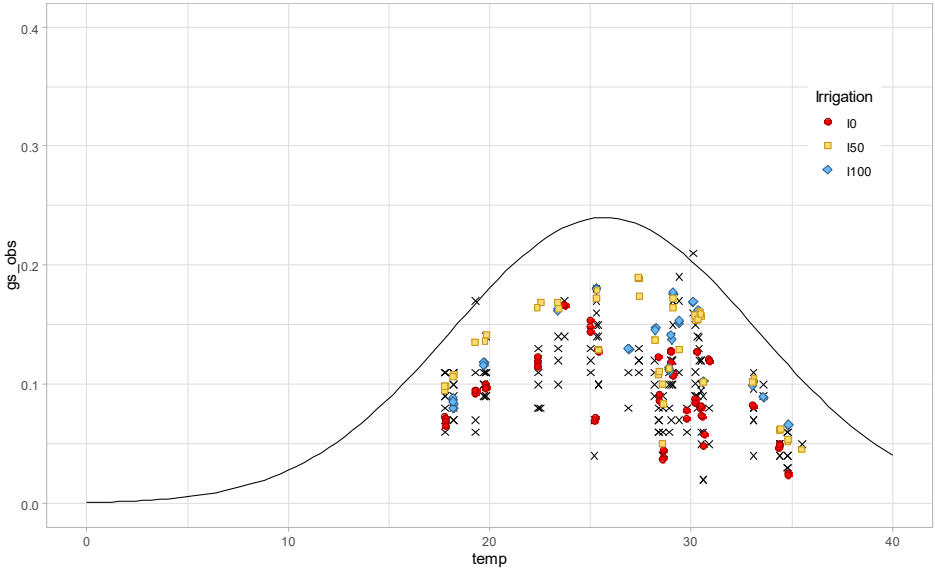

Figure 4 Stomatal conductance (gs) expressed in mol m^{-2} s^{-1} in relation to temperature (temp) expressed in °C. The observed values are shown as crosses, the simulated values are shown in different shapes and colours according to the irrigation level. The continuous line represents the equation 4.

In relation to the day of the year (doy), the maximum observed value has been observed at 161 days, while the minimum at 234 days. The relation between doy and simulated stomatal conductance has been modelled as a sigmoid function with the inflection point at 315 days (doe – k9).
The highest simulated stomatal conductance has been calculated at 158 days and the minimum at 220 days.

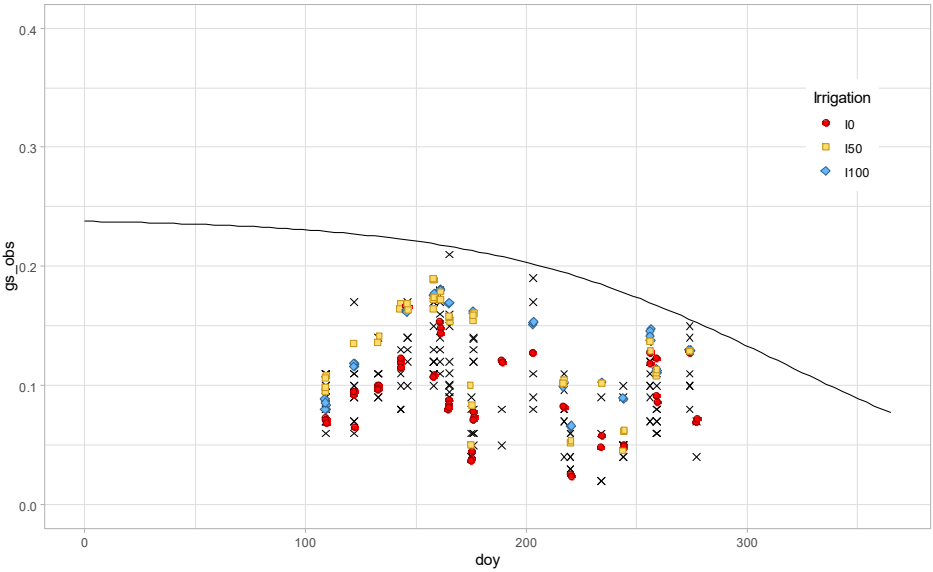

Figure 5 Stomatal conductance (gs) expressed in mol m^{-2} s^{-1} in relation to the day of the year (doy). The observed values are shown as crosses, the simulated values are shown in different shapes and colours according to the irrigation level. The continuous line represents the equation 5.

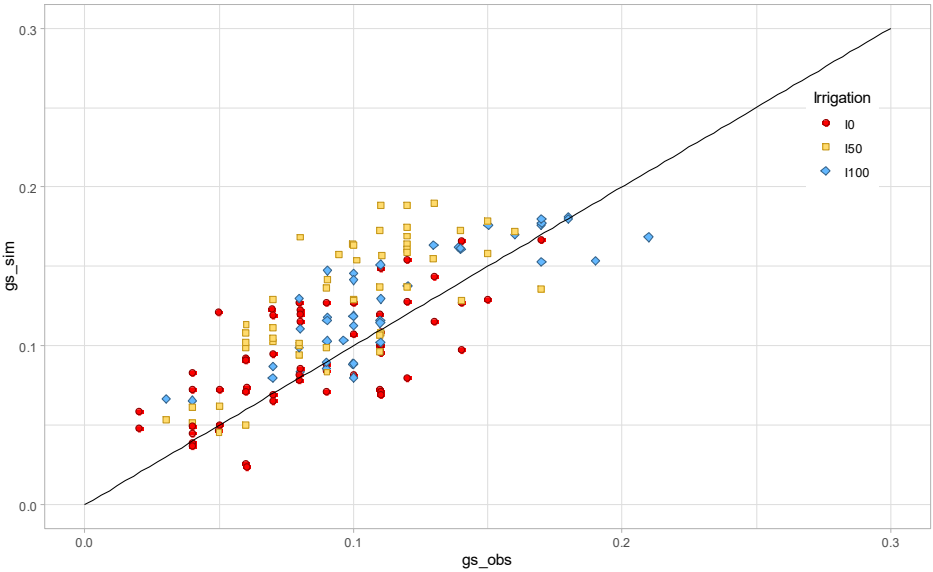

Figure 6 Relation between observed (gs_obs) and simulated values (gs_sim) of stomatal conductance expressed in mol m^{-2} s^{-1}. Values are shown in different shapes and colours according to the irrigation level. The continuous line represents the identity.

The coefficient of determination (R^2) of model predictions (gs_sim) versus observed values (gs_obs) was 0.87.

Observed net photosynthesis ranged between 5.9 and 32.4 µmol m^{-2} s^{-1}, while simulated stomatal conductance ranged between 5.8 and 30.7 µmol m^{-2} s^{-}. The highest observed net photosynthesis has been measured with the highest stomatal conductance of 0.22 mol m^{-2} s^{-1}. The relation between stomatal conductance and net photosynthesis has been modelled as an exponential function with the asymptote at 48.1 µmol m^{-2} s^{-1}. The highest simulated stomatal conductance has been calculated with a stomatal conductance of 0.191 mol m^{-2} s^{-1}.

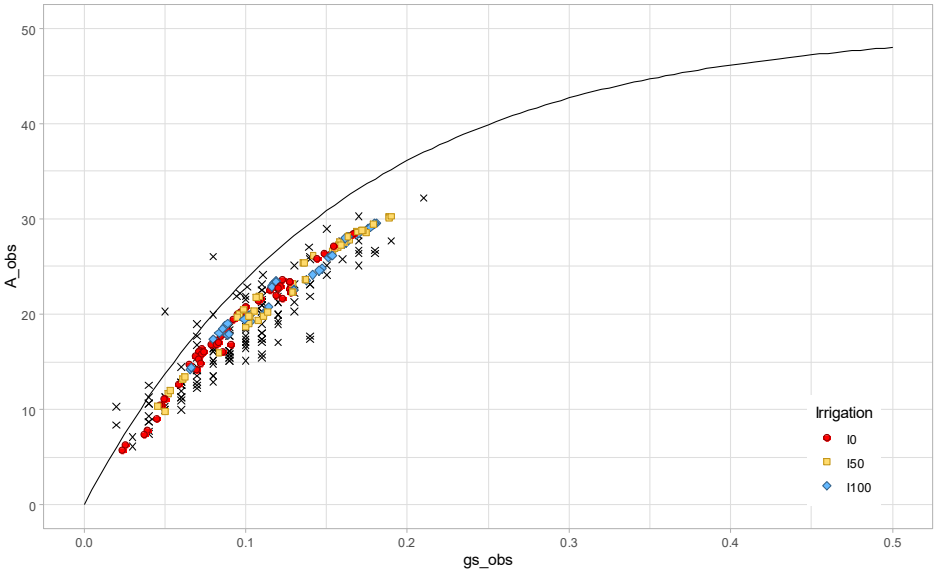

Figure 7 Net photosynthesis (A) expressed in µmol m^{-2} s^{-1} in relation to stomatal conductance (gs) expressed in mol m^{-2} s^{-1}. The observed values are shown as crosses, the simulated values are shown in different shapes and colours according to the irrigation level. The continuous line represents the equation 7.

The highest observed stomatal conductance has been measured with VPD at 1.64 kPa. Observed values tend to decrease at high level of VPD (above 2.5 kPa). The relation between VPD and simulated net photosynthesis has been modelled from the simulated values of stomatal conductance at a given VPD. The highest simulated stomatal conductance has been calculated at 1.24 kPa of VPD.

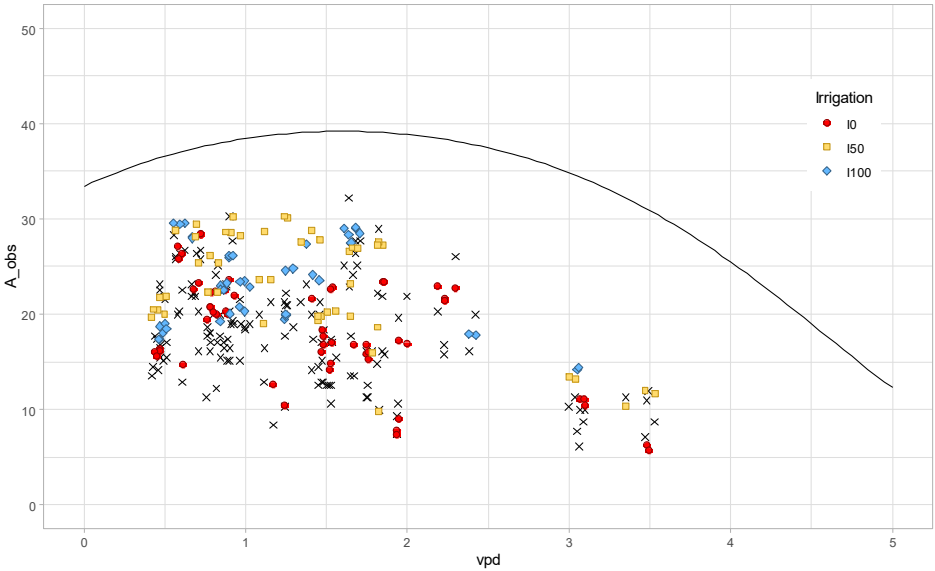

Figure 8 Net photosynthesis (A) expressed in µmol m^{-2} s^{-1} in relation to vapour pressure deficit (VPD). The observed values are shown as crosses, the simulated values are shown in different shapes and colours according to the irrigation level. The continuous line represents the equation 8.

In relation to available soil water (ASW), the maximum observed value has been observed at 71.3% of field capacity, while the minimum at 9.1% of field capacity. Observed values tend to decrease at ASW below 15% of field capacity. The relation between ASW and simulated net photosynthesis has been modelled from the simulated values of stomatal conductance at a given ASW. The highest simulated net photosynthesis has been calculated at 57.4% of field capacity.

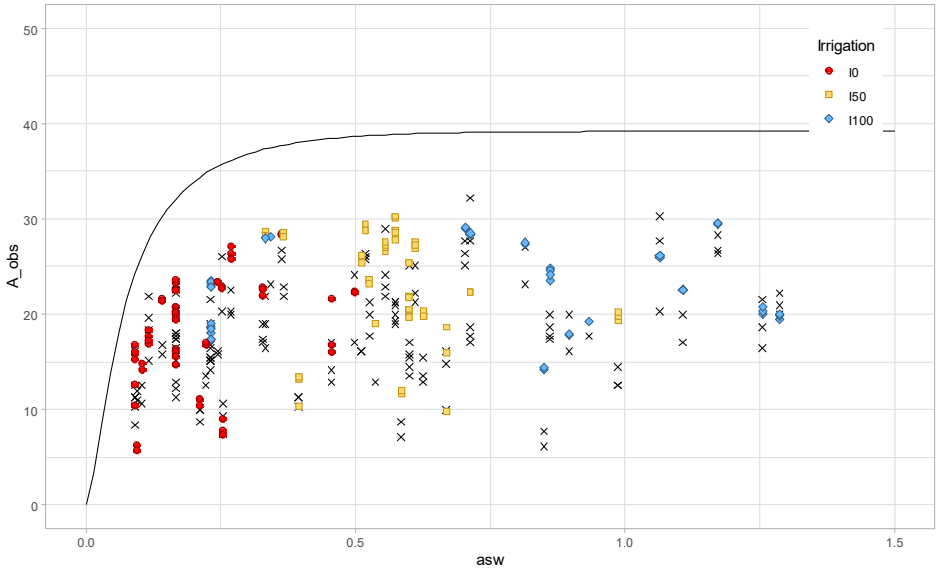

Figure 9 Net photosynthesis (A) expressed in µmol m^{-2} s^{-1} in relation to available soil water (ASW) expressed as fraction of the field capacity. The observed values are shown as crosses, the simulated values are shown in different shapes and colours according to the irrigation level. The continuous line represents the equation 9.

In relation to photosynthetically active radiation (Q), the maximum observed value has been observed at 1674 mol m^{-2} s^{-1}, while the minimum at 635 mol m^{-2} s^{-1}. The relation between Q and simulated net photosynthesis has been modelled as the product of a sigmoid function with the inflection point at 280 mol m^{-2} s^{-1} (c4) and the function that simulate net photosynthesis from the simulated values of stomatal conductance at a given Q. The highest simulated net photosynthesis has been calculated at 1655 mol m^{-2} s^{-1} and the minimum at 635 mol m^{-2} s^{-1}.

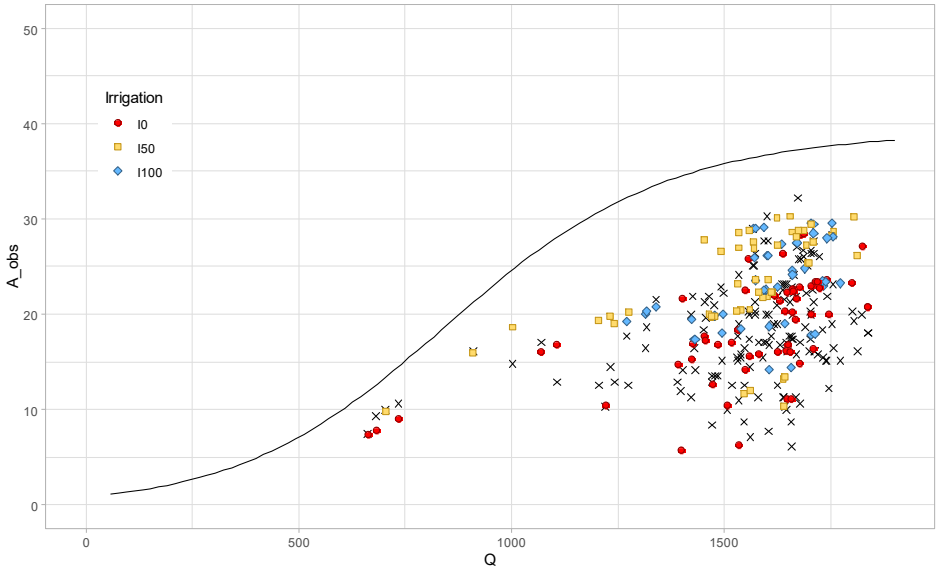

Figure 10 Net photosynthesis (A) expressed in µmol m^{-2} s^{-1} in relation to photosynthetically active radiation (Q) expressed in µmol m^{-2} s^{-1}. The observed values are shown as crosses, the simulated values are shown in different shapes and colours according to the irrigation level. The continuous line represents the equation 10.

In relation to temperature (temp), the maximum observed value has been observed at 30.5°C, while the minimum at 34.4°C. Observed values tend to decrease at temperature below 20°C or above 30°C. The relation between temperature and simulated net photosynthesis has been modelled as the product of a Gaussian function with an optimum at 25.7°C (c2), with the parameter c3=1.8, and the function that simulate net photosynthesis from the simulated values of stomatal conductance at a given temperature. The highest simulated net photosynthesis has been calculated at 27.4°C.

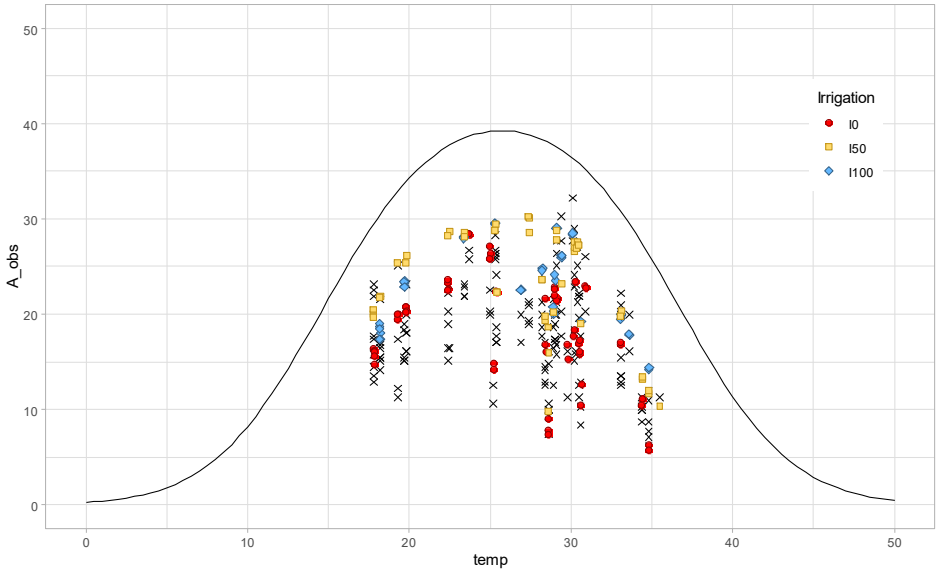

Figure 11 Net photosynthesis (A) expressed in µmol m^{-2} s^{-1} in relation to temperature (temp) expressed in °C. The observed values are shown as crosses, the simulated values are shown in different shapes and colours according to the irrigation level. The continuous line represents the equation 11

In relation to CO_2 concentration in the atmosphere (carbon), the maximum observed value has been observed at 403 ppm, while the minimum at 395 ppm. The relation between CO_2 concentration and simulated net photosynthesis has been modelled as an exponential function with a slope coefficient (c5) of 0.008.
The highest simulated net photosynthesis has been calculated at 392 ppm and the minimum at 395 ppm.

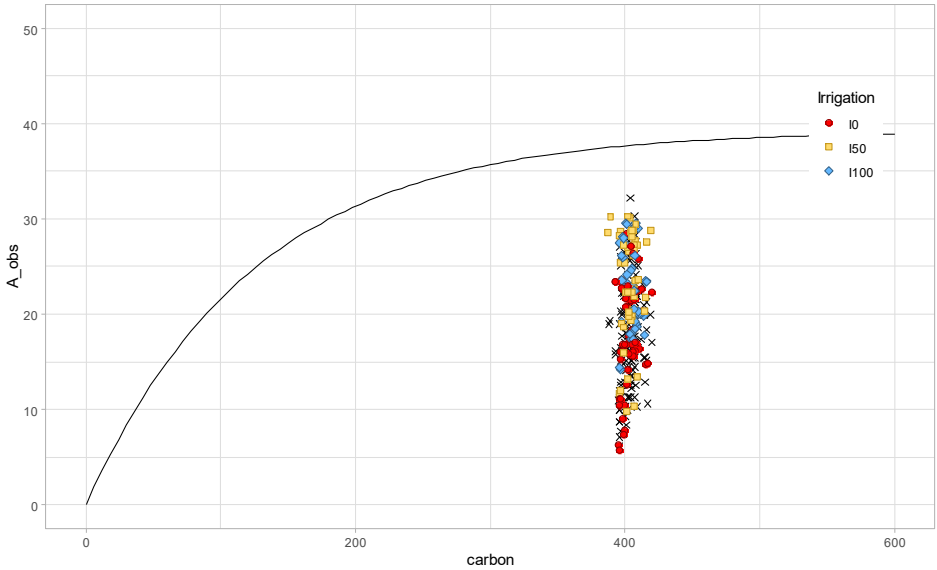

Figure 12 Net photosynthesis (A) expressed in µmol m^{-2} s^{-1} in relation to CO_2 concentration in the atmosphere (carbon) expressed in ppm. The observed values are shown as crosses, the simulated values are shown in different shapes and colours according to the irrigation level. The continuous line represents the equation 12.

In relation to the day of the year (doy), the maximum observed value has been observed at 161 days, while the minimum at 234 days. The relation between doy and simulated net photosynthesis has been modelled as the product of a sigmoid function with the inflection point at 315 days (doe – c9) and the function that simulate net photosynthesis from the simulated values of stomatal conductance at a given doy.
The highest simulated net photosynthesis has been calculated at 158 days and the minimum at 220 days.

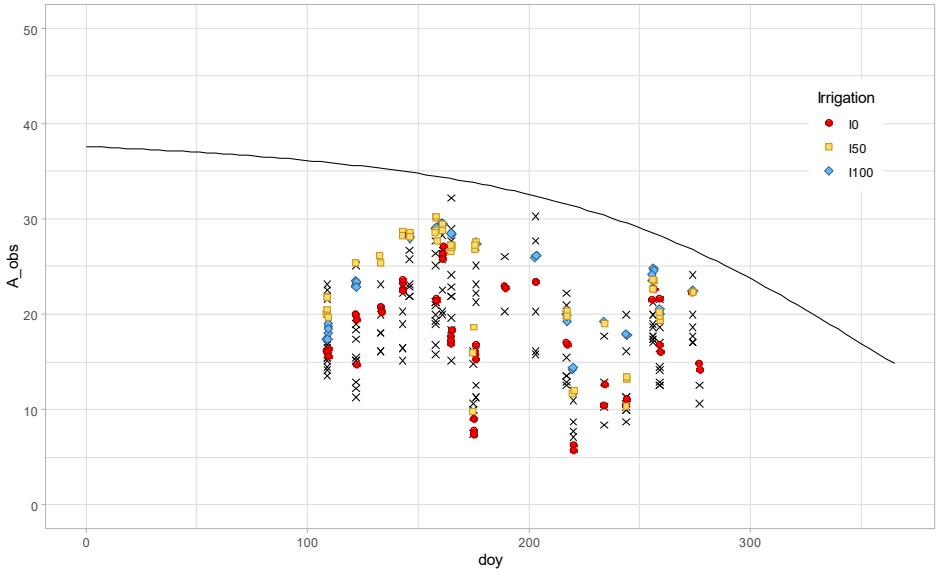

Figure 13 Net photosynthesis (A) expressed in µmol m^{-2} s^{-1} in relation to the day of the year (doy). The observed values are shown as crosses, the simulated values are shown in different shapes and colours according to the irrigation level. The continuous line represents the equation 13.

The coefficient of determination (R^2) of model predictions (A_sim) versus observed values (A_obs) was 0.89.

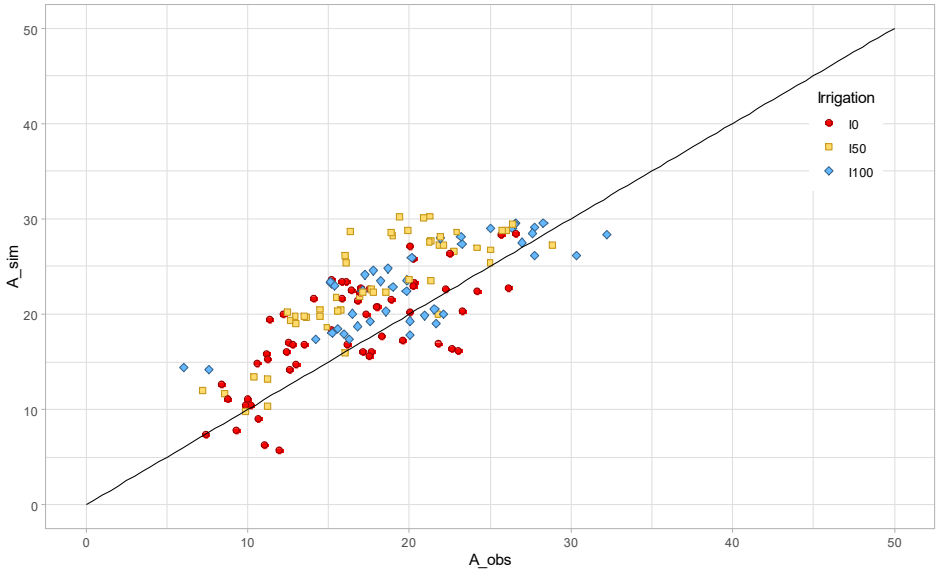

Figure 14 Relation between observed (A_obs) and simulated values (A_sim) of net photosynthesis rate expressed in µmol m^{-2} s^{-1}. Values are shown in different shapes and colours according to the irrigation level. The continuous line represents the identity.

4.3 References

Allen, R. G., Pereira, L. S., Raes, D., & Smith, M. (1998). Crop evapotranspiration-Guidelines for computing crop water requirements-FAO Irrigation and drainage paper 56. *Fao, Rome*, *300*(9), D05109.

5 Assessment of giant reed biomass potential (*Arundo donax* L.) In marginal areas of Italy via the application of Arungro simulation

5.1 Introduction

The identification of solutions to ethical concerns dealing with competition for land between food/feed and energy crops is a hot topic in the international public debate. The International Renewable Energy Agency (IRENA, 2016), which is in charge of supporting countries in their transition to a sustainable energy future, identified several actions to expand bioenergy production "without competing with food production or causing land use change". In this context, the recovery of marginal areas (MAs - i.e. areas with low productivity and profitability, which are prone to land abandonment (Sallustio et al., 2016)) to grow perennial, non-food and low-input energy crops represents a promising solution to produce renewable energy at low cost, while preserving environmental sustainability. Besides natural constraints to productivity, the cultivation of conventional crops in MAs is expected to become even less convenient in the near future due to projected detrimental effects of climate change on crop productivity and yield stability in Mediterranean countries, especially under no adaptation (Supit et al., 2012; Donatelli et al., 2015). As a result, farmers will be probably forced to use larger amounts of inputs to alleviate expected yield losses due to higher frequency of heat waves and drought during crucial phenological phases, with water playing a key role.

Among non-food energy crops, giant reed (*Arundo donax* L.) is an invasive high-yielding, low-input C3 perennial species, tolerant to a broad spectrum of soil conditions, and suitable as a feedstock for anaerobic digestion, as well as for electric and thermal energy production (Perdue et al., 1958). Giant reed

provides higher energy production per hectare than conventional crops in Italian environments, due to the favourable relationship between productivity, environmental sustainability and inputs/cost needed to achieve them (Schievano et al., 2012; Ceotto et al., 2013). Furthermore, model-based studies have shown that giant reed grown under optimal water conditions would even be able to increase biomass production rates in the future, both in plain (Cappelli et al., 2015) and in marginal wet areas around river beds in Northern Italy (Pedrazzi et al., 2017; Allesina et al., 2018; Ginaldi et al., 2018). However, the assessment of climate change impact on the productivity of this species under rainfed condition is still an open issue, despite the crucial implications for mid-term planning policies.

The main objective of this research was an extensive evaluation of future trends of giant reed rainfed productivity in MAs of Italy in the short and medium term, via the spatially explicit application of the process- based Arungro model (Stella et al., 2015). The analysis was conducted at 500 m spatial resolution by integrating the state-of-the art of crop growth models, IPCC climate change scenarios and databases with detailed information on soil physical/chemical properties, marginality and crop suitability to environment.

5.2 Materials and methods

5.2.1 *Model description*

The Arungro model was used for the simulation of giant reed development and growth, considering soil water balance and site-specific agricultural practices (i.e. transplanting and cutting times, stand density, irrigation scheduling and water supply). Arungro simulates gross photosynthesis and respiration costs to estimate net carbon fixation, depending on radiation interception and crop transpiration. The model provides a detailed

description of leaf area index dynamics at shoot and plant levels, considering leaf width/length heterogeneity on a single stem and among stem cohorts. The evolution of the stem number is simulated based on thermal time, with emission of new tillers regulated by rhizome biomass during sprouting.
The limitation to giant reed rates of gross photosynthesis due to soil water availability was simulated by a stress function (0^{-1}, 1 = no stress) based on the ratio between root water uptake and crop transpiration. Root water uptake was computed according to potential evapotranspiration demand, soil water content and root depth, based on the EPIC model (Williams et al., 1989). The soil water dynamics are simulated using a tipping- bucket approach (Ritchie et al., 1985), assuming that water can flow to downward soil layers when field capacity of the above layers is exceeded. For each layer, maximum and minimum soil water content were initialized at field capacity (m^3 m^{-3}) and wilting point (m^3 m^{-3}), respectively, with daily precipitation (mm) or irrigation (mm) refilling the soil water content.
The decline in biomass accumulation during the plant lifetime after the peak of production is not simulated. Model calibration and spatially distributed simulations were carried out under non-limiting conditions for nutrients, pests and weeds.

5.2.2 *Calibration*

Arungro was calibrated using multi-year experimental datasets collected in six locations across Italy in the period 1997-2013, in both rainfed and irrigated systems, under non-limiting conditions for nitrogen availability (**Figure** 1; **Table** 1).

Figure 1: Geographic distribution of experimental field datasets used in calibration.

The minimum experimental dataset to set-up the calibration included information related to transplanting and cutting times, stand density, water management and soil texture, as well as multiple in-season measurements of green leaf area index (GLAI, $m^2\ m^{-2}$), aboveground biomass (AGB, Mg ha^{-1}) and volumetric soil water content (SWC, $m^3\ m^{-3}$), the latter for water-limited experiments.

Table 1. Characterization of field experiments used in calibration.

	Landriano	Anzola	Ozzano	Pisa	Bellizzi	Catania
Years	2010-2013	2007-2011	1998-2007	2003-2004	2011-2013	1997-1999
Stand density *(rhizomes m^{-2})*	0.3	2.78	1.1	2.0	1.0	2.5
Soil	Silty-loam	Silty-loam	Clay-loam	Loam	Clay-loam	Sandy-clay-loam
Nitrogen *(kg ha^{-1})*	120	120	120	100	150	120
Water	NL	NL	Rainfed	NL	Rainfed	100, 50, 0% ET
Tavg *(°C)*	14.9 ± 8.6	15.1 ± 8.5	14.8± 8.5	17.1 ± 7.8	17.9 ± 6.7	18.5 ± 6.3
Rain *(mm)*	758 ± 80	632 ± 198	440 ± 237	766	702 ± 175	378 ± 148
AGB *(Mg ha^{-1})*	31 -74	41-61	15-26	30-32.5	19-22.5	38.5-42.8
Source	[12]	[7]	[15]	[16]	[17]	[18]

Daily minimum and maximum air temperatures (°C), cumulative rainfall (mm) and average wind speed (m s^{-1}) were retrieved from National Centers for Environmental Information (NOOA, https://www.ncdc.noaa.gov/) database. Global solar radiation (MJ m−2 d −1) was estimated based on Hargreaves and Samani (Hargreaves et al., 1982) equation. Field capacity and wilting point at model initialization were estimated according to the method of Wösten et al. (Wösten, 1999).

The parameters connected to leaf expansion and photosynthesis were tuned within the biophysical ranges reported in literature to achieve the highest accuracy between observed and simulated data. The multi-start downhill simplex (Acutis and Confalonieri, 2006) was used as optimization algorithm, and the average root mean square error (RMSE, minimum and optimum=0; maximum=+∞, it quantifies the average difference between simulated and measured data in the unit of the analysed variable; values lower than half of the standard deviation of the measurements reveal good results, (Moriasi et al., 2007) was chosen as objective function and evaluated after each iteration. The automatic optimization ended when the difference of RMSE between consecutive iterations felt below a tolerance fixed range. Besides RMSE, model performances in calibration were quantified using other standard metrics in crop modeling studies, as relative root mean square error (RRMSE, minimum and optimum=0%; maximum=+∞, (Jørgensen et al., 1986)), coefficient of residual mass (CRM, minimum=-∞, maximum=+∞, optimum=0, unitless, (Loague et al., 1991); if positive indicates model underestimation and vice versa) and the modelling efficiency (EF, minimum=-∞, optimum and maximum=1, unitless, (Nash, 1970); if positive, the model is a better predictor than the mean of measured values and results can be considered acceptable, (Moriasi et al., 2007).

5.2.3 *Spatially distributed simulation*

The Arungro model was coupled with a georeferenced database including information on baseline and climate change scenarios, farming practices, soil properties, marginality and crop suitability to environments (**Figure** 2).

Daily downscaled weather data (0.25° spatial resolution) for current and future climate conditions were retrieved from Duveiller et al. (Duveiller et al., 2017), who generated 30- year bias-corrected synthetic series using three climate models – DMIHIRHAM5-ECHAM5, ETHZ- CLMHadCM3Q0, METO-HCHadRM3Q0-HadCM3Q0 – for the IPCC emission scenario A1B (i.e. the most extreme among those provided by the IPCC's Fourth Assessment Report). Time frames centered on near past (2000), and future (2020 and 2030) were considered.

The minimum dataset of pedological characteristics including field capacity and wilting point was derived, on the fly, via pedo-transfer functions (Wösten, 1999), by soil texture and organic matter data available at 500 x 500 m resolution across Italy (L'Abate et al., 2020). Texture data were considered within the useful soil depth, i.e. soil profile without physical constraints to the deepening of roots.

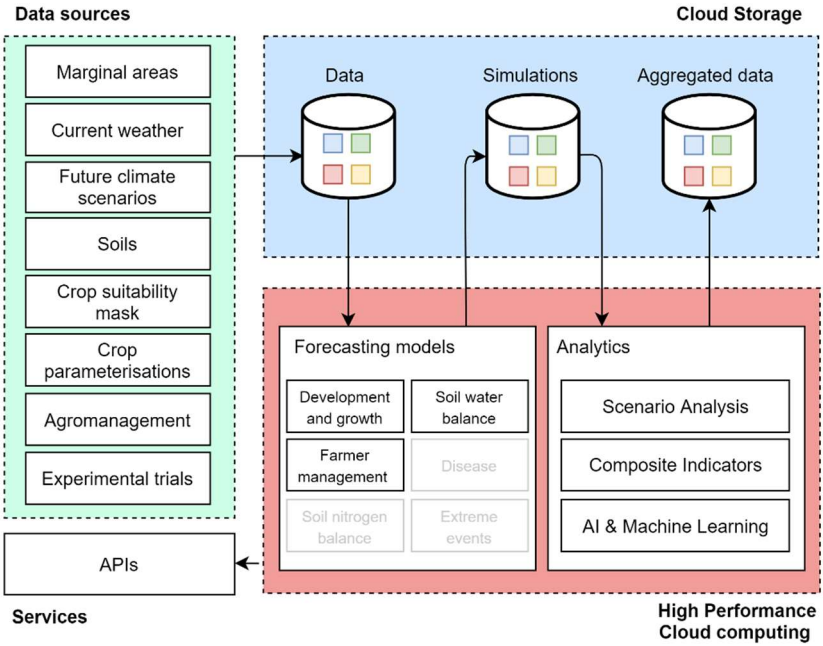

Figure 2: Schematic representation of the simulation environment developed for the AGROENER project (http://agroener.crea.gov.it/).

Maps of soil marginality and crop suitability were produced at 250 m spatial resolution in the framework of the AGROENER project [2, 28]. Marginal areas (i.e. MAs) were defined as non-protected areas, without natural constraints to productivity and an Average Value of Agricultural Land (AVAL) lower than the mean regional AVAL. Three classes of marginality were identified: i) high (< 30% of AVAL), intermediate (30– 60% of AVAL), and low (60–99% of the AVAL). The suitability assessment was based on a fuzzy Multi- Criteria Analysis, in which fuzzy functions were applied to score land suitability according to multiple environmental factors; the scores were then aggregated in a final suitability index ranging from 0 (no suitability) to 1 (complete suitability). Finally, three classes of

suitability were identified: (i) suitable land (score = 0.90- 1.00); (ii) marginally suitable land (score = 0.70-0.89); and (iii) low suitable land (score = 0.00-0.699).
Site-specific transplanting data were derived according to literature and expert knowledge. Cutting date was set at the end of November - i.e. before leaf senescence.
Soil grid-cells were defined as simulation units (SU) and georeferenced layers were univocally assigned to each SU depending on spatial attributes (i.e. geographic coordinates of centroids), via the use of GIS-based software applications according to Ginaldi et al. (Ginaldi et al., 2019). As a result, a total of 81,078 SUs was defined, considering high/intermediate marginality and high suitability classes. For each combination of IPCC emission scenario (1) × climate model (3) × time frame (3) × year (30) × grid cell (81,078) simulations were performed under water-limited conditions. The total number of simulations was 21,891,060, by considering all the possible combinations of the factors tested.

5.2.4 *Analysis of results*

Model outputs achieved in calibration were used to plot simulated daily dynamics of AGB and LAI versus reference data, distinguishing by site and production level (full irrigated vs rainfed) and to produce a table showing the statistical indices of agreement between simulated and measured data. The outputs of 30-year spatially distributed simulations were i) used to draw boxplots presenting the overall variability of AGB and water use efficiency (WUE, g l^{-1} ; i.e. the ratio between simulated AGB to cumulative potential evapotranspiration from re- sprouting to harvest) in the baseline and 2030, and ii) averaged on each grid cell, considering each combination emission scenario × climate model × time frame, and then used to evaluate the impact of climate change as percentage

difference compared to the baseline. This exploratory study focused on the grid-cells belonging to the provinces of Catania and Bologna, which were characterized by contrasting weather conditions and well represented in the calibration dataset. The combination ETHZ−CLM−HadCM3Q0 × 2030 time frame was selected as target climate change scenario, since representing the intermediate realization of A1B scenario among the three available (i.e. average temperature increases up to 1.4 °C and average decrease in cumulative daily precipitation up to -30% in the period April-September). As a result, the total number of simulations herein presented is 359,520 by considering the combination of IPCC emission scenario (1) × climate model (1) × time frame (2) × year (30) × grid cell (5,992).

5.3 Results and discussion

5.3.1 *Calibration*

The simulated dynamics of AGB (Mg ha^{-1}) and GLAI (m2 m -2) in the field trials used in calibration are presented in **Figure** 3 and 4, whereas the values of the statistical indices of agreement between simulated and observed data are presented in **Table** 2.

Table 2. Performances in reproducing leaf area index (GLAI, m2 m -2) and aboveground biomass (AGB, Mg ha- 1) in model calibration. RMSE: root mean square error (m 2 m -2 for GLAI and Mg ha^{-1} for AGB); RRMSE: relative root mean square error (%); EF: model efficiency (unitless); CRM: coefficient of residual mass (unitless).

Variable	Statistical indices			
	RMSE	*RRMSE*	*EF*	*CRM*
GLAI	1.73	32.52	0.70	0.13
AGB	6.47	27.96	0.81	0.11

The model accurately simulated the evolution of both growth variables along the vegetative season in all the experiments, with average RMSE of 1.73 m2 m -2 for GLAI (RRMSE=32.52%)

and of 6.47 Mg ha^{-1} for AGB (RRMSE=27.96%). Arungro explained the 78% and 85% of the year-to-year variability of GLAI (EF=0.70) and AGB (EF=0.81). Larger errors corresponded to the first year experiment in Pisa and the second year experiment in Bellizzi and Landriano, where Arungro underestimated both maximum GLAI and final AGB of about 3.6 m2 m^{-2} and 7.2 Mg ha^{-1}, respectively. CRM values indicated a systematic underestimation of GLAI (CRM=0.13) at mid and late vegetative stages, which resulted in an underestimation of AGB at the same phenological stage (CRM=0.11). Unexpectedly, in the third year experiment at Landriano the model markedly underestimated final AGB despite GLAI was correctly simulated. In this trial, the exceptional low values of measured GLAI compared to final AGB data were probably due to the device used to estimate this variable - i.e. PocketLAI - which denoted a saturation effect for GLAI values higher than 5 m^2 m^{-2}, especially for giant reed (Francone et al., 2014).

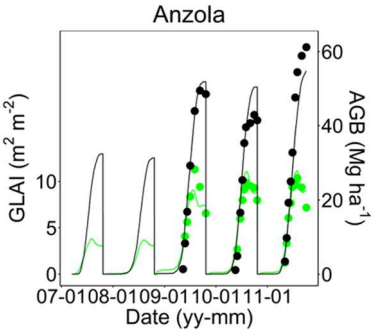
Anzola
GLAI (m² m⁻²)
AGB (Mg ha⁻¹)
0
5
10
0
20
40
60
07-01
08-01
09-01
10-01
11-01
Date (yy-mm)

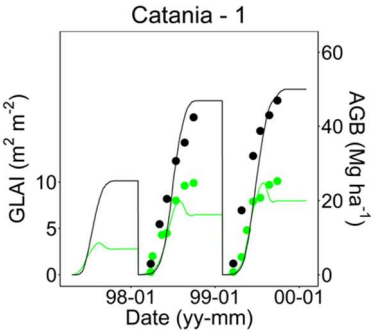
Catania - 1
GLAI (m² m⁻²)
AGB (Mg ha⁻¹)
0
5
10
0
20
40
60
98-01
99-01
00-01
Date (yy-mm)

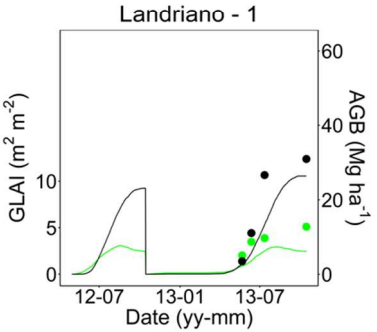
Landriano - 1
GLAI (m² m⁻²)
AGB (Mg ha⁻¹)
0
5
10
0
20
40
60
12-07
13-01
13-07
Date (yy-mm)

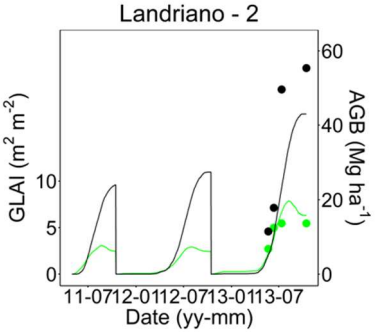
Landriano - 2
GLAI (m² m⁻²)
AGB (Mg ha⁻¹)
0
5
10
0
20
40
60
11-07
12-01
12-07
13-01
13-07
Date (yy-mm)

Pisa

Figure 3: Model performances in reproducing the dynamics of the green LAI (GLAI, green line) and the aboveground biomass (AGB, black line) during the vegetative season of giant reed. Measurements of GLAI (green dots) and AGB (black dots) were collected at the experimental sites in **Table** 1 from plots with no water stress and with different combinations of stand densities and harvest times.

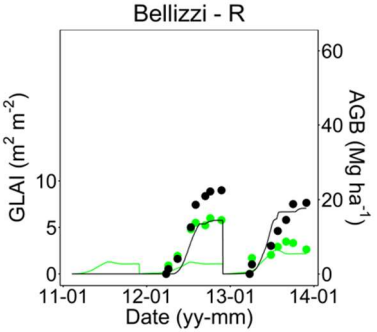
Bellizzi - R
GLAI (m2 m-2)
AGB (Mg ha-1)
0
5
10
0
20
40
60
11-01
12-01
13-01
14-01
Date (yy-mm)

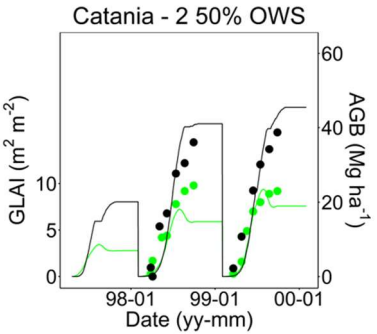
Catania - 2 50% OWS
GLAI (m2 m-2)
AGB (Mg ha-1)
0
5
10
0
20
40
60
98-01
99-01
00-01
Date (yy-mm)

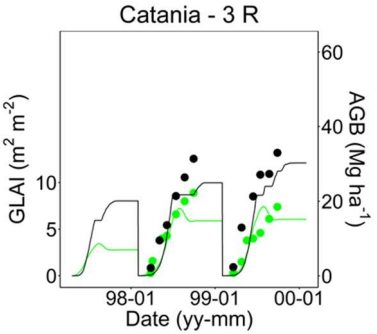
Catania - 3 R
GLAI (m2 m-2)
AGB (Mg ha-1)
0
5
10
0
20
40
60
98-01
99-01
00-01
Date (yy-mm)

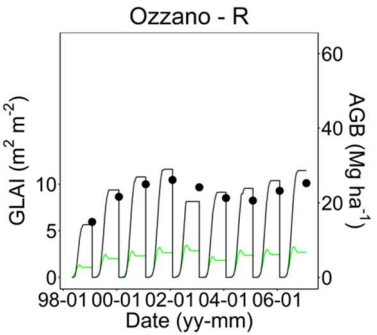
Ozzano - R
GLAI (m2 m-2)
AGB (Mg ha-1)
0
5
10
0
20
40
60
98-01
00-01
02-01
04-01
06-01
Date (yy-mm)

Figure 4: Model performances in reproducing the dynamics of the green LAI (GLAI, green line) and the aboveground biomass (AGB, black line) during the vegetative season of giant reed. Measurements of GLAI (green dots) and AGB (black dots) were collected at the experimental sites in **Table** 1 from plots with water limitation (OWS: optimum water supply, R: rainfed) and with different combinations of stand densities and harvest times.

In Catania, Arungro accurately reproduced the decrease in GLAI and AGB according to lower water availability, from full (i.e. 100% ET restitution) to medium (i.e. 50% ET restitution) and no irrigation treatments (i.e. 0% ET restitution), even if the dynamics of the simulated data were slightly delayed compared to the measured ones. As a matter of fact, the underestimation of GLAI in the early vegetative phase delayed the GLAI increase before the maximum number of tiller was reached, which in turn resulted in delayed rates of biomass accumulation. The underestimation of the GLAI value simulated at harvest was instead due to a more rapid onset of simulated leaf senescence compared to field measurements. In the second year experiment at Bellizzi, the overestimation of simulated water stress and suboptimal temperature conditions at early stages of crop development led to a low number of both simulated tillers and leaves, which resulted in reduced GLAI and AGB values. The model correctly simulated biomass values achieved in experimental sites of Emilia Romagna, with an increasing trend from rainfed (Ozzano) to non-limiting conditions for water availability (Anzola). Despite field trials were conducted on soils with similar characteristics, the climate of Anzola was characterized by very favourable precipitation amounts during giant reed growing season (average of 632 mm compared to the 440 mm in Ozzano) and more suitable temperatures for development and growth (mean temperature of 15.1 °C instead of 14.7 °C in Ozzano).

5.3.2 *Spatially distributed simulation*

The distribution of simulated AGB and WUE values in baseline and 2030 time frame for Bologna and Catania provinces is shown as boxplots in **Figure** 5 and 6. Average AGB simulated in 2030 and related variability remained almost unchanged compared to the baseline in both provinces, with values fluctuating around 20 and 22 Mg ha^{-1} respectively. The anticipation of the closed canopy stage and reduced thermal limitation to photosynthesis simulated under warmer scenarios were counteracted by higher transpiration rates, leading to average $^{-1}$0% decreases in WUE (**Figure** 6), regardless the province considered. Expected increases in water demand, together with the higher incidence of simulated water shortage even in water-rich areas determined less optimistic projections compared to previous studies carried out in Northern Italy, in which predicted gains in productivity under optimal water conditions were in the range +5/10% in MAs of Emilia Romagna (Ginaldi et al., 2018) and +20% in MAs of Lombardy plain (Cappelli et al., 2015).

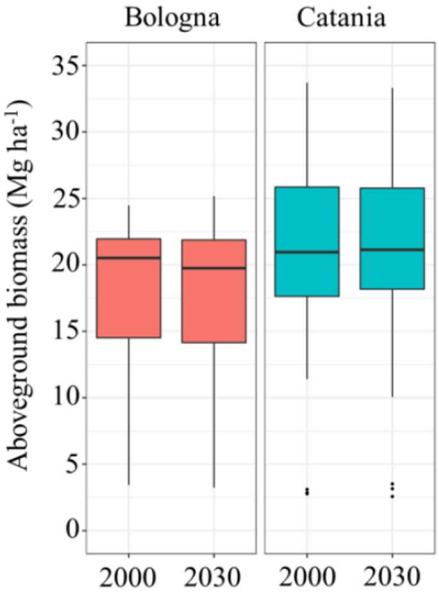

Figure 5: Boxplots of absolute aboveground biomass (AGB, Mg ha^{-1}) values simulated for the baseline (2000) and 2030 in the marginal areas of Bologna and Catania provinces. Each box derives from the values simulated for the combination year (30) × simulation units (1226 in Bologna; 4765 in Catania).

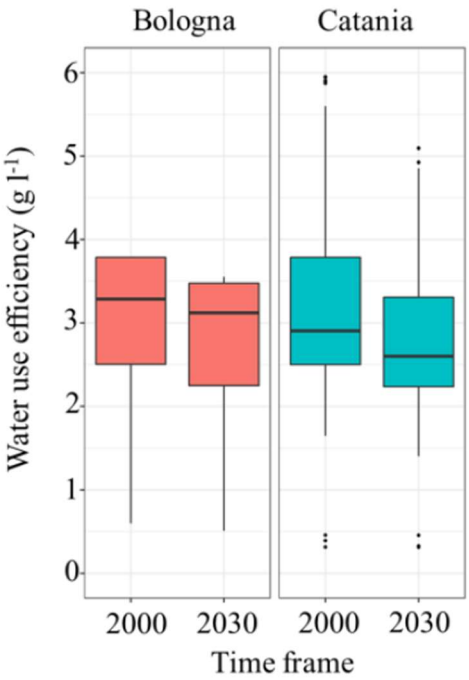

Figure 6: Boxplots of absolute water use efficiency (g l^{-1}) values simulated for the baseline (2000) and 2030 in the marginal areas of Bologna and Catania provinces. Each box derives from the values simulated for the combination year (30) × simulation units (1226 in Bologna; 4765 in Catania).

The spatial representation of AGB % variations compared to the baseline presented large heterogeneity of results across the study area, without outlining a clear geographic pattern (**Figure** 7). According to the spatial resolution of input data used, results revealed a predominant role of soil characteristics versus weather conditions in determining the spatial variability of AGB across the province, with soil texture and depth playing a key role. More than 1,200 SUs presented positive variations in the

range +1/+15%, whereas more than 1,500 SUs showed relative changes less than ±1 %. The 97% of remaining SUs showed declines in terms of biomass production ranging from $^{-1}$ to -5%, suggesting that, in these areas, thermal regimes are already close to the optimum for the species under baseline scenario.

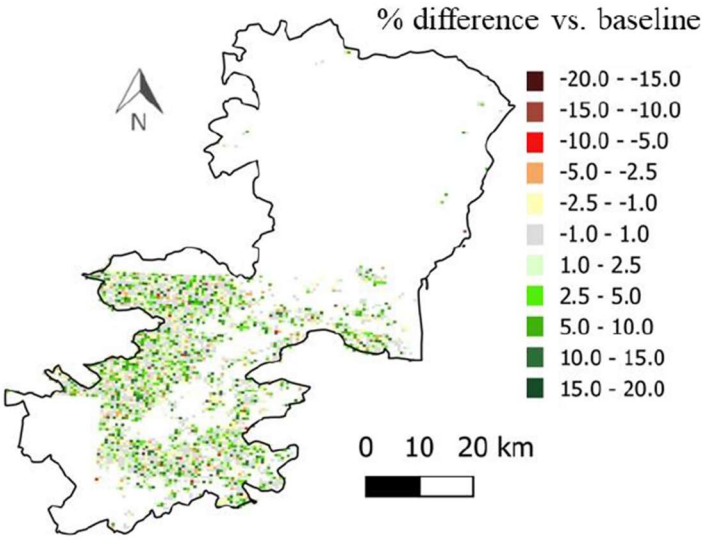

Figure 7: Percentage differences of aboveground biomass simulated in 2030 with respect to the baseline in the Catania province.

Conversely, results achieved for WUE (**Figure** 8) were decidedly less variable across the province and confirmed that a larger amount of water will be needed to maintain the current production levels under future scenarios in 94% of SUs. This means that SUs characterized by soils with low water holding capacity, such as shallow or sandy soils, could be no longer suitable to giant reed in the short term under intermediate climate projections.

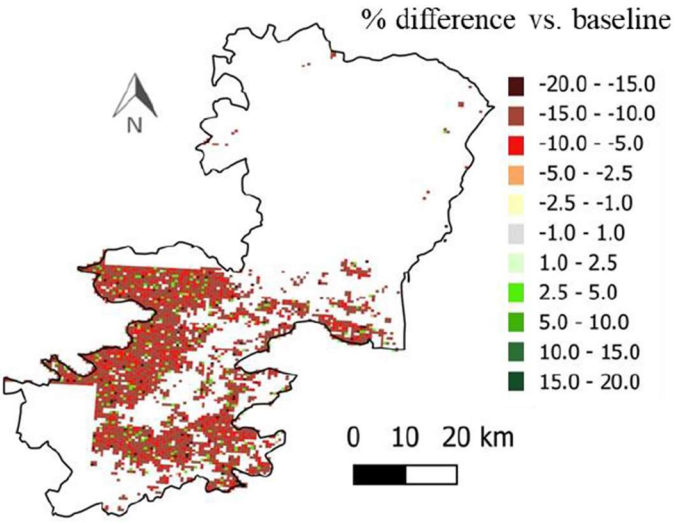

Figure 8: Percentage differences of water use efficiency simulated in 2030 with respect to the baseline in the Catania province.

Nevertheless, the results obtained here should be considered as encouraging; as a matter of fact, the noticeable tolerance for drought of this species will allow achieving higher biomass productions in most SUs. The variability in results confirms how they cannot be generalized to other provinces or MAs with different pedo-climatic conditions but, they should rather be analyzed locally, looking for site specific solutions.

5.4 Concluding remarks

Few studies on the prediction of the future trends of energy crops productivity in marginal areas under climate change scenarios have been carried out so far. We focused here on giant reed, considering the state-of-the art of crop growth models, an ensemble of climate change projections and databases with detailed information on Italian soil properties, marginality and crop suitability to environment. At field level, Arungro proved

to be capable of reproducing multiple in-season measurement of green leaf area index and aboveground biomass under varying management practices and pedo-climatic conditions. A slight general systematic underestimation of both variables was due to delayed leaf appearance and biomass accumulation simulated before the maximum number of tillers was reached. At province level, our study indicates a general stability in giant reed suitability over time and a large heterogeneity between spatial areas, depending on weather and soil characteristics considered. The expected gains in productivity due to the anticipation of the closed canopy stage and reduced thermal limitation to photosynthesis simulated under warmer scenarios were counterbalanced by higher transpiration rates, which markedly reduced water use efficiency. The consideration of local/regional-scale heterogeneity and water limitation to crop productivity allowed to i) identify critical spots and opportunities within the study area with high resolution detail and ii) to avoid overestimations in AGB projections compared to available studies performed in Northern Italy under potential conditions for water availability. This preliminary study should be extended to other Italian provinces and energy crops and may represent the basis for further analyses accounting for water use efficiency under increased atmospheric CO2 concentration and/or the consideration of qualitative aspects of production in order to identify the optimal harvest time according to the biochemical characteristics of raw materials and their destination. Despite the explicit limitations and assumptions, our work provides plausible indications on giant reed productivity trends in the short and medium term, which can be of interest for different stakeholders to expand Italian bioenergy production in a sustainable way.

5.5 References

M. Acutis, R. Confalonieri, Optimization algorithms for calibrating cropping systems simulation models. A case study with simplex-derived methods integrated in the WARM simulation environment, Italian Journal of Agrometeorology, 11 Vol. (2006), pag. 26.

G. Allesina, S. Pedrazzi, F. Ginaldi, G.A. Cappelli, M. Puglia, N. Morselli, et al.,. Energy production and carbon sequestration in wet areas of Emilia Romagna region, the role of *Arundo donax*, Advances in Modelling and Analysis A, 55 Vol. (2018), pag. 108.

A. Bonfante, A. Impagliazzo, N. Fiorentino, G. Langella, M. Mori, M. Fagnano, Supporting local farming communities and crop production resilience to climate change through giant reed (*Arundo donax* L.) cultivation: An Italian case study, Science of the Total Environment, 601 Vol. (2017), pag. 603.

G. Cappelli, S.S. Yamaç, T. Stella, C. Francone, L. Paleari, M. Negri, R. Confalonieri, Are advantages from the partial replacement of corn with second- generation energy crops undermined by climate change? A case study for giant reed in Northern Italy, Biomass and Bioenergy, 80 Vol. (2015), pag. 85.

E. Ceotto, M. Di Candilo, F. Castelli, F.-W. Badeck, F. Rizza, C. Soave, et al., Comparing solar radiation interception and use efficiency for the energy crops giant reed (*Arundo donax* L.) and sweet sorghum (*Sorghum bicolor* L. Moench), Field Crops Research, 149 Vol. (2013), pag. 159.

S.L. Cosentino, C. Patanè, E. Sanzone, G. Testa, D. Scordia, Leaf gas exchange, water status and radiation use efficiency of

giant reed (*Arundo donax* L.) in a changing soil nitrogen fertilization and soil water availability in a semi-arid Mediterranean area, European Journal of Agronomy, 72 Vol. (2016), pag. 56.

M. Donatelli, A. K. Srivastava, G. Duveiller, S. Niemeyer, D. Fumagalli, Climate change impact and potential adaptation strategies under alternate realizations of climate scenarios for three major crops in Europe, Environmental Research Letters, 10 Vol. (2015), 075005.

G. Duveiller, M. Donatelli, D. Fumagalli, A. Zucchini, R. Nelson, B. Baruth, A dataset of future daily weather data for crop modelling over Europe derived from climate change scenarios, Theoretical and Applied Climatology, 127 Vol. (2017), pag. 573.

C. Francone, V. Pagani, M. Foi, G. Cappelli, R. Confalonieri, Comparison of leaf area index estimates by ceptometer and PocketLAI smart app in canopies with different structures. Field Crops Research, 155 Vol. (2014), pag. 38.

F. Ginaldi, G.A. Cappelli, E. Ceotto, Modelling- based procedure to evaluate energy crops productivity in marginal humid areas of low po valley (Northern Italy), Proceedings of 26 th EUBCE European Biomass Conference and Exhibition, (2018), pag. 259.

F. Ginaldi, S. Bajocco, S. Bregaglio, G. Cappelli, Spatializing Crop Models for Sustainable Agriculture. In: M. Farooq, M. Pisante (Eds.), Innovations in Sustainable Agriculture, Springer, Cham, (2019), pag. 599.

G.H. Hargreaves, Z.A. Samani, Estimating potential evapotranspiration, Journal of the Irrigation and Drainage Division, 108 Vol. (1982), pag. 223.

IRENA, 2016, Boosting Biofuels: Sustainable Paths to Greater Energy Security, www.irena.org/publications.

S.E. Jørgensen, L. Kamp-Nielsen, T. Christensen, J. Windolf-Nielsen, B. Westergaard, Validation of a prognosis based upon a eutrophication model, Ecological Modelling, 35 Vol. (1986), pag. 165.

G. L'Abate, M. Fantappie, S. Priori, L. D'Avino, R. Barbetti, R. Lorenzetti, E.A.C. Costantini, Italian Derived Soil Profile's Database. 1.0. Consiglio per la ricerca in agricoltura e l'analisi dell'economia agraria (CREA-AA), Online database, (Last access 30/06/2020).

K. Loague, R.E. Green, Statistical and graphical methods for evaluating solute transport models: overview and application, Journal of contaminant hydrology, 7 Vol. (1991), pag. 51.

A. Monti, W. Zegada-Lizarazu, Sixteen-year biomass yield and soil carbon storage of giant reed (*Arundo donax* L.) grown under variable nitrogen fertilization rates, BioEnergy research, 9 Vol. (2016), pag. 248.

D.N. Moriasi, J.G. Arnold, M.W. van Liew, R.L. Bingner, R.D. Harmel, T.L., Veith, Model evaluation guidelines for systematic quantification of accuracy in watershed simulations, Transactions of the ASABE, 50 Vol. (2007), pag. 885.

J.E. Nash, J.V. Sutcliffe, River flow forecasting through conceptual models, part I-a discussion of principles, Journal of hydrology, 10 Vol. (1970), pag. 282.

N. Nassi o Di Nasso, N. Roncucci, F. Triana, C. Tozzini, E. Bonari, Seasonal nutrient dynamics and biomass quality of giant reed (*Arundo donax* L.) and *Miscanthus* (*Miscanthus* x *giganteus* Greef et Deuter) as energy crops, Italian Journal of Agronomy, 6 Vol. (2011), pag. 152.

S. Pedrazzi, G. Allesina, N. Morselli, M. Puglia, L. Barbieri, I. Lancellotti, et al., The energetic recover of biomass from river maintenance: The REBAF project. Proceedings of 25th EUBCE European Biomass Conference and Exhibition, (2017), pag. 52.

R.E. Perdue, *Arundo donax* - Source of musical reeds and industrial cellulose, Economic Botany, 12 Vol. (1958), pag 368.

J.T. Ritchie, S. Otter, Description and performance of CERES-wheat: a user- oriented wheat yield model. In: W.O. Willis (Ed.), ARS Wheat Yield Project. U.S. Dept. of Agriculture, Agricultural Research Service. ARS-38, Washington DC, (1985) pp. 159.

L. Sallustio, D. Pettenella, P. Merlini, R. Romano, L. Salvati, M. Marchetti, P. Corona, Assessing the economic marginality of agricultural lands in Italy to support land use planning, Land use policy, 76 Vol. (2016), pag. 526.

L. Sallustio, A. Harfouche, M. Marchetti, L. Salvati, P. Corona, Evaluating the potential of marginal lands available for sustainable cellulosic biofuel production in Italy, Renewable and Sustainable Energy Reviews, (2020), (submitted).

A. Schievano, G. D'Imporzano, L. Corno, F. Adani, F Cerino Badone, S.R. Pilu. Più biogas a costi inferiori con Arundo o doppia coltura. Articolo pubblicato sul supplement a l'Informatore Agrario, 25 Vol. (2012), pag. 21, Italian.

T. Stella, C. Francone, S.S. Yamaç, E. Ceotto, V. Pagani, R. Pilu, R. Confalonieri, Reimplementation and reuse of the Canegro model: From sugarcane to giant reed, Computers and Electronics in Agriculture, 113 Vol. (2015), pag. 193.

I. Supit, C.A. van Diepen, A.J.W. de Wit, J. Wolf, P. Kabat, B. Baruth, F. Ludwig, Assessing climate change effects on European crop yields using the Crop Growth Monitoring System and a weather generator, Agricultural and Forest Meteorology, 164 Vol. (2012), pag. 96.

J.R. Williams, C.A. Jones, J.R. Kiniry, D.A. Spanel, The EPIC growth model, Transactions of the American Society of Agricultural Engineers, 32 Vol. (1989), pag. 497.

J.H.M. Wösten, A. Lilly, A. Nemes, C. Le Bas, Development and use of a database of hydraulic properties of European soils, Geoderma, 90 Vol. (1999), pag. 169.

6 Photothermal zoning of castor (*Ricinus communis* L.) growing season in the semi-arid Mediterranean area

6.1 Introduction

Castor (*Ricinus communis* L.) is a perennial shrub or a small tree native to Ethiopia (Kiran and Prasad, 2017), tropical Africa, that has become naturalized throughout the tropical and sub-tropical regions of the world (Anastasi et al., 2015). All parts of castor are toxic to humans and other mammals due to the presence of the ricinine, a toxic alkaloid (Severino et al., 2012), while the seeds are toxic because of the presence of ricin, a lectin (carbohydrate-binding protein), produced in the endosperm (Smith and Hayoun, 2019). Nonetheless, castor has been cultivated as an industrial oilseed crop, because of its wide range of application, mainly in non-food, oil-based industries (Anastasi et al., 2015).

Castor is also a promising feedstock for biodiesel production, because of its high seed oil content, fatty acid composition profile and potentially high oil yields. Furthermore, due to the non-edible nature of its oil and the possibility to be grown on marginal lands, including heavy metal contaminated lands, castor is a viable alternative to minimize land-use competition for food production, and its adverse effects (direct or indirect) on food security, land based GHG emissions and biodiversity loss (Severino et al., 2012; Kiran and Prasad, 2017). A drawback of castor oil for biodiesel production is, however, the high concentration of ricinoleic acid which limits the possibility to blend castor oil in conventional diesel up to 10% in volume (Berman et al., 2011). On the other hand, the high concentration of ricinoleic acid in castor oil improves the solubility in alcohol at 30°C, facilitating transesterification without heating and thus

reducing the cost and the energy of production, and improves the oxidative stability of the oil extending the shelf-life of the product (Lavanya et al., 2012). Furthermore, plant residues as bark can provide cellulose fibres suitable for the production of plastic composite with polypropylene (Vinayaka et al., 2017).

Castor presents a high adaption to a wide range of climate and soil conditions. Although it is a considered a long-day plant, with a day-length >12 h favoring the formation of female flowers (Mendoza and Reyes, 1985), it is well suited to regions with photoperiods not shorter than 9 h and good exposure to solar radiation (Beltrão and Silva, 1999; Kumar et al., 1997). Falasca et al. (2012), estimated that an economic threshold of castor cultivation can be achieved in areas with 400–500 mm of rainfall during the whole growing cycle, or ideally until the onset of flowering to get most out its potential yield.

In tropical and sub-tropical areas, castor is cultivated as a perennial crop, although it is often grown as annual crop to ease mechanical harvest (Severino et al., 2012). In Mediterranean and warm-temperate environments it is a spring-summer annual crop, due mainly to the high thermal requirements for germination and the drop of temperatures during winter. It has been reported that minimum temperature required for germination is $14^{-1}5$°C, and optimum temperature for growth around 24-27°C. Lower soil temperatures delay germination and seedling emergence, while temperature below -8°C cause the death of most-cold resistant castor genotypes in few hours (Moshkin, 1986).

In semi-arid Mediterranean climatic areas of southern Italy, castor is usually considered as an annual spring-summer crop that requires irrigation, whose sowing is generally performed on April when soil temperature reaches a stable level of $16^{-1}7$°C (Anastasi et al., 2015). Satisfactory castor seed yields are attained by at least 180 days growing season in arid and semi-

arid regions, and a $140^{-1}60$ frost free day season is more desirable (Falasca et al., 2012; Amorim Neto et al., 1999). In regions where daily minimum temperature during the winter months is high enough to allow the survival of the plants, as in some zones of semi-arid Mediterranean environments, it would be worth to explore the ecological flexibility of the species by performing autumn sowings. In this case, the extended growing season would allow a greater vegetative development of the plant, enhancing its productivity, and the early seed ripening stage might be reached before the onset of the dry season, thus enabling the rainfed cropping system. Anastasi et al. (2015) explored the feasibility of growing castor as semi-perennial plant in the coastal areas of Sicily (south Italy) under rainfed regime by adopting the autumnal sowing and keeping the crop over a two-year period, through the evaluation of plant surviving, seed yield and oil quality. The experiment indicated that the thermal regime and rainfall amount during the two cropping seasons were adequate to satisfy crop requirements.

Despite the wide adaptability and flexibility of this feedstock, global production of castor oil is concentrated in a few countries (mostly India, China, Brazil and Mozambique) (FAOSTAT, 2018), while about one quarter of the world castor oil production is processed by the European oleo-chemical industry (Zanetti et al., 2017). Information about crop adaption to climatic conditions would foster the introduction of this species in other countries where castor might be profitably grown in low-input, rainfed cropping systems. This is particularly true in the region of southern Italy, where the need for crop diversification is particularly important by adopting agronomic strategies also for macro-thermal species in favor of soil water conditions, although optimal thermal requirements might not be meet. The wide variability of the climatic events occurring during crop development makes, however, difficult to predict the length of

the growing season in terms of number of days. This issue has been little investigated in castor. Therefore, a field research was conducted in two subsequent growing seasons in a coastal area of Sicily, aiming at developing thermal and photothermal units to predict the length of the main phenological intervals in castor, either in autumn-winter and in spring-summer growing seasons. On the basis of the best formula a 'zonation' was carried out to identify the areas were thermal conditions allow to cultivate castor in autumn or spring sowings irrespective of water supply.

6.2 Materials and methods

6.2.1 *Field experiment*

The field experiment was conducted during the 2009-2010 and 2010-2011 growing seasons at Pozzallo, a site of South-eastern coast of Sicily (10 m a.s.l., 36°44' N Lat, 14°51' E Long). The soil of the experimental field is classified as Calcixerollic Xerochrepts (USDA, Soil Taxonomy) having the following characteristics: clay 38.0%, sand 37.0%, silt 25.0%, organic matter 2.6%, pH 8.5, total N 1.6‰, available P_2O_5 52.3 ppm, exchangeable K_2O 325.0 ppm. Hybrid 'Hazera' (Hazera Genetics Ltd., Israel) of castor was used for the experiment.
To intercept a wide range of air temperature and photoperiod conditions, eight different sowings were performed in the two growing seasons, from middle autumn to late spring: 20 November, 22 January, 12 March and 8 May, in the first season (2009-2010); 18 December, 12 February, 16 April and 16 June, in the second season (2010-2111).
The experiment was arranged in a completely randomized blocks design with three replicates. Treatments in the experimental design were represented by sowing dates. Single

plot measured 14 m^2 (5 x 2.8 m) and a density of 5.7 plants/m^2 was adopted. At sowing, basic fertilisation with 40 kg/ha N as ammonium sulphate, and 60 kg/ha P_2O_5 as mineral perphosphate, was applied. A further 40 kg/ha N (as ammonium nitrate) was supplied as top dressing, approximately a month after sowing. Irrigation was applied up to plant establishment when needed, and periodically up to field capacity to restore crop evapotranspiration only to spring sowing dates (approximately 450 mm averaged the two growing seasons).
Throughout the growing seasons, maximum (H) and minimum (L) air temperature and rainfall were recorded in a daily scale using a data logger (CR10, Campbell Scientific, Logan, UT, USA) near the experimental field. The reference crop evapotranspiration (ET_0) was calculated from the evaporation pan (mm/d) multiplied by the pan coefficient of 0.80 (Doorenbos and Pruitt, 1977).
During the experiment, the date of occurrence of the main crop phenological stages (seedling emergence, flowering, seed physiological maturity) was recorded when more than 50% of the plants within each plot reached the specific stage. Harvest was performed manually when seed physiological maturity was reached, namely when all plants in each plot had 95% capsules ripened in each sowing date. Dry seed yield (Mg/ha) was then calculated for each sowing date at 10% moisture content.

6.2.2 Procedures for thermal and photothermal unit calculation

Sums of daily thermal (TU) and photothermal units (PTU) (°Cd) were calculated from minimum and maximum daily temperature, according to the procedures reported in **Table** 1. Briefly, several methods to calculate growing degree units (GDU) were considered: a general GDU equation, a photoperiod corrected GDU and five modifications to these equations.

For PTU calculation, photoperiod (P_i) was considered, calculated as follows:

$$P_i = 7.64 \cdot \cos^{-1}\left[0.1 - \frac{\sin\left(\frac{Latitude}{180}\right) \cdot 3.14) \cdot \theta}{\cos\left(\frac{Latitude}{180} 3.14\right) \cdot \cos(\sin^{-1}\theta)}\right]$$

where:

$$\theta = \sin^{-1}\{0.39785 \cdot \sin[4.869 + 0.0172 \cdot \mathrm{DOY} + 0.03345 \cdot \sin(6.224 + 0.0172 \cdot \mathrm{DOY})]\}$$

DOY= day of the year

GDU accumulated along each interval (sowing-plant emergence, plant emergence-flowering, flowering-seed ripening) and the whole growing period (sowing-seed ripening) were then calculated for each sowing time. Three different values (8, 9 and 10°C) were adopted each time as base temperature (t_b) (i.e., below which development is assumed to cease) in thermal and photothermal unit calculations. Maximum cardinal or ceiling air temperature at which development of castor ceases was considered 30°C.

Values for the length of the intervals of growing season, expressed in GDU sums (hereinafter referred as GDUs) or number of days, were compared for the coefficient of variation (CV = st. deviation/mean). The calculation procedure leading to the lowest CV was considered as the best predicting the length of the interval considered.

Table 1 Thermal and photothermal units sums calculation procedures.

Code	Method	Formula
Tu1	Standard	$\Sigma((H_i + L_i)/2) - t_b$
Tu2	Standard modified 1	$\Sigma((H'_i + L_i)/2) - t_b$
Tu3	Standard modified 2	$\Sigma((H''_i + L_i)/2) - t_b$
Tu4	Standard modified 3	$\Sigma((H_i + L'_i)/2) - t_b$
Tu5	Standard modified 4	$\Sigma((H'_i + L'_i)/2) - t_b$
Tu6	Standard modified 5	$\Sigma((H''_i + L'_i)/2) - t_b$
PTu1	Moltiplicative photothermal	$\Sigma(((H_i + L_i)/2) - t_b) \times P'_i$
PTu2	Moltiplicative photothermal modified 1	$\Sigma(((H'_i + L_i)/2) - t_b) \times P'_i$
PTu3	Moltiplicative photothermal modified 2	$\Sigma(((H''_i + L_i)/2) - t_b) \times P'_i$
PTu4	Moltiplicative photothermal modified 3	$\Sigma(((H_i + L'_i)/2) - t_b) \times P'_i$
PTu5	Moltiplicative photothermal modified 4	$\Sigma(((H'_i + L'_i)/2) - t_b) \times P'_i$
PTu6	Moltiplicative photothermal modified 5	$\Sigma(((H''_i + L'_i)/2) - t_b) \times P'_i$

N= number of days the thermal units were cumulated
H_i= maximum temperature (°C) for day i
L_i= minimum temperature (°C) for day i
t_b= base temperature (8°, 9° or 10°C)
$H'_i = H_i$ if $H_i < 30$; $=30$ if $H_i > 30$
$L'_i = L_i$ if $L_i > t_b$; $= t_b$ if $L_i < t_b$

$H''_i = H_i$ if $H_i < 30$; $= 30 - (H_i - 30)$ if $H_i > 30$
P_i= photoperiod (h d^{-1}) for day i
$P'_i = P_i/24$

6.2.3 *Weather dataset creation*

A weather dataset was created using data from 93 weather stations distributed across the Sicilian Region within the SIAS network (http://www.sias.regione.sicilia.it) (**Table** 2). The stations were selected for data continuity from 1 January 2007 to 31 December 2016. The data were recorded with a 5-day frequency for potential evapotranspiration and a 10-day frequency for minimum, maximum and average temperature, solar radiation and rainfall.

Station	Longitude East [°]	Latitude North [°]	Altitude (m a.s.l.)	Site	Longitude East [°]	Latitude North [°]	Al (m
Agrigento Scibica	13.549	37.341	225	San Fratello	14.624	37.955	1
Agrigento Mandrascava	13.636	37.238	40	San Pier Niceto	15.360	38.130	4
Aragona	13.624	37.459	305	Torregrotta	15.340	38.196	
Bivona	13.415	37.596	350	Alia	13.746	37.742	5
Cammarata	13.736	37.632	379	Camporeale	13.101	37.905	4
Canicattì	13.773	37.358	475	Castelbuono	14.090	37.975	4
Licata	13.889	37.156	80	Contessa Entellina	13.043	37.731	2
Ribera	13.266	37.439	30	Corleone	13.251	37.805	4
Sciacca	13.040	37.592	90	Montalbano Elicona	14.967	37.986	1
Caltanissetta	14.050	37.430	350	Sclafani Bagni	13.850	37.706	4
Delia	13.926	37.349	360	Lascari	13.920	38.000	
Gela	14.334	37.159	70	Mezzojuso	13.495	37.852	3
Butera	14.114	37.135	54	Misilmeri	13.443	38.032	1
Mazzarino	14.214	37.298	480	Monreale Vigna Api	13.203	38.026	6
Mussomeli	13.827	37.516	375	Palermo	13.328	38.131	
Riesi	14.089	37.276	300	Partinico	13.095	38.067	1
Bronte	14.787	37.755	424	Gangi	14.194	37.816	8
Catania	15.069	37.443	10	Petralia Sottana	14.012	37.634	7
Caltagirone	14.575	37.232	260	Polizzi Generosa	13.996	37.825	6
Riposto	15.198	37.685	50	Termini Imerese	13.613	37.973	3
Linguaglossa	15.131	37.828	590	Ragusa	14.677	36.955	7
Maletto	14.873	37.828	1040	Comiso	14.591	37.016	2
Mazzarrone	14.562	37.096	300	Ispica	14.994	36.730	
Mineo	14.726	37.321	205	Modica	14.902	36.883	3
Paterno	14.855	37.516	100	Acate	14.401	36.975	
Pedara	15.049	37.644	803	Giuliana	13.230	37.633	2
Randazzo	14.980	37.889	680	Prizzi	13.422	37.689	1
Aidone	14.467	37.451	350	Monreale Bifarera	13.368	37.879	7
Enna	14.176	37.517	350	Santa Croce Camerina	14.502	36.836	
Nicosia	14.424	37.764	700	Scicli	14.677	36.761	
Piazza Armerina	14.367	37.317	540	Augusta	15.150	37.283	
Caronia Buzza	14.490	38.029	50	Siracusa	15.159	37.062	
Caronia Pomiere	14.487	37.897	1470	Francofonte	14.894	37.246	1
Cesaro Vignazza	14.680	37.839	820	Lentini	14.926	37.342	
Agira	14.502	37.623	467	Noto	15.058	36.846	
Antillo	15.261	37.979	796	Pachino	15.095	36.682	
Calascibetta	14.227	37.671	650	Palazzolo Acreide	14.872	37.062	6
Cesarò Monte Soro	14.694	37.933	1840	Calatafimi	12.882	37.857	2
Fiumedinisi	15.375	38.035	440	Castellammare del Golfo	12.890	38.015	
Leni (Salina)	14.834	38.563	315	Castelvetrano	12.853	37.648	1
Messina	15.561	38.259	420	Erice	12.585	38.033	5

Militello Rosmarino	14.667	38.040	460	Marsala	12.569	37.802	1
Mistretta	14.340	37.863	690	Mazara del Vallo	12.675	37.680	1
Naso	14.786	38.107	468	Salemi	12.720	37.819	2
Novara di Sicilia	15.142	38.026	750	Trapani Fontanasalsa	12.553	37.944	1
Patti	15.020	38.141	88	Trapani Fulgatore	12.661	37.948	1
Pettineo	14.290	37.974	210				

Table 2 List of the 93 weather stations located in different areas of Sicily.

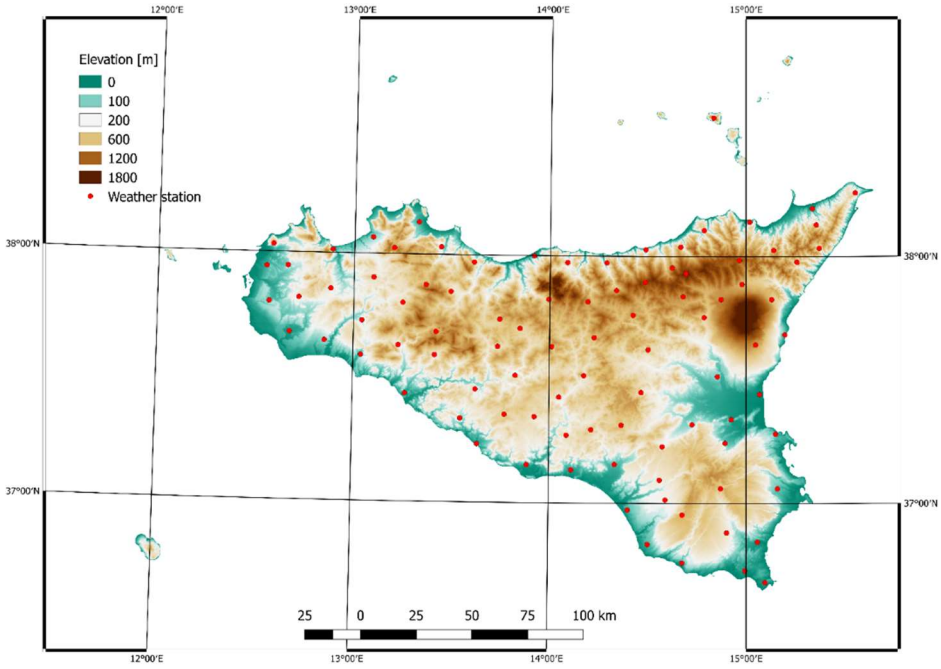

Fig 1. Map of distribution of the weather stations

6.2.4 *Decade average temperature maps creation*

The temperature dataset was used to generate the maximum and minimum 10-day temperature average maps of Sicily. The average 10-day (hereinafter referred as decade) temperature was calculated over the 10 years of observations:

$$H_{dec} = \sum_{n=1}^{10} H_{dec_n} \cdot \frac{1}{10} \qquad (1)$$

$$L_{dec} = \sum_{n=1}^{10} L_{dec_n} \cdot \frac{1}{10} \qquad (2)$$

Where $1 \leq dec \leq 36$ is the decade, H_{dec} is the average decade maximum temperature and L_{dec} is the average decade minimum temperature.

A process of temperature normalization for altitude was performed in order to take account of the variability between stations due to the presence of elevations and thus to improve the map accuracy (Drago, 2005). In particular, the average decade temperature was normalized by subtracting the elevation effect, calculated by multiplying the thermal vertical gradient by the elevation of the station (**Table** 3):

$$H'_{dec} = H_{dec} - \nabla H_{dec} \cdot elev \quad (3)$$

$$L'_{dec} = L_{dec} - \nabla L_{dec} \cdot elev \quad (4)$$

Where H'_{dec} and L'_{dec} are the normalized average decade maximum and minimum temperature, respectively, ∇H_{dec} and ∇L_{dec} are the vertical maximum and minimum temperature gradients for the decade, respectively, and $elev$ is the elevation of the weather station above sea level. The 8 x 10^7 cells raster maps of the H'$_{dec}$ and L'$_{dec}$ was obtained by interpolating the georeferenced data from the SIAS weather stations using the Inverse Distance Weighting method (Ozelkan et al., 2013).

The effect of the elevation was subsequently introduced by using the QGIS raster calculation tool to multiply the thermal vertical gradient by the elevation attribute of the Sicilian 40x40 Digital Elevation Model (DTM) raster (SITR – Sistema Informativo Territoriale Regionale) and thus adding the effect of the elevation to the normalized average decade temperature raster:

$$H_{dec} = H'_{dec} + \nabla H_{dec} \cdot elev \quad (5)$$

$$L_{dec} = L'_{dec} + \nabla L_{dec} \cdot elev \quad (6)$$

where H_{dec} and L_{dec} are the average decade maximum and minimum temperature in the raster and $elev$ is the elevation in the DTM raster.

The maps of the monthly average maximum and minimum temperature were obtained by calculating the three decades mean trough the QGIS raster calculation tool.

6.2.5 *Determination of the sowing date*

By using the procedure described above, two raster maps representing autumn and spring sowing date were generated, considering H_{dec} and L_{dec} raster maps as inputs. The sowing of castor can be performed when soil temperature reaches a stable value of 15°C, to allow rapid seed germination and uniform crop establishment (Anastasi et al., 2015). To ensure survival of the seedlings during winter, several assumptions were checked for the autumn sowing: average temperature of the sowing decade greater than 15°C and L_{month} greater than 5°C for the whole growing season. The autumn sowing date was set as the latest day with a decade mean temperature above 15°C, as determined by the following equation:

Decade	Thermal vertical gradient H (°C/100 m)	Thermal vertical gradient L (°C/(100 m)
1	-0.72	-0.67
2	-0.72	-0.67
3	-0.72	-0.67
4	-0.69	-0.67
5	-0.69	-0.67
6	-0.69	-0.67
7	-0.6	-0.62
8	-0.6	-0.62
9	-0.6	-0.62
10	-0.5	-0.57
11	-0.5	-0.57
12	-0.5	-0.57
13	-0.34	-0.47
14	-0.34	-0.47
15	-0.34	-0.47
16	-0.19	-0.46
17	-0.19	-0.46
18	-0.19	-0.46
19	-0.19	-0.42
20	-0.19	-0.42
21	-0.19	-0.42
22	-0.2	-0.47
23	-0.2	-0.47
24	-0.2	-0.47
25	-0.34	-0.56
26	-0.34	-0.56
27	-0.34	-0.56
28	-0.51	-0.63
29	-0.51	-0.63
30	-0.51	-0.63
31	-0.64	-0.66
32	-0.64	-0.66
33	-0.64	-0.66
34	-0.7	-0.66
35	-0.7	-0.66
36	-0.7	-0.66

$$Sowing\ date = -5 + dec \cdot 10 + \frac{(Tavg_{dec} - 15°C)}{Tavg_{dec-1} - Tavg_{dec+1}} \cdot 20 \quad (7)$$

where $1 \leq dec \leq 36$ is the last decade with $T\text{avg}_{dec} > 15°C$, $T\text{avg}_{dec}$ is the decade average temperature, calculated as the mean of H_{dec}

and L_{dec}. If the $Tavg_{dec}$ of the n^{th} decade is less than 15°C, the algorithm considers the n^{-1th} decade. In locations where these thermal conditions were not satisfied, sowing was set in spring, to allow plant thermal requirements to be satisfied. The spring sowing date was determined by Eq. (7), with $1 \leq dec \leq 36$ is the first decade with $Tavg_{dec} > 15°C$ and if the $Tavg_{dec} < 15°C$ of the n^{th} decade, the algorithm considers the $n+1^{th}$ decade.

Table 1 Thermal vertical gradient for each decade of the year.

6.2.6 *Determination of the ripening date*

Ripening date was estimated for both autumn and spring sowing by adding GDUs to the GDU sum from the day of sowing until the sum reaches the ripening threshold. An average GDU sum of the eight sowing dates of 949°C was considered representative as ripening threshold. In order to perform this calculation, an algorithm was developed both on R coding and trough the QGIS raster calculation tool.

$$Ripening\ date = \sum_{month=1}^{N} n\ days_{month} - n\ days_N \cdot \frac{GDU_N - GDU_{ripening}}{GDU_N} \quad (8)$$

where $GDU_{ripening}$ is the growing degree days threshold for seed ripening (949°C), N is the number of the first month that solves the equation $\Sigma^{N}_{month=1}\ GDU_{month} \geq GDU_{ripening}$, , GDU_N is growing degree days cumulation for the month N, $n\ days_{month}$ is the number of days in the month.

6.2.7 *Statistical analysis*

Phenological intervals (sowing-emergence, emergence-flowering, flowering-seed ripening, and whole growing season) and dry seed yield were evaluated by one-way ANOVA

according to the experimental layout, considering the sowing date as fixed effect, and the experimental year as random effect. Mean were separated by the Tuckey's test at 95% confidence level using the Minitab 17.0 Statistical software.
Relationships between minimum soil temperature and plant emergence, and between minimum soil temperature and mean emergence time were calculated by non-linear models. The Shapiro–Wilk test was developed to test residuals for normality. Coefficients were considered significant at $P \leq 0.05$. The goodness of fit was assessed by calculating R^2 (SigmaPlot11, Systat Software Inc., San Jose, CA, USA). The standard deviation of the estimated harvesting date among the 10 years of observations for each weather station was calculated by the software RStudio, an integrated development environment for R (R Core Team, 2013). The values of the standard deviation from all the weather stations were interpolated using the Inverse Distance Weighting method (Ozelkan et al., 2013) to generate a raster map of the standard deviation of the estimated harvesting date for both autumn and spring sowings.

6.3 Results

6.3.1 *Meteorological conditions and plant phenology*

Air temperatures decreased from autumn to winter sowings, followed by an increase from winter to spring ones (**Figure** 1). The first season was slightly cooler and wetter than the second. Mean temperature was at or slightly lower than 10°C in the coldest months of the year (January and February) at the second growing seasons, while at the first season 6°C were registered in a few days of January and 8°C through February and beginning of March. Rainfall distribution was wider at the first year, that

also exhibited a higher rainfall amount with an extreme event (260 mm) in February.

The crop growing season was significantly affected by sowing dates (**Table** 4). Generally, the earlier the sowing the longer the growing season. It ranged from 240 days with the sowing of November to 99 days with the sowing of May (**Figure** 2). The interval "sowing-emergence" was longer at the sowing of November (77.0 days), and shorter on May and on June (6.1 days averaged). As sowing was moved from colder to warmer dates, this interval decreased. The interval "emergence-flowering" was again significantly longer on autumn sowings (110.0 days across the average of November and December), followed by winter sowings (77.0 days across the average of January and February) and the sowing of March (57.6 days). April, May and June sowings showed similar "emergence-flowering" intervals (38.5 days across the average). The interval "flowering-maturation", although significantly different, showed a small variation as compared with the previous intervals. It was shorter on April sowing (50.0 days) than the remaining dates (55.4 days across the average).

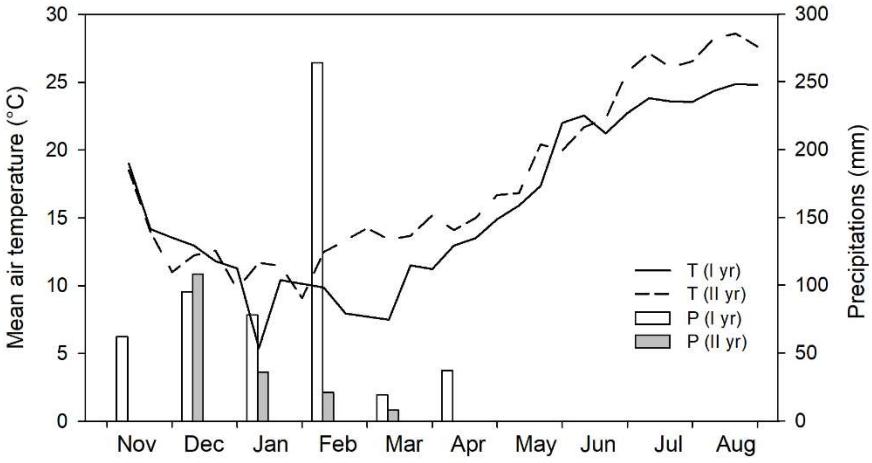

Figure 1. Mean air temperature (T, °C) and precipitation (P, mm) through the two experimental years.

6.3.2 *Prediction of phenological intervals*

The length of the different phenological intervals and that of the whole growing season, in relation to sowing date is reported in **Table** 5-8. The intervals are expressed either in days or in GDUs, calculated according to procedures reported in **Table** 1. The "sowing-plant emergence" interval was progressively reduced from 77 to 5 days by shifting the sowing dates from November to June (**Table** 5). The variation among values expressed in days was quite high (CV >70%), indicating that this procedure to predict the duration of seed germination up to plant emergence in field is not reliable. When the interval was expressed in GDU, this variation was reduced (CV <50%); a further reduction was achieved when photoperiod was included into GDU calculation (PTu_s formulas, CV <35%). In addition,

the variability within PTu_s formulas further decreased when t_b replaced the daily minimum temperature (L), especially when a t_b of 10°C was included (CV <30%), demonstrating that castor is highly sensitive to low temperature during seed germination. Overall, the lowest CV (27.6%) was obtained in PTu4, whereby castor requires an average of 62.2 °Cd from sowing to emergence in field conditions.

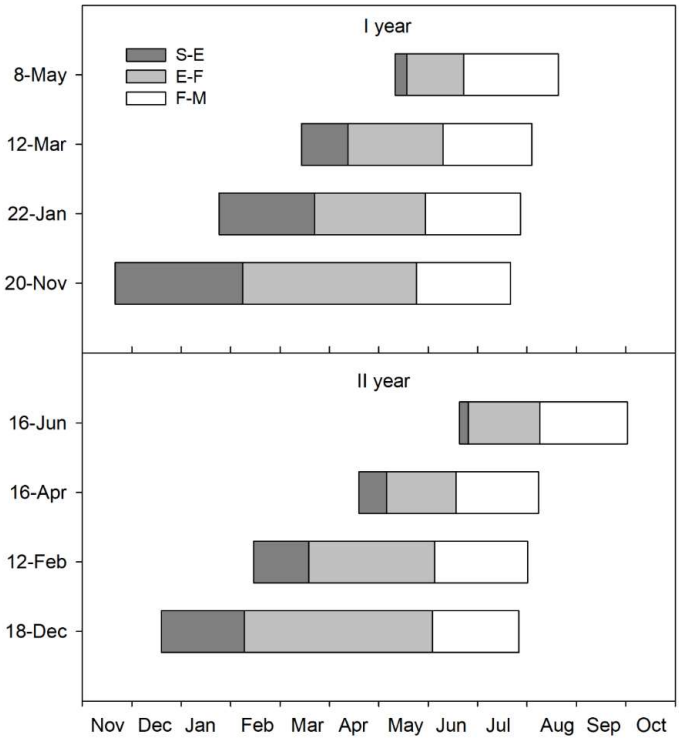

Figure 2. Main phenological phases (sowing-emergence, S-E; emergence-flowering, E-F; flowering-maturation, F-M) of castor under different sowing dates and experimental years.

The "emergence-flowering" interval (**Table** 6), which ranged from 115 (sowing of December) to 35 days (sowing of May), exhibited a lower variability when compared with the previous interval, both in terms of days (CV 43.7%) and GDUs (CV <35%). Even in this case, values of GDUs where photoperiod was included (PTu_s) were slightly less variable (CV from 34.4 to 23.5%) than those calculated by Tu_s (CV from 34.1 to 25.4%). This reflect the behavior of this long-day plant, where photoperiod exceeding 15 h (as in late spring-early summer in Sicily) triggers castor flowering. When the sowing is delayed to late spring, seed germination and plant emergence is shorter in field, however plants start flowering more or less at the same period of those sown in autumn and winter. Thus, the interval "emergence-flowering" is gradually shortened, but a progressively longer photoperiod compensates for the gradual reduction. As a result, GDUs that included photoperiod were more constant with changing sowing time. In all cases, CV attained lower values when a t_b of 8°C was considered, indicating that the growth period just after plant emergence is less sensitive to low temperature than seed germination. Overall, the lowest CV (23.5%) corresponded to GDUs calculated by the PTu6 formula.

The interval "flowering-seed ripening" (**Table** 7) was the least variable, lasting from 50 to 58 days (CV 5.2%). Indeed, onset of fruit (capsule) requires more or less the same time from flowering to take place and seeds to ripen, therefore the extent of this period was rather constant. Nonetheless, the variability was further reduced (CV <3.5%) when PTu formulas with a t_b of 8°C were adopted to predict the length of this interval in terms of GDUs.

The whole growing season (sowing-seed ripening) lasted 157 days across the average of all experimental conditions (**Table** 8), ranging from 240 (sowing of November) to 99 days (sowing of

May) (CV 34.2%). As observed for single intervals, the variability within sowing dates was reduced when GDUs were adopted (CV <17%). Indeed, this period is shortened when air temperatures progressively increase, and since both terms (number of days and temperature) are included into the formula of GDUs, the length of the growing season expressed in GDUs was rather constant with sowing time. In particular, the variation coefficient calculated for GDUs obtained by using PTu6 formula did not exceed 10% (8.4% with t_b 8°C).

Table 2 Length of the interval 'sowing-plant emergence' in castor bean in relation to sowing date (tb: base temperature).

	d	Tu1			Tu2			Tu3			Tu4			Tu5			Tu6			PTu1			PTu2			PTu3			PTu4			PTu5			PTu6		
		t_b (°C)			t_b (°C)			t_b (°C)			t_b (°C)			t_b (°C)			t_b (°C)			t_b (°C)			t_b (°C)			t_b (°C)			t_b (°C)			t_b (°C)			t_b (°C)		
Sowing date		**10**	**9**	**8**	**10**	**9**	**8**	**10**	**9**	**8**	**10**	**9**	**8**	**10**	**9**	**8**	**10**	**9**	**8**	**10**	**9**	**8**	**10**	**9**	**8**	**10**	**9**	**8**	**10**	**9**	**8**	**10**	**9**	**8**	**10**	**9**	**8**
20/11/92	77	115.5	170.5	233.5	115.5	170.5	233.5	115.5	170.5	233.5	204.5	249.0	297.5	204.5	249.0	297.5	204.5	249.0	297.5	51.3	75.8	104.0	51.3	75.8	104.0	51.3	75.8	104.0	91.4	111.2	132.9	91.2	111.2	132.9	91.2	111.2	132.9
22/1/93	58	20.0	46.0	83.0	20.0	46.0	83.0	20.0	46.0	83.0	118.0	146.5	176.5	118.0	146.5	176.5	118.0	146.5	176.5	10.0	22.8	40.9	10.0	22.8	40.9	10.0	22.8	40.9	58.1	72.0	86.7	58.1	72.0	86.7	58.1	72.0	86.7
12/3/93	28	47.0	74.0	102.5	47.0	74.0	102.5	47.0	74.0	102.5	100.5	115.5	131.5	100.5	115.5	131.5	100.5	115.5	131.5	25.8	40.5	56.0	25.8	40.5	56.0	25.8	40.5	56.0	54.7	62.9	71.6	54.7	62.9	71.6	54.7	62.9	71.6
8/5/93	7	52.5	60.5	68.5	52.5	60.5	68.5	52.5	60.5	68.5	54.0	60.5	68.5	54.0	60.5	68.5	54.0	60.5	68.5	32.4	37.3	42.3	32.4	37.3	42.3	32.4	37.3	42.3	33.3	37.3	42.3	33.3	37.3	42.3	33.3	37.3	42.3
18/12/93	50	59.4	97.4	144.4	59.4	97.4	144.4	59.4	97.4	144.4	133.9	161.9	191.4	133.9	161.9	191.4	133.9	161.9	191.4	26.8	43.8	64.9	26.8	43.8	64.9	26.8	43.8	64.9	60.2	72.8	86.0	60.2	72.8	86.0	60.2	72.8	86.0
12/2/94	33	118.3	152.3	186.3	118.3	152.3	186.3	118.3	152.3	186.3	151.0	169.9	193.9	151.0	169.9	193.9	151.0	169.9	193.9	59.5	76.6	93.7	59.5	76.6	93.7	59.5	76.6	93.7	76.0	85.5	97.6	76.0	85.5	97.6	76.0	85.5	97.6
16/4/94	17	112.5	130.5	148.3	112.5	130.5	148.5	112.5	130.5	148.5	116.5	132.0	148.5	116.5	132.0	148.5	116.5	132.0	148.5	66.7	77.4	88.1	66.7	77.4	88.1	66.7	77.4	88.1	69.1	78.3	88.1	69.1	78.3	88.1	69.1	78.3	88.1
16/6/94	5	84.5	90.5	96.5	79.0	85.0	91.0	79.0	85.0	91.0	84.5	90.5	96.5	79.0	85.0	91.0	79.0	85.0	91.0	54.5	58.4	62.3	51.0	54.9	58.7	51.0	54.9	58.7	54.5	58.4	62.3	51.0	54.9	58.7	51.0	54.9	58.7
CV%	***74.4***	***48.5***	***43.3***	***42.4***	***48.8***	***43.8***	***43.0***	***48.8***	***43.8***	***43.0***	***37.6***	***40.5***	***43.1***	***38.3***	***41.2***	***43.8***	***38.3***	***41.2***	***43.8***	***48.6***	***38.9***	***34.4***	***48.4***	***39.1***	***34.8***	***48.4***	***39.1***	***34.8***	***27.6***	***29.7***	***31.9***	***28.1***	***30.4***	***32.6***	***28.1***	***30.4***	***32.6***

Table 3 Length of the interval 'plant emergence-flowering' in castorbean in relation to sowing date (tb: base temperature).

	d	Tu1			Tu2			Tu3			Tu4			Tu5			Tu6			PTu1			PTu2			PTu3			PTu4			PTu5			PTu6		
		°C d																																			
		t_b (°C)			t_b (°C)			t_b (°C)			t_b (°C)			t_b (°C)			t_b (°C)			t_b (°C)			t_b (°C)			t_b (°C)			t_b (°C)			t_b (°C)			t_b (°C)		
Sowing date		**10**	**9**	**8**	**10**	**9**	**8**	**10**	**9**	**8**	**10**	**9**	**8**	**10**	**9**	**8**	**10**	**9**	**8**	**10**	**9**	**8**	**10**	**9**	**8**	**10**	**9**	**8**	**10**	**9**	**8**	**10**	**9**	**8**	**10**	**9**	**8**
20/11/92	106	283.5	364.5	452.5	283.5	364.5	452.5	283.5	364.5	452.5	409.0	474.0	545.5	408.5	474.0	546.0	408.5	474.0	546.0	168.4	214.3	263.7	168.4	214.3	263.7	168.4	214.3	263.7	234.83	271.3	311.6	234.8	271.4	311.9	234.6	271.4	311.9
22/1/93	67	314.5	380.5	448.0	314.5	380.5	448.0	314.5	380.5	448.0	370.0	418.5	472.0	370.0	418.5	472.5	370.0	418.5	472.5	189.5	228.4	268.1	189.5	228.4	268.1	189.5	228.4	268.1	220.92	249.8	281.6	220.9	249.8	281.8	220.9	249.8	281.8
12/3/93	58	410.5	469.5	528.5	404.0	463.0	522.0	397.5	456.5	515.5	432.5	482.0	535.5	426.0	475.5	529.5	419.5	469.0	523.0	253.9	289.9	325.9	249.8	285.8	321.8	245.6	281.6	317.6	266.91	297.2	330.0	262.8	293.1	326.2	258.6	289.0	322.0
8/5/93	35	394.0	430.0	466.0	383.5	419.5	455.5	373.0	409.0	445.0	394.5	430.0	466.0	384.0	419.5	455.5	373.5	409.0	445.0	251.4	274.3	297.2	244.6	267.6	290.5	237.9	260.8	283.8	251.68	274.2	297.2	245.0	267.6	...	238.2	260.9	283.8
18/12/93	115	648.3	764.3	880.3	648.3	764.3	880.3	648.3	764.3	880.3	704.5	793.9	890.4	704.5	793.9	890.4	704.5	793.9	890.4	375.7	440.5	505.3	375.7	440.5	505.3	375.7	440.5	505.3	404.6	455.7	510.5	404.6	455.7	510.5	404.6	455.7	510.5
12/2/94	77	529.8	607.8	685.8	529.8	607.8	685.8	529.8	607.8	685.8	546.3	615.3	686.8	546.3	615.3	686.8	546.3	615.3	686.8	318.3	364.3	410.3	318.3	364.3	410.3	318.3	364.3	410.3	327.5	368.5	410.9	327.5	368.5	410.9	327.5	368.5	410.9
16/4/94	42	422.8	465.8	508.8	422.8	465.8	508.8	422.8	465.8	508.8	422.8	465.8	508.8	422.8	465.8	508.8	422.8	465.8	508.8	266.7	293.8	320.9	266.7	293.8	320.9	266.7	293.8	320.9	266.8	293.8	320.9	266.8	293.8	320.9	266.8	293.8	320.9
16/6/94	44	740.0	785.0	830.0	681.5	726.5	771.5	623.0	668.0	713.0	740.0	785.0	830.0	681.5	726.5	771.5	623.0	668.0	713.0	468.2	496.7	525.2	431.2	459.7	488.2	394.2	422.7	451.2	468.2	496.7	525.2	431.2	459.7	488.2	394.2	422.7	451.2
CV%	***43.7***	***34.1***	***31.2***	***29.2***	***32.1***	***29.7***	***28.2***	***30.5***	***28.6***	***27.6***	***29.0***	***27.7***	***26.9***	***27.3***	***26.5***	***26.0***	***26.0***	***25.6***	***25.4***	***34.4***	***30.9***	***28.4***	***32.0***	***29.0***	***27.0***	***29.9***	***27.5***	***25.9***	***29.0***	***27.3***	***26.0***	***26.8***	***25.6***	***24.2***	***24.9***	***24.1***	***23.5***

Table 4 Length of the interval 'flowering-ripening' in castorbean in relation to sowing date (tb: base temperature).

	d	Tu1			Tu2			Tu3			Tu4			Tu5			Tu6			PTu1			PTu2			PTu3			PTu4			PTu5			PTu6		
		°C d																																			
		t_b (°C)			t_b (°C)			t_b (°C)			t_b (°C)			t_b (°C)			t_b (°C)			t_b (°C)			t_b (°C)			t_b (°C)			t_b (°C)			t_b (°C)			t_b (°C)		
Sowing date		**10**	**9**	**8**	**10**	**9**	**8**	**10**	**9**	**8**	**10**	**9**	**8**	**10**	**9**	**8**	**10**	**9**	**8**	**10**	**9**	**8**	**10**	**9**	**8**	**10**	**9**	**8**	**10**	**9**	**8**	**10**	**9**	**8**	**10**	**9**	**8**
20/11/92	57	726.0	784.0	842.0	711.0	769.0	827.0	696.0	754.0	812.0	726.0	784.0	842.0	711.0	769.0	827.0	696.0	754.0	812.0	464.8	502.0	539.1	455.2	492.4	529.5	445.6	482.8	519.9	464.8	502.0	539.1	455.2	492.4	529.5	445.6	482.8	519.9
22/1/93	58	754.0	813.0	872.0	738.5	797.5	856.5	723.0	782.0	841.0	754.0	813.0	872.0	738.5	797.5	856.5	723.0	782.0	841.0	482.2	520.0	557.7	472.3	510.0	547.8	462.4	500.1	537.9	482.2	520.0	557.7	472.3	510.0	547.8	462.4	500.1	537.9
12/3/93	54	710.0	765.0	820.0	701.0	756.0	811.0	692.0	747.0	802.0	710.0	765.0	820.0	701.0	756.0	811.0	692.0	747.0	802.0	452.7	487.8	522.9	447.0	482.1	517.1	441.2	476.3	511.4	452.7	487.8	522.9	447.0	482.1	517.1	441.2	476.3	511.4
8/5/93	57	780.0	830.0	896.0	777.0	835.0	893.0	765.0	823.0	881.0	780.0	838.0	896.0	777.0	835.0	893.0	765.0	823.0	881.0	489.2	525.6	562.0	487.2	523.6	560.0	479.8	516.2	552.6	489.2	525.6	562.0	487.2	523.6	560.0	479.8	516.2	552.6
18/12/93	52	776.0	829.0	882.0	728.5	781.5	834.5	686.5	739.5	792.5	776.0	829.0	882.0	728.5	781.5	834.5	686.5	739.5	792.5	496.5	530.5	564.4	466.2	500.1	534.0	439.3	473.3	507.2	496.5	530.5	564.4	466.2	500.1	534.0	439.3	473.3	507.2
12/2/94	56	845.5	902.5	959.5	791.5	848.5	905.5	743.0	800.0	857.0	845.5	902.5	959.5	791.5	848.5	905.5	743.0	800.0	857.0	539.6	576.0	612.4	505.1	541.5	577.9	474.3	510.7	547.1	539.6	576.0	612.4	505.1	541.5	577.9	474.3	510.7	547.1
16/4/94	50	811.0	862.0	913.0	749.5	800.5	851.5	639.5	744.5	795.5	811.0	862.0	913.0	749.5	800.5	851.5	693.5	744.5	795.5	514.7	547.1	579.5	475.7	508.0	540.4	440.2	472.6	504.9	514.7	547.1	579.5	475.7	508.0	540.4	400.2	472.6	505.0
16/6/94	53	911.0	965.0	1019.0	840.5	894.5	948.5	770.0	824.0	878.0	911.0	965.0	1019.0	840.5	894.5	948.5	770.0	824.0	878.0	520.6	551.4	582.1	480.0	510.3	541.0	438.5	469.2	500.0	520.6	551.4	582.1	479.6	510.3	541.0	438.5	469.2	500.0
CV%	5.2	8.3	7.7	7.1	6.1	5.7	5.3	6.2	4.6	4.4	8.3	7.7	7.1	6.1	5.7	5.3	4.8	4.6	4.4	5.9	5.3	4.8	3.8	3.6	3.5	3.7	3.8	3.9	5.9	5.3	4.8	3.8	3.6	3.5	5.6	3.8	3.9

Table 5 Length of the interval 'sowing-ripening' in castorbean in relation to sowing date (tb: base temperature).

	d	Tu1			Tu2			Tu3			Tu4			Tu5			Tu6			PTu1			PTu2			PTu3			PTu4			PTu5			PTu6		
		°C d																																			
		$t_{b\,(°C)}$			t_b (°C)			t_b (°C)			t_b (°C)			t_b (°C)			t_b (°C)			t_b (°C)			t_b (°C)			t_b (°C)			t_b (°C)			t_b (°C)			t_b (°C)		
Sowing date		**10**	**9**	**8**	**10**	**9**	**8**	**10**	**9**	**8**	**10**	**9**	**8**	**10**	**9**	**8**	**10**	**9**	**8**	**10**	**9**	**8**	**10**	**9**	**8**	**10**	**9**	**8**	**10**	**9**	**8**	**10**	**9**	**8**	**10**	**9**	**8**
20/11/92	240	1115.5	1307.5	1514.5	1100.5	1292.5	1499.5	1085.5	1277.5	1484.5	1327.0	1493.0	1669.5	1311.5	1478.0	1655.0	1296.5	1463.0	1640.0	678.5	785.0	898.6	668.9	775.4	889.0	659.3	765.8	879.4	783.6	876.3	974.4	773.8	866.7	965.1	764.2	857.1	955.5
22/1/93	182	1074.0	1223.0	1384.5	1058.5	1207.5	1369.0	1043.0	1192.0	1353.5	1225.5	1360.0	1501.0	1210.0	1344.5	1486.0	1194.0	1329.0	1470.5	672.8	761.1	855.5	662.9	751.2	845.6	653.0	741.3	835.7	751.3	830.9	914.2	741.3	821.0	904.6	731.2	811.0	894.7
12/3/93	140	1155.0	1294.0	1434.5	1139.5	1278.5	1419.0	1124.0	1263.0	1403.5	1230.5	1348.0	1470.5	1215.0	1332.5	1455.5	1199.5	1317.0	1440.0	724.8	809.3	894.7	714.8	799.4	884.8	704.9	789.5	874.9	766.7	839.1	914.4	756.8	829.2	904.8	746.9	819.3	894.9
8/5/93	99	1210.0	1310.0	1410.0	1196.5	1296.5	1396.5	1174.0	1274.0	1374.0	1211.5	1310.0	1410.0	1198.0	1296.5	1396.5	1175.5	1274.0	1374.0	762.4	825.4	888.4	753.7	816.7	879.7	739.6	802.5	865.5	763.4	825.4	888.4	754.7	816.7	879.7	740.5	802.6	865.5
18/12/93	217	1469.8	1674.8	1888.8	1422.3	1627.3	1841.3	1380.3	1585.3	1799.3	1599.2	1768.2	1945.7	1551.7	1720.7	1898.2	1509.7	1678.7	1856.2	890.5	1005.2	1123.9	860.1	974.8	1093.5	833.3	948.0	1066.7	952.3	1049.0	1150.1	922.0	1018.7	1119.7	895.1	991.8	1092.9
12/2/94	166	1478.6	1645.6	1812.6	1424.6	1591.6	1758.6	1376.1	1543.1	1710.1	1527.3	1670.8	1821.3	1473.3	1616.8	1767.3	1424.8	1568.3	1718.8	909.0	1006.4	1104.8	873.6	972.0	1070.3	842.7	941.1	1039.5	933.5	1019.5	1109.3	899.1	985.1	1074.8	868.2	954.2	1044.0
16/4/94	109	1330.3	1440.3	1550.3	1268.8	1378.8	1488.8	1212.8	1322.8	1432.8	1334.3	1441.8	1550.3	1272.8	1380.3	1488.8	1216.8	1324.3	1432.8	838.2	907.0	975.9	799.1	868.0	936.9	763.7	832.5	901.4	840.5	907.9	975.9	801.5	868.9	936.9	766.0	833.4	901.4
16/6/94	102	1703.5	1806.5	1909.5	1571.5	1674.5	1777.5	1454.5	1548.0	1651.0	1703.5	1860.5	1909.5	1571.5	1674.5	1777.5	1445.0	1548.0	1651.0	1023.4	1085.0	1147.1	980.0	1045.7	1111.4	903.5	969.2	1034.9	1085.2	1147.1	943.3	1005.1	1067.0	866.7	928.6	990.4	943.3
CV%	34.2	16.6	14.9	13.7	14.4	12.9	12.2	12.5	11.4	11.1	13.6	13.6	12.6	11.7	11.4	11.4	10.2	10.3	10.7	15.3	13.5	12.2	14.0	12.4	11.3	11.9	10.7	9.9	14.0	12.8	9.7	11.7	10.9	9.7	9.8	9.3	8.4

6.3.3 *Seed yield*

Seed yield of castor was significantly affected by sowing time (**Table** 9). Seed yield was the highest with the winter sowings of January and February (3.9 Mg/ha), and the lowest with the sowing of April (1.8 Mg/ha). However, the sowing of early spring (March, 3.65 Mg/ha) was not significantly different from the most productive sowing dates. Satisfactory yields were also observed with the late autumn sowing in rainfed conditions (December), and the middle spring by using the irrigation (May). Late spring sowing in June or early sowing in November led to significant yield reductions.

Table 6 Seed yield of castorbean in relation to sowing date. Values followed by the same letter do not differ at $p \leq 0.05$ (L.S.D test)

Sowing date	Seed yield (t/ha)
November 20, 1992	2.63 cd
January 22, 1993	3.93 a
March 12, 1993	3.65 ab
May 8, 1993	3.12 bc
December 18, 1993	3.06 bc
February 12, 1994	3.91 a
April 16, 1994	1.79 e
June 16, 1994	2.15 de
Significance	***

***significant at $p \leq 0.001$

3.4 Plant emergence in field vs. soil temperature

The relationship of plant emergence in field *vs*. minimum soil temperature, considering the pooled data of the two growing

seasons, was calculated (**Figure** 3). This relationship was well described (R^2 >0.84) by the function $y = a/(1+(x/x_0)^b)$ where *a* indicates maximum plant emergence, x_0 is temperature to 50% of maximum plant emergence, *b* is a fitting parameter of the curve, and whose trend showed how plant emergence sharply increases as soil temperature raised up to approximately 15°C; afterwards, the raise in germination percentage became negligible. The speed of plant emergence in field, was also greatly affected by soil temperature. Consequently, mean emergence time (MET, days) to 30% plant emergence dropped to less than 30 days with the increase of soil temperature from 12.5°C to approx. 15°C; beyond this temperature, the increase in plant emergence speed was less evident. According to these results, 15°C was assumed as minimum thermal threshold for drawing the suitability maps of estimated sowing dates and seed ripening of castor across Sicily.

Figure 38 Relationships of minimum soil temperature vs. plant emergence in field and Mean Germination time (MET).

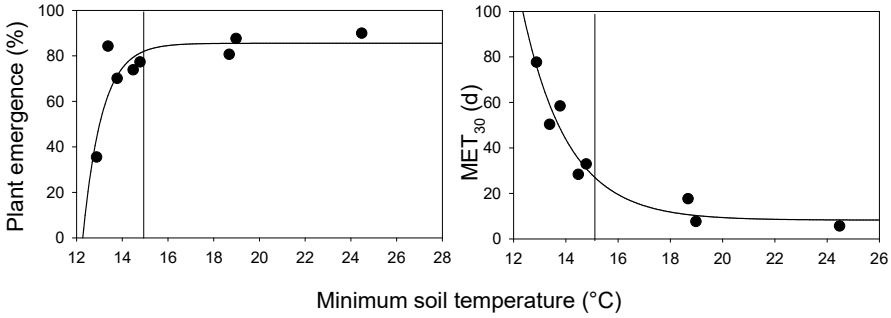

6.3.4 *Sowing date estimation*

The suitability map of the estimated latest autumn sowing date in Sicily, starting from the first of November in areas that meet the requirements for autumn sowings (T_{avg} during the sowing

decade >15°C and L_{month} >5°C for the whole growing season), is shown in **Figure** 4. Only coastal and lowland to moderate hilly areas were adapted to autumn sowings. In coastal and lowland areas, sowing can be delayed up to 5 December. In hilly areas, sowing should be performed earlier, before 10 November.

The suitability map of the estimated earliest spring sowing date in Sicily is shown in **Figure** 5. The earliest spring sowing can be performed at the end of March in Northern coasts, several locations in Southern coasts (Licata and plains around Gela) and in the lowland south of Simeto river. Latest spring sowing must be performed on mid-May in the inland hill areas up to an altitude of 800 m. Unsuitable areas are characterized by monthly average temperature <15°C until May, where castor cycle length is not enough for seed ripening.

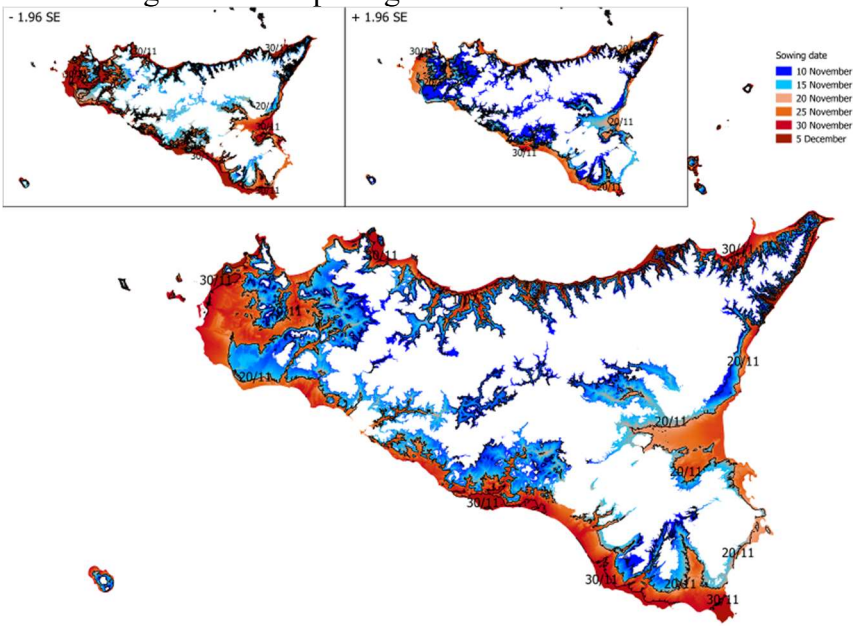

Figure 39 Autumn sowing date

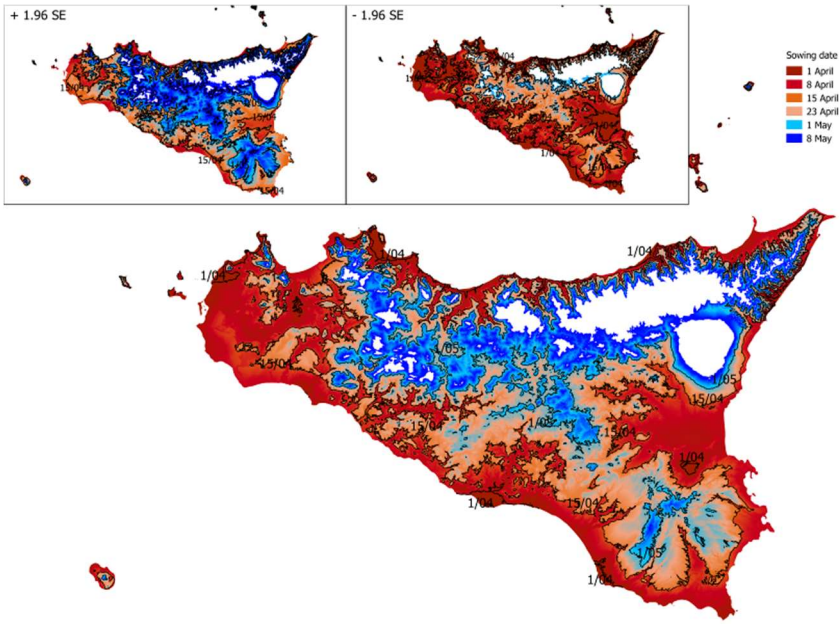

Figure 40 Spring sowing date

6.3.5 *Ripening date estimation*

The suitability map representing predicted date of seed ripening achieved by plants sown in autumn sowing is shown in **Figure** 6. The earliest seed ripening was reached at the end of June in several locations of Southern coasts (around Licata), the plain around Palermo and an area of Catania plain located south of the Simeto river. The latest seed ripening was reached on mid-July in areas of altitude up to 400 m and in the valleys connected to the coastal areas, where wind blowing from the Mediterranean Sea prevent the thermal inversion and keep the L_{month} above 5°C in wintertime. The areas with the widest variability over the years are located in the North-Eastern coastal.

The suitability map of seed ripening achieved by plants sown in spring sowings is shown in **Figure** 7. The earliest seed ripening was reached at the end of July in Northern coasts, several locations in Southern coasts, the plains around Trapani, the lowland coastal from Taormina to Messina and the lowland south of Simeto river. The latest seed ripening stage was reached on mid-September in the inland hills up to 800 m altitude. The areas with the greatest variability over the years are the inland hilly areas and the North coast.

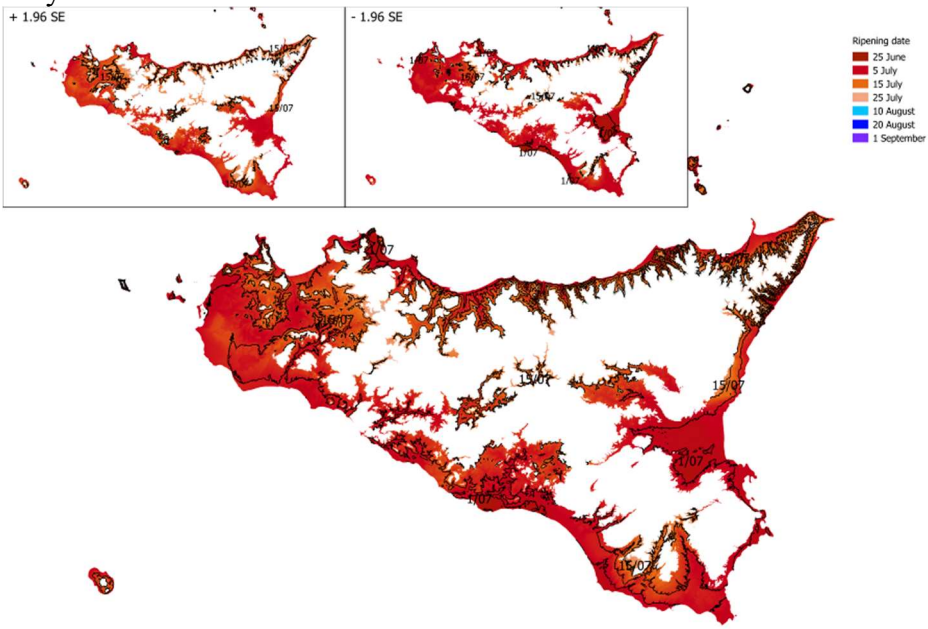

Figure 41 Ripening date with autumn sowing

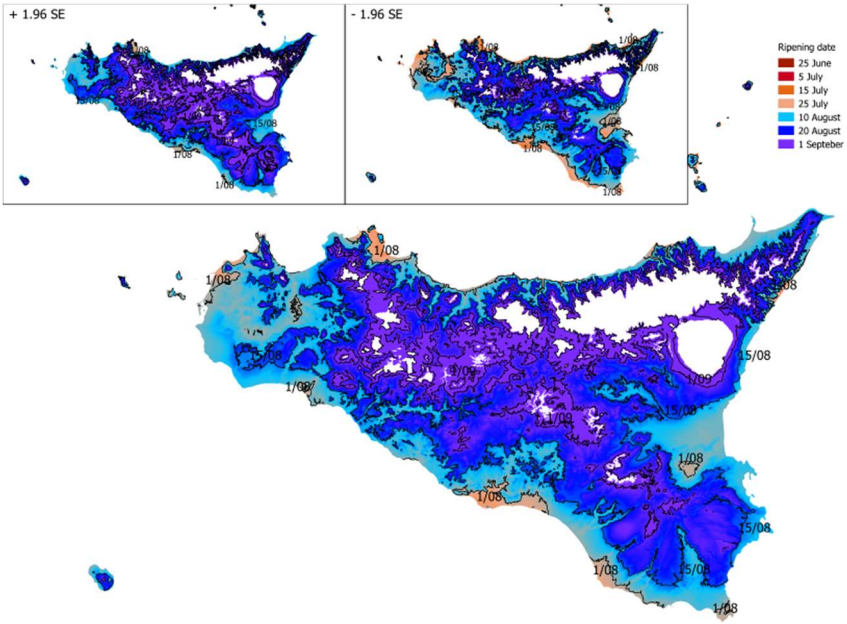

Figure 42 Ripening date with spring sowing

6.4 Discussion

Castor well adapts to a wide range of climate and soil conditions, and it can be grown either as perennial or annual crop, expected that thermal, water and photoperiod requirements are met. In semi-arid Mediterranean climate, castor holds great promise as oilseed crop mainly due to its potential seed yield, as well as to the possibility to be grown in low-input systems (i.e., rainfed conditions) and to exploit the perennial habit as compared with other macrothermal oilseed crops (Anastasi et al., 2015).
Several studies reported castor yields in temperate or subtropical areas performing spring sowings. A recent study on four castor hybrids in two Mediterranean locations, a North Mediterranean lowland area in Italy and a central Mediterranean lowland in

Greece, showed mean seed yield of 4.02 Mg/ha and 3.87 Mg/ha, respectively. Sowing was performed in spring at both locations, and hybrids were kept rainfed in Italy, while 100 mm of supplemental irrigations were provided in Greece (Alexopoulou et al., 2015a; Zanetti et al., 2017). Kumar et al. (1997) reported higher yields with a sowing in June in a tropical climate, as compared with sowings in July and August, with a shifting of the contribution to seed yield of different raceme orders: primary raceme contribution decreased, while secondary and tertiary raceme contribution increased as sowing was delayed.

Seed yield of castor in the present study was outstanding with winter sowings in rainfed conditions (3.9 Mg/ha). With late winter sowing in March, seed yield did not differ from that of most productive sowing dates, however, irrigation was applied. In general, too long (as in early autumn sowings) or too short (as in late spring sowings) growing season led to lower seed yields. Polynomial equations of seed yield and growing season duration in days showed an optimum of seed yields at about $170^{-1}80$ days, both at the first and second growing season (R^2 0.96 and 0.89, respectively; data not shown). These results matched those of Falasca et al. (2012) in Argentinian semi-arid zones. On the other hand, $90^{-1}35$ day season was reported for tropical zones (Kumar et al., 1997).

However, crop growth and development is generally dependent on thermal index or heat units, and a physiological clock is usually developed based on GDU sum. As argued by Dwyer et al. (1999), an ideal index would estimate a constant number of heat units for a given genotype to reach a specific development stage. The abovementioned polynomial equations were not significant when GDU sums were used instead of calendar days, since GDU sums were rather constant across sowing dates, with an average of 949°C.

The present study found that a base temperature of 8°C is the most suited to predict the length of growing season in terms of GDU sum for the genotype of castor used in this study; a low temperature of 5°C was set as critical for castor survival, and 15°C was assumed as minimum thermal threshold for an adequate seed germination.
Falasca et al. (2012) combined annual mean rainfall data and thermal data to define the climatologic aptitude of the Argentinean semiarid and arid zones to grow castor. A base temperature of 15°C for germination and growth, and 8°C as critical low temperature was used. The study mainly focused on frost free spring-summer period as suitable areas for castor. Kumar et al. (1997) considered a base temperature of 10°C for castor reproductive phases in a tropical environment. They observed that the length of the day in combination with the growing degree units, significantly affected seed yield of the primary raceme.
Results from this study confirm the photoperiodism of castor, since the prediction of the length of phenological stages was more accurate when photoperiod was included into the formula used for growing degree unit calculations.
Present findings confirmed the productive potential of castor in the coastal area of Sicily even in rainfed conditions. By using an inductive approach, it might be assumed to reach similar yields in other coastal and lowlands areas of Sicily, where autumn/winter sowing is feasible according to the thermal regime.

6.5 Conclusions

Castor is grown as an annual spring-summer crop in temperate areas prone to winter frost due to its high thermal requirements. However, temperate areas with infrequent frost are suitable for exploiting management strategies. Climate of lowlands and

coastal areas of Sicily, and generally of the semi-arid Mediterranean, present cool winter with infrequent light frost, spring prone to dry spells, dry summer and the peak of annual precipitation during autumn and winter. In these areas, sowing of castor can be performed in autumn, shifting crop cycle during a period of the year with a suitable pluviometric regime, escaping the summer drought and thus enabling a rainfed cropping system. Moreover, lower temperatures during winter increase the length of the growing season, allowing a greater vegetative development of the plant and a greater leaf area duration, which may increase the potential yield.

Otherwise, spring sowing in lowlands and coastal areas of Sicily should be performed at the end of March or beginning of April to satisfy the thermal requirement for germination, but exposing this phase to the risk of dry spells. Sicilian hilly areas are not suitable to autumnal sowing. In these areas, sowing can be performed in spring, shifting growing season during a period of the year with a not suitable pluviometric regime, thus requiring irrigation to achieve adequate yields.

6.6 References

Alexopoulou, E., Papatheohari, Y., Zanetti, F., Tsiotas, K., Papamichael, I., Christou, M., Namatov, I., Monti, A., 2015. Comparative studies on several castor (*Ricinus communis* L.) hybrids: Growth, yields, seed oil and biomass characterization. Ind. Crops Prod., 75, 8-13. doi:10.1016/j.indcrop.2015.07.015

Amorim Neto, M., Araújo, A., Beltrão, N., Silva, L., Gomes, D.C., 1999. Zoneamento e época de plantio para a mamoneira no Estado da Paraiba. Campina Grande: EMBRAPA-CNPA. Comunicado Técnico 108, 5 pp., http://ainfo.cnptia.embrapa.br/digital/bitstream/CNPA-2009-09/14450/1/COMTEC108.pdf.

Anastasi, U., Sortino, O., Cosentino, S.L., Patanè, C., 2015. Seed yield and oil quality of perennial castor bean in a Mediterranean environment. Int. J. Plant Prod. 9, 99-116.

Beltrão, N.E., Silva, L.C., 1999. Os múltiplos uso do óleo da mamoneira (*Ricinus communis* L.) e a importância do seu cultivo no Brasil. Revista Brasileira de Oleaginosas Fibrosas 31, 1-7.

Berman, P., Nizri, S., Wiesman, Z., 2011. Castor oil biodiesel and its blends as alternative fuel. Biomass Bioenergy 35, 2861-2866. doi:10.1016/j.biombioe.2011.03.024

Doorenbos, J, Pruitt, W.O., 1977. Guidelines for predicting crop water requirements. Irrigation and Drainage Paper No. 24. (Food and Agriculture Organization of the United Nations: Rome).

Drago, A., 2005. Atlante climatologico della Sicilia - Seconda Edizione. Riv. Ital. Agrometeorol. 2, 67-83.

Dwyer, L.M., Steward, D.W., Carrigan, L., Ma, B.L., Neave, P., Balchin, D., 1999. A general thermal index for maize. Agron. J. 91, 940-946. doi:10.2134/agronj1999.916940x

Falasca, S.L., Ulberich, A.C., Ulberich, E., 2012. Developing an agro-climatic zoning model to determine potential production

areas for castor bean (*Ricinus communis* L.). Ind. Crops Prod. 40, 185-191. https://doi.org/10.1016/j.indcrop.2012.02.044
FAOSTAT [WWW Document], 2018. FAOSTAT. URL http://www.fao.org/faostat/en/#home (accessed 9.18.18).
Kiran, B.R., Prasad, M.N.V., 2017. *Ricinus communis* L. (Castor bean), a potential multi-purpose environmental crop for improved and integrated phytoremediation. EuroBiotech. J. 1, 101-116. doi:10.24190/ISSN2564-615X/2017/02.01
Kumar, P.V., Ramakrishna, Y.S., Rao, B.V.R., Victor, U.S., Srivastava, N.N., Subba Rao, A.V.M., 1997. Influence of moisture, thermal and photoperiodic regimes on the productivity of castor beans (*Ricinus communis* L.). Agric. For. Meteorol. 88, 279-289. doi:10.1016/S0168-1923(97)00019-1
Lavanya, C., Murthy, I., Nagaraj, G., Mukta, N., 2012. Prospects of castor (*Ricinus communis* L.) genotypes for biodiesel production in India. Biomass Bioenergy 39, 204-209. doi:10.1016/j.biombioe.2012.01.008
Mendoza, Z.H, Reyes, T.S., 1985. Guía del cultivo de higuerilla. Boletín Divulgativo. INIAP. 1985.08. Portoviejo. Ecuador.
Moshkin, V.A., editor. 1986. Castor. Amerind, New Delhi.
Ozelkan, E., Bagis, S., Ustundag, B.B., Ozelkan, E.C., Yucel, M., Ormeci, C., 2013. Land surface temperature - Based spatial interpolation using a modified Inverse Distance Weighting method. Second International Conference on Agro-Geoinformatics (Agro-Geoinformatics). doi:10.1109/Argo-Geoinformatics.2013.6621890
Severino, L.S., Auld, D.L., Baldanzi, M., Cândido, M.J.D., Chen, G., Crosby, W., Tan, D., He, X., Lakshmamma, P., Lavanya, C., Machado, O.L.T., Mielke, T., Milani, M., Miller, T.D., Morris, J.B., Morse, S.A., Navas, A.A., Soares, D.J., Sofiatti, V., Wang, M.L., Zanotto, M.D., Zieler, H., 2012. A Review on the Challenges for Increased Production of Castor.

Agron. J. 104, 853-880. https://doi.org/10.2134/agronj2011.0210
Smith, M.E., Hayoun, M.A., 2019. Ricin toxicity. StatPearls Publishing LLC. National Center for Biotechnology Information, U.S. National Library of Medicine 8600 Rockville Pike, Bethesda MD, 20894 USA.
Vinayaka, D.L., Guna, V., Madhavi, D., Arpitha, M., Reddy, N., 2017. *Ricinus communis* plant residues as a source for natural cellulose fibers potentially exploitable in polymer composites. Ind. Crops Prod. 100, 126-131. http://dx.doi.org/10.1016/j.indcrop.2017.02.019
Zanetti, F., Chieco, C., Alexopoulou, E., Vecchi, A., Bertazza, G., Monti, A., 2017. Comparison of new castor (*Ricinus communis* L.) genotypes in the mediterranean area and possible valorization of residual biomass for insect rearing. Ind. Crops Prod. 107, 581-587. doi:10.1016/j.indcrop.2017.04.055